

UNCLASSIFIED

AD NUMBER

AD844980

LIMITATION CHANGES

TO:

Approved for public release; distribution is unlimited.

FROM:

Distribution authorized to U.S. Gov't. agencies and their contractors; Critical Technology; JUL 1968. Other requests shall be referred to Air Force Cambridge Research Laboratory, CRDM, Hanscom AFB, MA 01730. This document contains export-controlled technical data.

AUTHORITY

afcr1 ltr 22 dec 1971

THIS PAGE IS UNCLASSIFIED

AN EXPERIMENTAL STUDY OF THE BREAKDOWN  
CHARACTERISTICS OF MICROWAVE AND VHF ANTENNAS  
VOLUME I OF 2

by:

Richard C. Warder, Jr., and John A. Thornton

SPACE SCIENCES LABORATORIES  
Litton Systems, Inc.  
336 N. Foothill Road  
Beverly Hills, California 90213

This research was sponsored by:

Advanced Research Projects Agency  
Department of Defense  
Project DEFENDER  
ARPA Order No. 693

Prepared for:

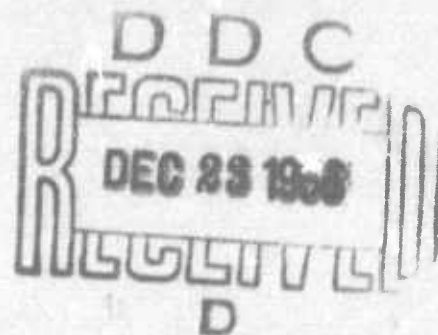
Air Force Cambridge Research Laboratories  
Office of Aerospace Research  
United States Air Force  
Bedford, Massachusetts

FINAL REPORT (Vol. I)  
July 1967 - July 1968  
July 1968

Contract No. F19628-68-C-0001  
Project No. 8671

Contract Monitor  
Walter Rotman  
Microwave Physics Laboratory

THIS DOCUMENT IS SUBJECT TO SPECIAL EXPORT CONTROLS AND EACH TRANSMITTAL  
TO FOREIGN GOVERNMENTS OR FOREIGN NATIONALS MAY BE MADE ONLY WITH PRIOR  
APPROVAL OF AFCRL (CRDM/~~XXXXXXXXXX~~) L. G. Hanscom Field, BEDFORD,  
MASSACHUSETTS (01730)



AD 844980

**BEST  
AVAILABLE COPY**

AN EXPERIMENTAL STUDY OF THE BREAKDOWN  
CHARACTERISTICS OF MICROWAVE AND VHF ANTENNAS  
VOLUME I OF 2

by:

Richard C. Warder, Jr., and John A. Thornton

SPACE SCIENCES LABORATORIES  
Litton Systems, Inc.  
336 N. Foothill Road  
Beverly Hills, California 90213

This research was sponsored by:

Advanced Research Projects Agency  
Department of Defense  
Project DEFENDER  
ARPA Order No. 693

Prepared for:

Air Force Cambridge Research Laboratories  
Office of Aerospace Research  
United States Air Force  
Bedford, Massachusetts

FINAL REPORT (Vol. I)  
July 1967 - July 1968  
July 1968

Contract No. F19628-68-C-0001  
Project No. 8671

Contract Monitor  
Walter Rotman  
Microwave Physics Laboratory

THIS DOCUMENT IS SUBJECT TO SPECIAL EXPORT CONTROLS AND EACH TRANSMITTAL  
TO FOREIGN GOVERNMENTS OR FOREIGN NATIONALS MAY BE MADE ONLY WITH PRIOR  
APPROVAL OF AFCRL (CRDM/~~Walter Rotman~~) L. G. Hanscom Field, BEDFORD,  
MASSACHUSETTS (01730)



ACKNOWLEDGMENT

This research was supported by the  
Advanced Research Projects Agency,  
Project DEFENDER,  
and was monitored by the  
Air Force Cambridge Research Laboratories  
under Contract No. F19628-68-C-0001.

## ABSTRACT

This document is part of the final report describing an investigation of the breakdown characteristics of selected microwave and VHF transmitting antennas under both cold air and simulated re-entry conditions. The purpose of the program was to provide experimental data which will aid in the selection of re-entry jammers. Of particular interest were the power handling capabilities, the pattern of the radiated fields, and the input impedance, of antennas which are compatible with the geometry of a conical re-entry vehicle.

The report is divided into two volumes. This volume is unclassified and describes the investigation of a microwave slot antenna. Volume II, which is classified SECRET, describes the investigation of a VHF antenna.

The microwave antenna consisted of a teflon-filled X-band slot located on a conical surface which served as a conducting plane. The microwave experiments consisted of performing initiate and extinguish breakdown tests with both cold gas, and a plasma environment over the antenna. Transmitted and reflected power measurements were also made, together with preliminary ablation tests.

The antenna plasma tests were conducted in the large size, steady state, plasma flow environment produced by the Litton electrodeless MHD plasma accelerator.

#### AUTHORS' ACKNOWLEDGMENTS

The authors wish to acknowledge the contributions of Dr. A.S. Penfold, Mr. R.M. Rosen, Mr. D.L. Curtis, and Mr. G. Fonda-Bonardi to the antenna testing program. Mr. C.A. Cullian and Mr. W. Umphres contributed to the design and construction of the plasma diagnostic instrumentation and operated the plasma test facility. Mr. R. de Craene provided major support, suggestions and contributions throughout the entire measurement program.

It is a pleasure to acknowledge the cooperation and contributions of Mr. W. Scott and Mr. C.W. Westermann of Philco-Ford to the VHF testing program. Their willingness to perform measurements on the VHF antenna and to supply additional detailed information was a major aid in developing an understanding of the power handling capabilities of the VHF antenna.



## TABLE OF CONTENTS

1.	INTRODUCTION	1
2.	PLASMA TEST CONDITIONS AND BOUNDARY LAYER MEASUREMENTS	5
2.1	INTRODUCTION	5
2.2	CONE DIAGNOSTIC INSTRUMENTATION	6
2.3	BOUNDARY LAYER DIAGNOSTIC INSTRUMENTATION	8
2.4	PLASMA TEST CONDITIONS	10
2.5	EXPERIMENTAL RESULTS	17
2.6	ELECTRON COLLISION FREQUENCY	34
2.7	SELECTION OF PLASMA CONDITIONS FOR MICROWAVE EXPERIMENTS	37
3.	MICROWAVE SLOT ANTENNA TESTING	41
3.1	INTRODUCTION	41
3.2	MICROWAVE ELECTRICAL INSTRUMENTATION	43
3.3	PRELIMINARY EXPERIMENTS	49
3.4	COLD GAS BREAKDOWN EXPERIMENTS	53
3.5	X-BAND SLOT ANTENNA-PLASMA LAYER EXPERIMENTS	61
4.	MICROWAVE EXPERIMENTS, SUMMARY AND CONCLUSIONS	83
4.1	INTRODUCTION	83
4.2	ANTENNA BREAKDOWN CHARACTERISTICS	85
4.3	INPUT IMPEDANCE CHARACTERISTICS	91
4.4	ANTENNA PATTERN MEASUREMENTS	92
5.	REFERENCES	95

## LIST OF FIGURES AND TABLES

Figure 2-1.	Schematic of Test Cone	7
Figure 2-2.	Turret with Boundary Layer Probes	9
Figure 2-3.	Summary of Utilization of Experimental Data	11
Figure 2-4.	Calibration of Cone Diagnostic Instrumentation	15
Figure 2-5.	Plasma Flow over Cone under Various Operating Conditions	16
Figure 2-6.	Comparison of Electron Density Obtained Using Various Data Reduction Theories	20
Figure 2-7.	Influence of Electron Temperature on Experimental Electron Density Profiles	21
Figure 2-8.	Electron Density Profiles at Various Axial Stations	23
Figure 2-9.	Electron Density Profiles over Microwave Slot Aperture	24
Figure 2-10.	Electron Density Profiles over Microwave Slot Aperture	25
Figure 2-11.	Axial Variation in Electron Density Along Cone Surface	26
Figure 2-12.	Typical Electron Temperature Profile over Microwave Slot Aperture	29
Figure 2-13.	Gas Temperature Profiles at Various Axial Stations	31
Figure 2-14.	Gas Temperature Profiles over Microwave Slot Aperture	32

Figure 2-15.	Gas Number Density Profiles over Microwave Slot Aperture	33
Figure 2-16.	Gas Velocity Profile over Microwave Slot Aperture	35
Figure 2-17.	Flow Field over Microwave Test Cone	36
Figure 3-1.	Schematic of Microwave Power Measurement Circuit	45
Figure 3-2.	Schematic of Reflectometer Bridge Arrangement	46
Figure 3-3.	Photograph of Experimental Arrangement	47
Figure 3-4.	Test Chamber and Model Layout	48
Figure 3-5.	Results of Cold Air Breakdown Studies	55
Figure 3-6.	Results of Cold Argon Breakdown Studies	57
Figure 3-7.	Comparison of Breakdown Results for Several Gas Mixtures	58
Figure 3-8.	Reflection Coefficient Amplitude in Cold Air Experiments	59
Figure 3-9.	Phase and Amplitude of Reflection Coefficient in Cold Air Experiments	60
Figure 3-10.	Power Transmitted During Plasma Experiments	65
Figure 3-11.	Power Transmitted and Reflected During Plasma Experiment	66
Figure 3-12.	Reflected Power Characteristics	67
Figure 3-13.	Variation of Antenna Input Impedance for Overdense Plasma Layer	68
Figure 3-14.	Power Transmitted and Reflected During Plasma Experiment	70
Figure 3-15.	Power Transmitted and Reflected During Plasma Experiment	71



Figure 3-16.	Power Transmitted and Reflected During Plasma Experiment	72
Figure 3-17.	Power Transmitted During Plasma Experiments	73
Figure 3-18.	Peak Power Transmitted During Plasma Experiments	74
Figure 3-19.	Effect of Ambient Plasma on Breakdown Power Level	76
Figure 3-20.	Photograph of Ablated Teflon-covered Cone Tip	80
Figure 3-21.	Power Transmitted and Reflected During Ablation Experiments.	82
Table 2-I.	Summary of Plasma Tunnel Diagnostic Runs	13
Table 2-II.	Summary of Boundary Layer Diagnostic Measurements	14
Table 2-III.	Experimental Conditions Selected for Microwave Antenna Tests	39
Table 3-I.	Summary of Microwave Measurements made During Plasma Tunnel Tests	63

## 1. INTRODUCTION

This is Volume I of the final report describing experimental antenna test studies performed by the Space Sciences Laboratories of Litton Systems, Inc. for the Air Force Cambridge Research Laboratories under Contract F19628-68-C-0001, ARPA Order No. 693, Project DEFENDER.

The objective of the program was to evaluate the breakdown and transmission characteristics of selected microwave and VHF transmitting antennas under both ambient (cold air), and simulated re-entry conditions, at high altitudes. The purpose of the program was to provide experimental data which will aid in the selection of re-entry jammers. Of particular interest were the:

- Power-handling capabilities
- Pattern of radiated fields
- Input impedance

A teflon-filled X-band slot located in a surface, which serves as a conducting plane, was selected for the microwave investigation. This configuration was chosen since the analytical problem of a slot located in a conducting plane, which is covered with plasma, has received extensive attention in the literature.

In the VHF facet of the investigation it was considered important to utilize, to the fullest extent possible, advances that were occurring in VHF antenna design. Accordingly, a conical type antenna, which has recently been developed by Philco-Ford, was selected for these tests.

Both test programs were conducted with the antenna incorporated



into a slender cone. In the microwave study the slot was located 45 cm from the cone nose with the E-plane parallel to the direction of flow. In the VHF case the conical antenna structure constituted essentially the entire cone assembly.

Both the microwave and the VHF tests were conducted in a large vacuum facility (8 feet in diameter and 15 feet long) in which the walls were lined with appropriate anechoic material to minimize wall reflections of electromagnetic energy.

The power handling capabilities of an antenna are limited by gaseous breakdown. Even in the laboratory, the process of gaseous breakdown is a dynamic phenomenon which involves a delicate balance of many kinetic processes. Indeed, the gaseous breakdown has been called "the phenomenon in which nature reveals herself in her most fundamental way".<sup>1</sup> The gas breakdown that occurs in the electric field of an ECM antenna during re-entry is subject to additional complication since:

- The breakdown occurs in a high velocity flow.
- The ambient gas is at a temperature of several thousand degrees Kelvin and significant ionization may be present.
- The composition of the flow field may be complicated by the presence of ablation products.
- The vehicle shape, gas dynamic boundary layer, and antenna electric field distribution constitute an extremely complex geometry.

The complexity of the problem suggests an experimental approach. However, the pursuit of such an approach is made difficult by the following:

- The re-entry antenna breakdown situation cannot be simulated completely in the laboratory.
- It is not possible to make sufficiently detailed on-board measurements in actual re-entry tests to permit a systematic determination of the required design information.

Thus, the required approach is a co-ordinated program involving laboratory experiments, analytical studies, and flight tests. Since

various laboratory facilities can simulate various aspects of the re-entry situation, but since no one facility can provide a complete steady state simulation of the re-entry flow field, the laboratory test programs must be based on a careful analysis of the overall re-entry transmission problem.

In the re-entry simulation portion of the present program the emphasis was on surrounding the antenna with a controlled environment in which the electron density, and the electron density profile, could be accurately determined. Determination of the electron density profile required that detailed electrostatic probe measurements be made in the vicinity of the test antenna. Since the probe and traversing equipment would obviously affect the performance of the antenna, the approach was (1) to make detailed measurements of the plasma properties adjacent to the antenna structure, and (2) to remove the diagnostic equipment and perform the antenna tests. These objectives, and this approach, placed the following requirements on the experimental facility:

- It had to have sufficient range of operation so that (1) the electron density could be varied from a very low value to a value such that the plasma frequency was well above the operating frequency for the antenna in question, with (2), the gas density in a range such that the electron-neutral collision frequency was of the order of magnitude encountered during high altitude re-entry.
- It had to permit steady state operation so that detailed spatially resolved measurements could be made of the plasma properties.
- It had to be capable of sufficient control so that a given set of operating conditions could be generated reproducibly on a day to day basis.
- It had to be capable of providing a flow stream with sufficient total enthalpy to cause ablation on the test surface.
- It had to be large enough to permit testing of a full-sized conical antenna assembly.

The Litton electrodeless MHD accelerator was used for the re-entry simulation tests, since it is capable of providing flow conditions



which satisfy the above requirements over models placed in the large anechoic lined vacuum chamber.

This report is divided into two volumes. Volume I, which is unclassified, describes the detailed measurements of the plasma flow over the cone containing the slot antenna (Chapter 2), and the microwave experiments (Chapter 3). The microwave experiments consisted of performing initiate and extinguish breakdown tests with both a cold gas and a plasma environment over the antenna. Transmitted and reflected power, and impedance measurements were also made together with preliminary ablation tests. The results are summarized and compared with the findings of other investigators (Chapter 4).

Volume II, which is classified SECRET, describes the VHF experiments. As the program developed it became increasingly apparent that, because of the complexity of the processes involved, it was premature to perform plasma tests on the selected VHF antenna. Accordingly, in the VHF investigation, cold air breakdown studies were emphasized (Chapter 2), together with the identification of potential problem areas that would be encountered in a program involving extensive plasma testing. The results are examined in terms of their significance with respect to the selection and design of VHF re-entry jammers (Chapter 3). Detailed recommendations are given for a subsequent program of VHF antenna investigations (Chapter 4 and Appendix A).

## 2. PLASMA TEST CONDITIONS AND BOUNDARY LAYER MEASUREMENTS

### 2.1 INTRODUCTION

As noted in Chapter 1, the approach taken in the program was to perform the antenna experiments in a well-defined plasma environment. Accordingly, the measurement of the plasma parameters associated with the boundary layer over the test cone constituted an important facet of the program.

In particular, it was important that the spatial distribution of the following parameters be determined in the boundary layer over the cone:

- Electron Density -  $N_e$
- Gas Density -  $N_A$
- Gas Temperature -  $T_g$
- Electron Temperature -  $T_e$
- Gas Velocity -  $U$

The presence of diagnostic instrumentation for probing the spatial variations of the boundary layer plasma would perturb the measurement of antenna radiation patterns. Accordingly, it was necessary to obtain the plasma properties separately from the antenna data. This in turn required that plasma flow over the test cone be reproducible and that the index of reproducibility rely upon diagnostic instrumentation located on the cone surface.

Therefore, the purpose of this section is to describe the experiments that were performed to establish the relationship between the detailed plasma conditions that exist over the slot



antenna and the observables provided by the cone instrumentation. This section also describes the selection of several plasma conditions for the actual microwave tests.

## 2.2 CONE DIAGNOSTIC INSTRUMENTATION

The basic test model used for the microwave tests consisted of a  $6^{\circ} 20'$  half-angle cone, approximately 90 cm long, connected to a hollow cylindrical afterbody. An impact pressure port and a double (electrostatic) probe, both located at the nose of the cone, were chosen as indices of the plasma flow conditions. The choice of these particular sensors was based on measurements<sup>2-4</sup> which indicated that the impact pressure and the ion saturation current were quite sensitive indices of the plasma flow conditions.\*

In addition to the nose electrostatic probe and impact pressure port described above, the following diagnostic instrumentation was located on the cone: two double electrostatic probes, four static pressure ports, and a thermocouple (located so as to provide surface temperature measurements near the X-band slot antenna). Figure 2-1 shows schematically the test model and the associated diagnostic instrumentation.

The electrostatic probe located at the nose of the cone consisted of two cylindrical tungsten electrodes, 1 mm in diameter and 6.35 mm long, spaced 13 mm apart with a boron nitride insulator. The two electrostatic probes located near the rear of the cone were used to verify the azimuthal symmetry of the electron density distribution over the cone. These probes, which were used primarily to provide indices of the flow conditions and not to obtain basic diagnostic

---

\* The ion saturation current is a function of the gas density and temperature and the electron density and temperature (see Section 2.5.2.2).

- Ⓔ - ELECTROSTATIC ( DOUBLE ) PROBE
- Ⓟ - STATIC PRESSURE TAP
- Ⓢ - IMPACT PRESSURE PORT
- Ⓣ - THERMOCOUPLE

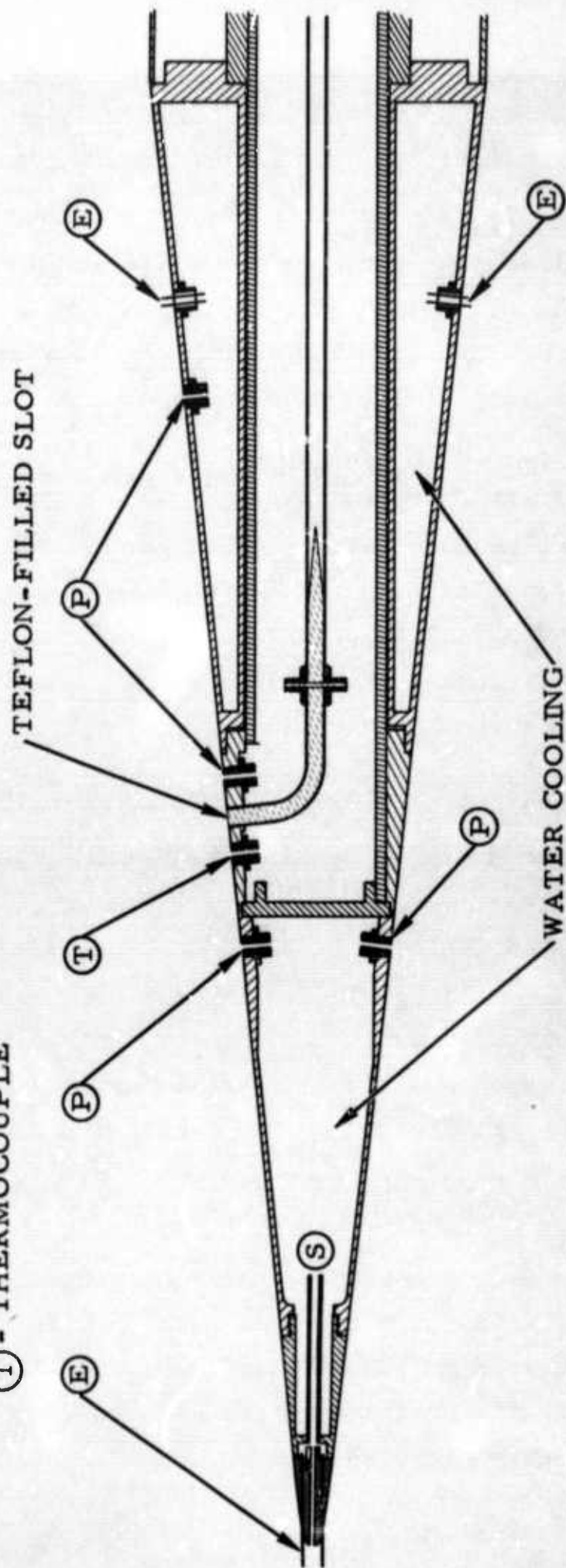


Figure 2-1. Schematic of Test Cone



information, also had cylindrical tungsten electrodes with the above described dimensions, but which were spaced 3.2 mm apart by a boron nitride insulator.

The impact pressure port was 1.6 mm in diameter. It was located between the electrodes of the nose electrostatic probe as indicated in Figure 2-1. The impact pressure was sensed by a calibrated Veeco DV 4 AM thermocouple gauge.

Four static pressure ports were used to measure axial and azimuthal variations in the static pressure at the cone surface. The pressures were measured with calibrated Veeco DV 1 AM thermocouple gauges. The cone surface temperature near the X-band slot antenna was determined by an iron-constantan thermocouple in a 1 mm diameter stainless steel jacket which in turn was press-fitted into a brass plug threaded into the cone wall.

### 2.3 BOUNDARY LAYER DIAGNOSTIC INSTRUMENTATION

Three types of diagnostic probes were used to measure the primary boundary layer properties. These included: a double electrostatic probe; an impact pressure probe, and a thermocouple temperature probe. The three boundary layer probes were mounted on a remotely controlled traversing mechanism that permitted measurement of the boundary layer profiles at various axial stations along the cone. A rotatable turret mounted on the traversing mechanism was used to interchange the boundary layer probes. This turret and the boundary layer probes are shown in Figure 2-2.

The impact pressure probe had an 18 mm diameter snout with a flat face. The impact pressure sensing orifice was 1.6 mm in diameter and was located 1.6 mm from the bottom surface of the water-cooled probe. The pressure was measured with a calibrated Veeco DV 4 AM thermocouple gauge.

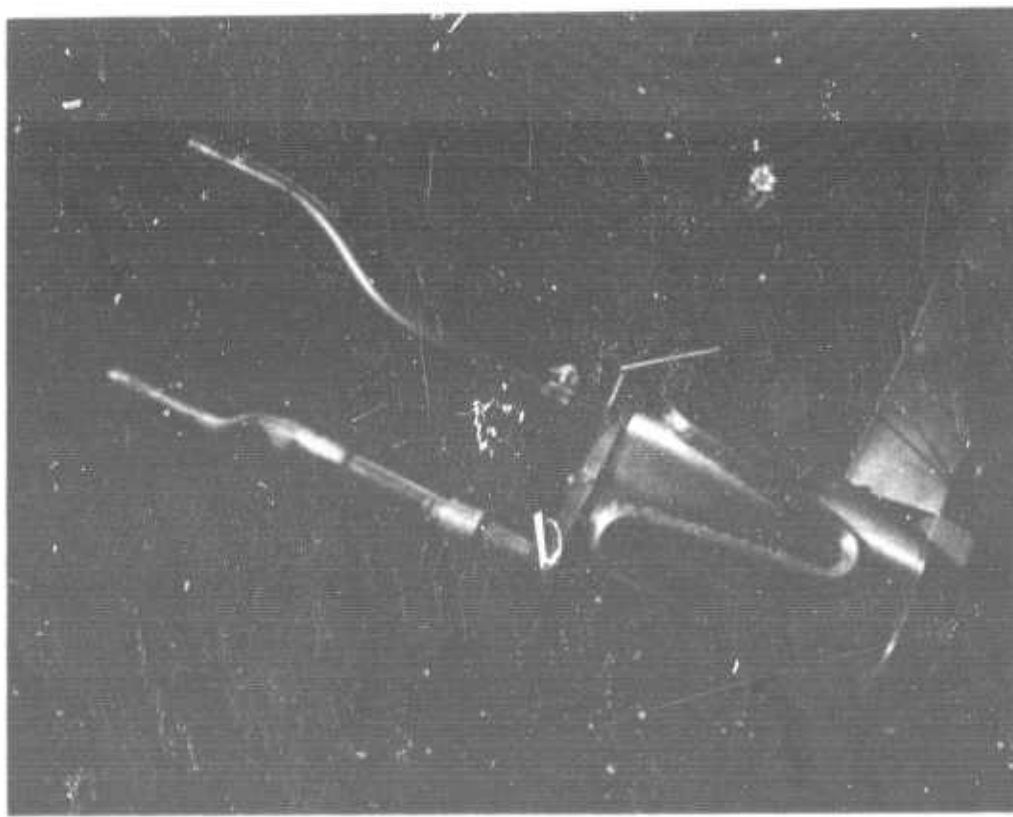
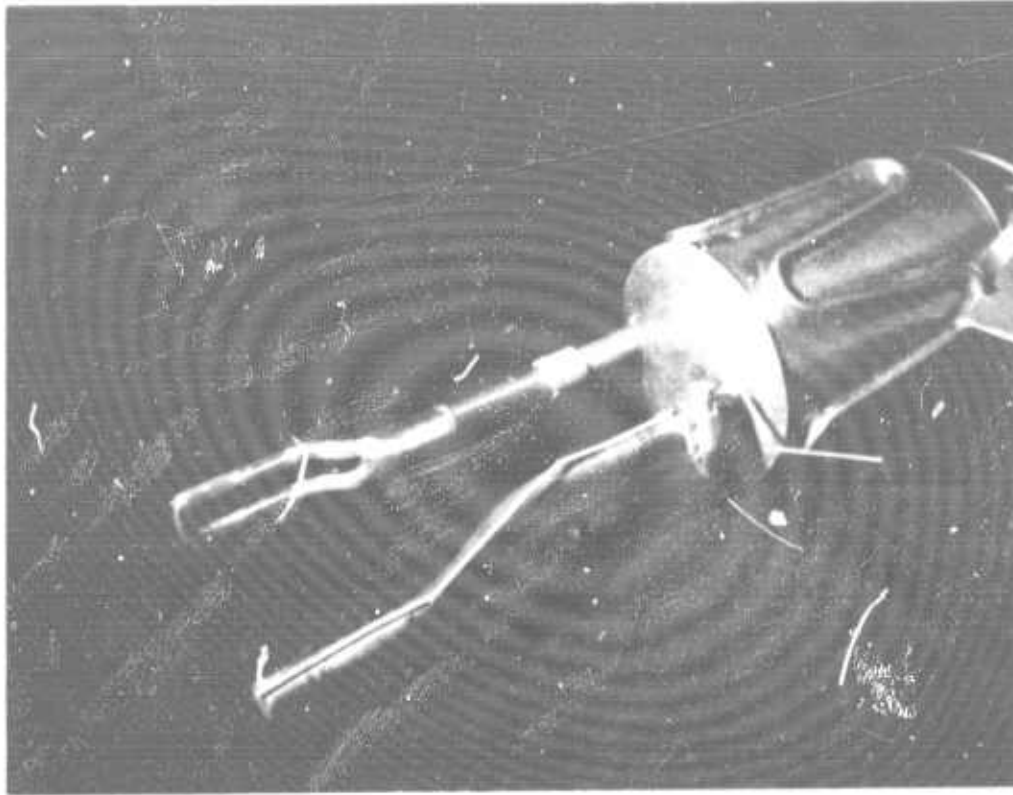


Figure 2-2. Turret with Boundary Layer Probes



The boundary layer electrostatic probe was manufactured from Pyrex glass with cylindrical tungsten electrodes, 0.5 mm in diameter and 10 mm long, separated by a distance of 17 mm. The probe was water cooled. The probe current-voltage characteristics were plotted using an XY recorder.

The temperature probe was an iron-constantan thermocouple mounted in a 1 mm diameter stainless steel jacket. All but the sensing tip of the thermocouple was sheathed in a ceramic tube for thermal insulation. The thermocouple sensing tip was exposed to the plasma convective effects and therefore temperatures measured with this probe were assumed to be impact temperatures. The temperature probe assembly was mounted on the impact pressure probe for boundary layer traversing.

Figure 2-3 summarizes the principal boundary layer diagnostic techniques and schematically illustrates the use of the experimental data to obtain the plasma properties.

#### 2.4 PLASMA TEST CONDITIONS

The plasma flow used in the antenna testing program was produced by the Litton electrodeless traveling wave accelerator. The general performance characteristics of this facility, as well as those features of particular interest from the viewpoint of antenna testing, have been described extensively in previous documents.<sup>2-7</sup>

A series of preliminary plasma tunnel tests was conducted in order to establish that the cone diagnostic data could indeed provide a reproducible index to the conditions in the plasma flow, and to select a set of environmental conditions for the detailed antenna testing program. A major objective during these tests was to obtain a range of electron densities over the region of the cone encompassing the slot antenna. The electron density over the slot was determined using the boundary layer electrostatic probe described in

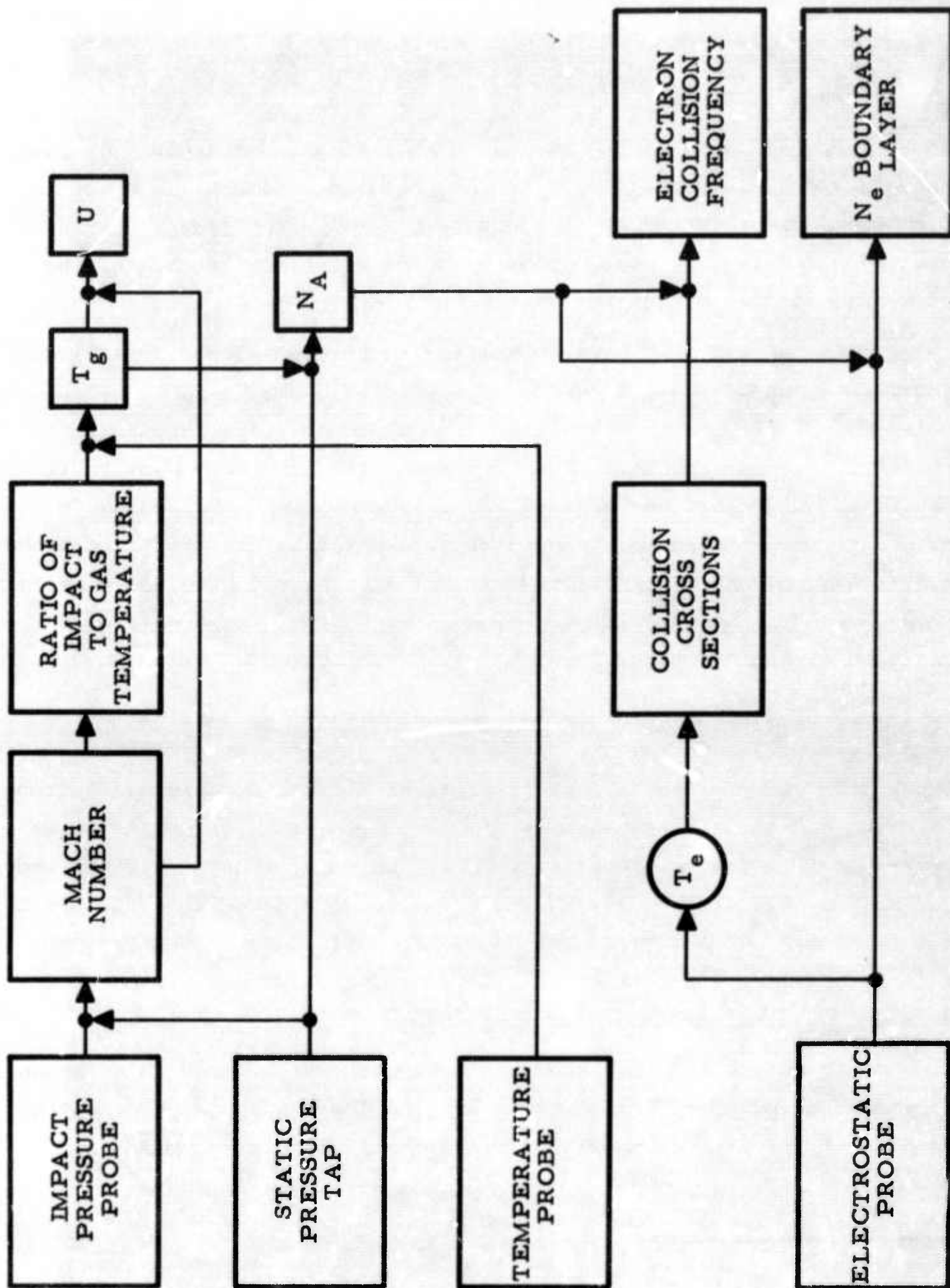


Figure 2-3. Summary of Utilization of Experimental Data



the previous section.

During these tests, the gas composition (pure argon and argon/air mixtures), the power input to the plasma accelerator, and the background pressure in the test chamber, were varied over a sufficiently wide range to obtain conditions of interest for the testing of X-band microwave slot antennas.\*

The series of plasma tunnel tests included a total of eleven individual runs. The test conditions for these eleven runs are summarized in Table 2-I. The particular boundary layer measurements that were made during these runs are summarized in Table 2-II. (It should be noted that the acquisition of a complete set of data, including impact pressures, temperatures, and radial electrostatic probe profiles at a number of selected axial stations, required approximately three hours of running time). With one exception, these data were obtained during continuous runs.

Figure 2-4 shows a plot of the peak electron density in the boundary layer above the microwave slot, as a function of the ion saturation current measured by the reference probe located at the cone nose and the ambient pressure in the test chamber. The data at 0.25 Torr show that the reference probe does indeed provide a reliable index to the peak electron density. The pressure dependence is indicated by the data taken at 1 Torr. Measurements of the electron density profiles associated with these peak electron densities are presented in Section 2.5.2.

In Figure 2-5 the upper photograph shows the cone in an argon flow corresponding to Run Number 1 and the lower photograph shows the cone under the argon/20% air mixture conditions corresponding to Run Number 2.

---

\* Subsequent to these particular tests, the plasma tunnel has been operated satisfactorily on a 100% air flow.

TABLE 2-I

## SUMMARY OF PLASMA TUNNEL DIAGNOSTIC RUNS

Run #	% Air By Weight	Test Chamber Ambient Pressure (Torr)	Teflon Ablation On Model	Ion Saturation Current Nose Elec- trostatic Probe ( $\mu$ amps)	Cone Nose Impact Pressure (Torr)	Remarks
1	0	~ 0.25	No	$1.4 \times 10^4$	~ 0.40	Similar to Run #2
2	20	~ 0.25	No	$3.5 \times 10^2$	~ 0.35	
3	20	~ 0.20	No	$1.0 \times 10^2$	~ 0.30	
4	20	~ 0.25	No	$4.4 \times 10^2$	~ 0.35	
5	20	~ 1.0	No	$1.85 \times 10^2$	~ 1.10	
6	0	~ 0.25	No	$1.25 \times 10^4$	~ 0.35	Similar to Run #5
7	10	~ 0.25	No	$1.7 \times 10^3$	~ 0.35	
8	20	~ 0.25	No	$3.5 \times 10^2$	~ 0.30	
9	20	~ 1.0	No	$1.0 \times 10^2$	~ 1.10	
10	0	~ 0.25	Yes	-*	~ 0.40	
11	20	~ 1.0	Yes	-*	~ 1.40	

\* The electrostatic probe located on the test cone nose is not a reliable index of the electron density over the X-band slot when ablation products are present.

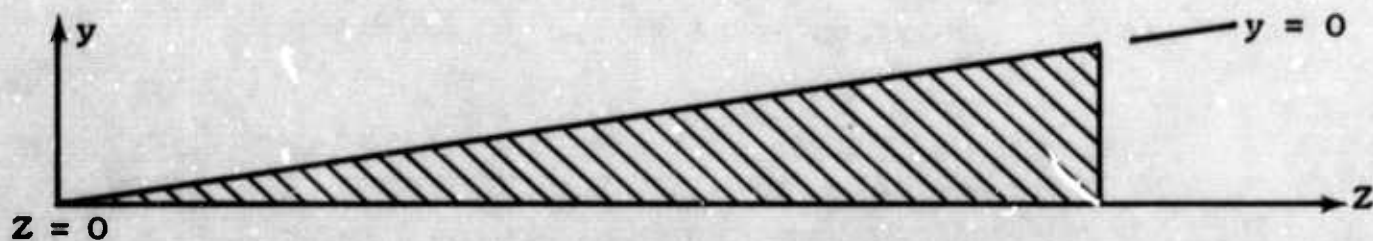


TABLE 2-II

## SUMMARY OF BOUNDARY LAYER DIAGNOSTIC MEASUREMENTS

Run #	Cone Nose $Z = 0$ cm	$Z = 23$ cm	Waveguide $Z = 45$ cm	$Z = 69$ cm	$Z = 83$ cm
1	$N_e(f)^*$	$N_e(y)$ $P_I(y)$ $T_I(y)$	$N_e(y)$ $P_I(y)$ $T_I(y)$	$N_e(y)$ $P_I(y)$ $T_I(y)$	
2	$N_e(f)$	$N_e(3.5\text{cm})$ $P_I(y)$ $T_I(y)$	$N_e(y)$ $P_I(y)$ $T_I(y)$	$N_e(3.5\text{cm})$ $P_I(y)$ $T_I(y)$	$N_e(3.5\text{cm})$ $P_I(1.6\text{cm})$ $T_I(1.6\text{cm})$
3	$N_e(f)$	$N_e(3.5\text{cm})$ $P_I(y)$ $T_I(y)$	$N_e(y)$ $P_I(y)$ $T_I(y)$	$N_e(3.5\text{cm})$ $P_I(y)$ $T_I(y)$	$N_e(3.5\text{cm})$ $P_I(1.6\text{cm})$ $T_I(1.6\text{cm})$
4	$N_e(f)$		$N_e(3.5\text{cm})$		
5	$N_e(f)$		$N_e(3.5\text{cm})$		
6	$N_e(f)$		$N_e(y)$ $P_I(y)$ $T_I(y)$		
7	$N_e(f)$		$N_e(y)$ $P_I(y)$ $T_I(y)$		
8	$N_e(f)$		$N_e(y)$		
9	$N_e(f)$		$N_e(y)$		
10	$N_e(f)$		$N_e(3.5\text{cm})$		
11	$N_e(f)$		$N_e(3.5\text{cm})$		

\* (f) refers to freestream values just in front of the cone tip.



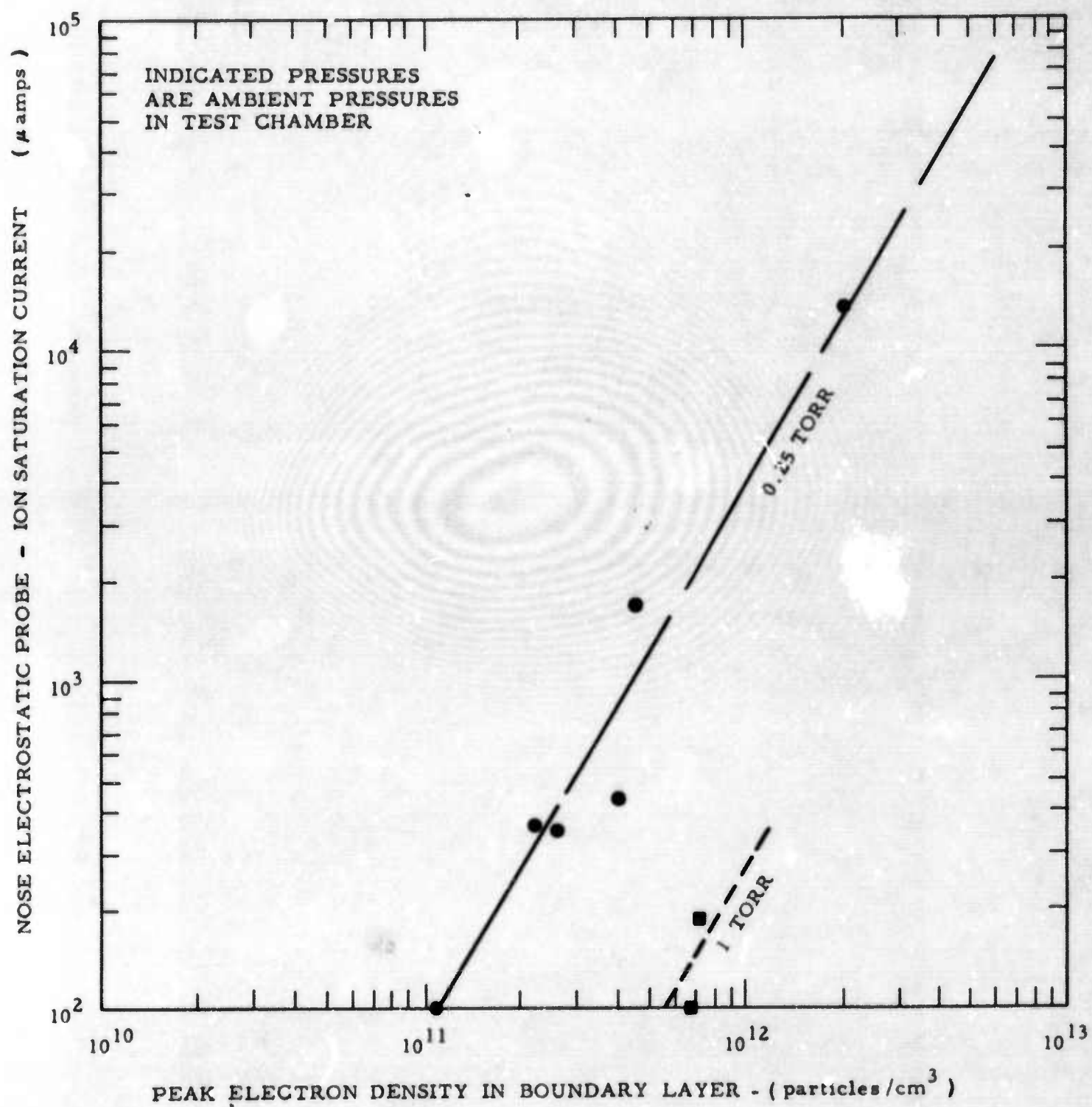


Figure 2-4. Calibration of Cone Diagnostic Instrumentation

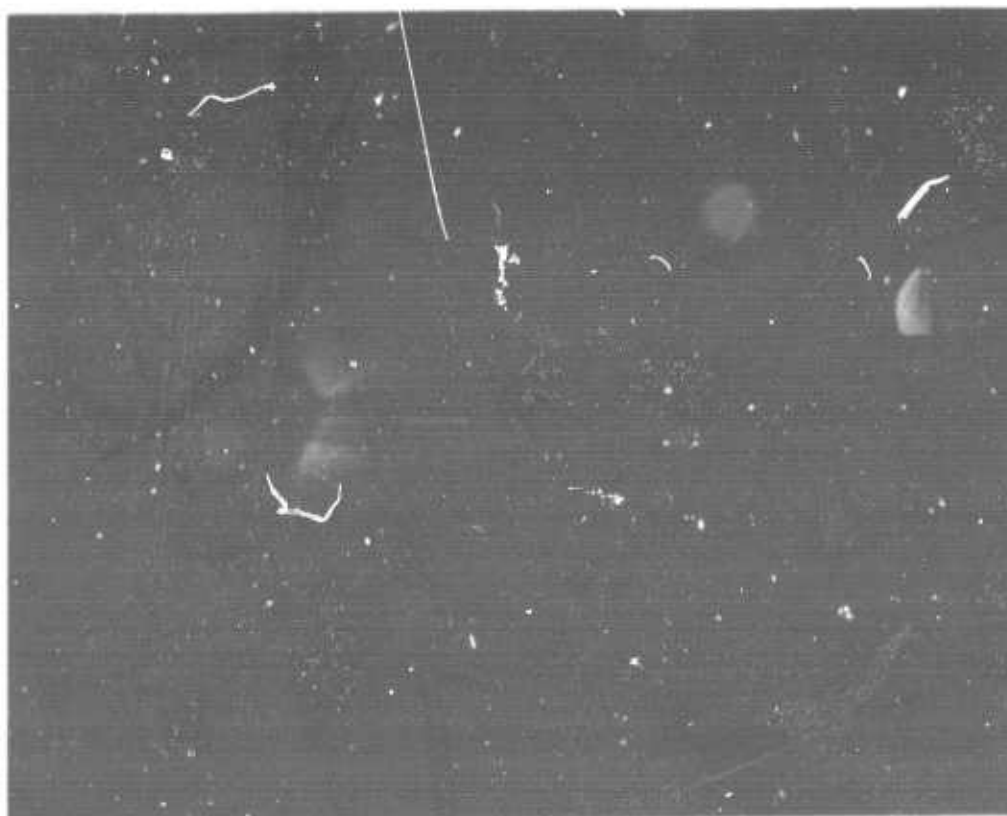
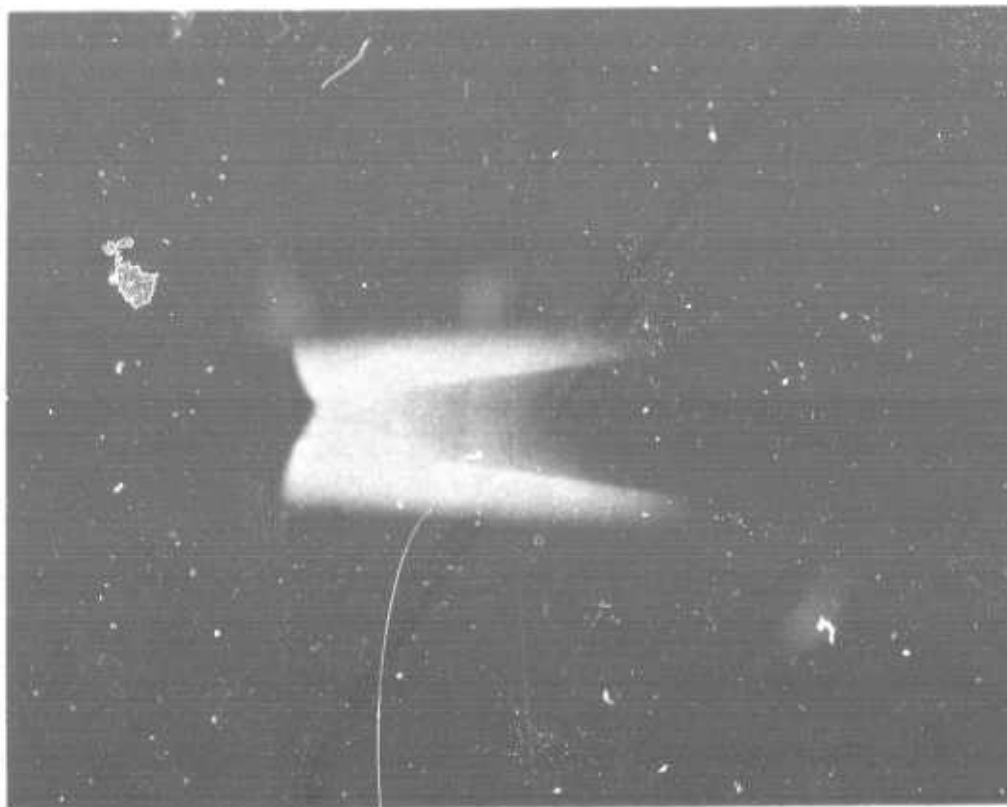


Figure 2-5. Plasma Flow over Cone under Various Operating Conditions



## 2.5 EXPERIMENTAL RESULTS

### 2.5.1 Introductory Remarks

In this section, a representative set of boundary layer plasma property profiles, as deduced from the experimental measurements, is presented. The particular parameters discussed in detail include the following:

- Electron density                    -  $N_e$
- Electron Temperature            -  $T_e$
- Gas Temperature                 -  $T_g$
- Gas Density                      -  $N_A$
- Gas Velocity                     -  $U$

Because the experimental data are subject to a number of uncertainties in interpretation (as opposed to acquisition), where appropriate, the particular method of data reduction utilized will be elaborated upon.

### 2.5.2 Electron Density Results

#### 2.5.2.1 Introduction

It is difficult to design an electrostatic probe system that is rugged enough to withstand the high temperature environment in the plasma tunnel, and that yields data which can be easily interpreted. This difficulty arises, due to the effect of collisions, because of the relatively high heavy particle densities that are of interest for re-entry and therefore for antenna testing. It was recognized at the outset of the present program that a simple interpretation of the probe data using the conventional collisionless theories would not be satisfactory for the relatively high-density plasmas produced by the plasma tunnel. Therefore, as a part of Litton's participation in this and other re-entry testing programs, an approximate theory was developed in which the effects of collisions were included.<sup>8</sup> This theory was used to reduce the electrostatic



probe data and thus to obtain electron density profiles over the test cone.

#### 2.5.2.2 Electrostatic Probe Data Interpretation

The double electrostatic probe voltage-current characteristic can easily be interpreted to yield a value for the ion saturation current collected by the probes and, subject to certain limitations discussed in Section 2.5.3, can also yield an electron temperature. However, a rigorous calculation relating the ion saturation current to the plasma properties is difficult, even for the collision-free condition (ion and electron mean free paths larger than the probe and sheath size), because of the complexity of the plasma sheaths that form over the two probe electrodes.

When the electron density is sufficiently large so that the sheath thickness is small compared to the probe radius, the collision-free thin-sheath formula due to Bohm<sup>9</sup> provides a convenient method for estimating the electron density from the ion saturation current. The Bohm relationship can be written as

$$I_+ \approx 0.5N_e \left( \frac{kT_e}{m_+} \right)^{\frac{1}{2}} A \quad \text{Eq. 2.1}$$

where  $I_+$  is the ion saturation current,  $N_e$  is the electron density (which is assumed equal to the ion density),  $T_e$  is the electron temperature,  $m_+$  is the ion mass,  $A$  is the probe area, and  $k$  is Boltzmann's constant. Bohm's equation properly accounts for the acceleration of ions by the electric fields that penetrate beyond the sheath but neglects large sheath size and collisional effects, in the sheath and presheath. Convective effects are also neglected; however, they are not important for the probe orientations and the plasma conditions used in the present program.

When the thickness of the plasma sheath is significant, as compared with the probe radius, and/or when collision effects are

present, a more extensive probe theory, such as the one described in Reference 8, must be used to deduce the electron density from the ion saturation current. In some antenna test studies, the Bohm theory has incorrectly been applied to situations where thick-sheath and collisional effects are important. Unfortunately, this approach can result in significant errors in the deduced electron density (see Section 4.3). To illustrate the errors that result from incorrectly using the Bohm theory, or, for that matter, any theory that does not properly include collisions and thick-sheath effects, a comparison is made in Figure 2-6 of the electron density profile over the slot aperture as calculated using the Bohm formula and as calculated from the theory by Thornton.<sup>8</sup> It is immediately obvious that, for these operating conditions, a large error would result if one proceeded on the basis of the Bohm theory. (It should be noted that for cylindrical probes, over these operating conditions, the theory given in Reference 8 yields results that are similar to the theory of Zakharova.<sup>10</sup>)

It is particularly revealing to note that, while the Bohm theory indicates a peak electron density such that  $\omega_p/\omega = 0.5$ , the theory of Reference 8 indicates that the peak electron density was substantially greater than the cutoff value for the microwave frequency used in the X-band experiments. That the plasma was, indeed, above cutoff in this particular experiment was verified experimentally, as discussed in Chapter 3.

Finally it should be noted that, for the operating conditions of interest, the electron temperature or electron energy enters essentially linearly in the more detailed theory as opposed to a square root dependence in the Bohm theory. Thus, errors in electron temperature have a greater influence on the electron densities than would be anticipated from the Bohm theory (see Figure 2-7).

#### 2.5.2.3 Electron Density Profiles

Electron density profiles in the boundary layer at various



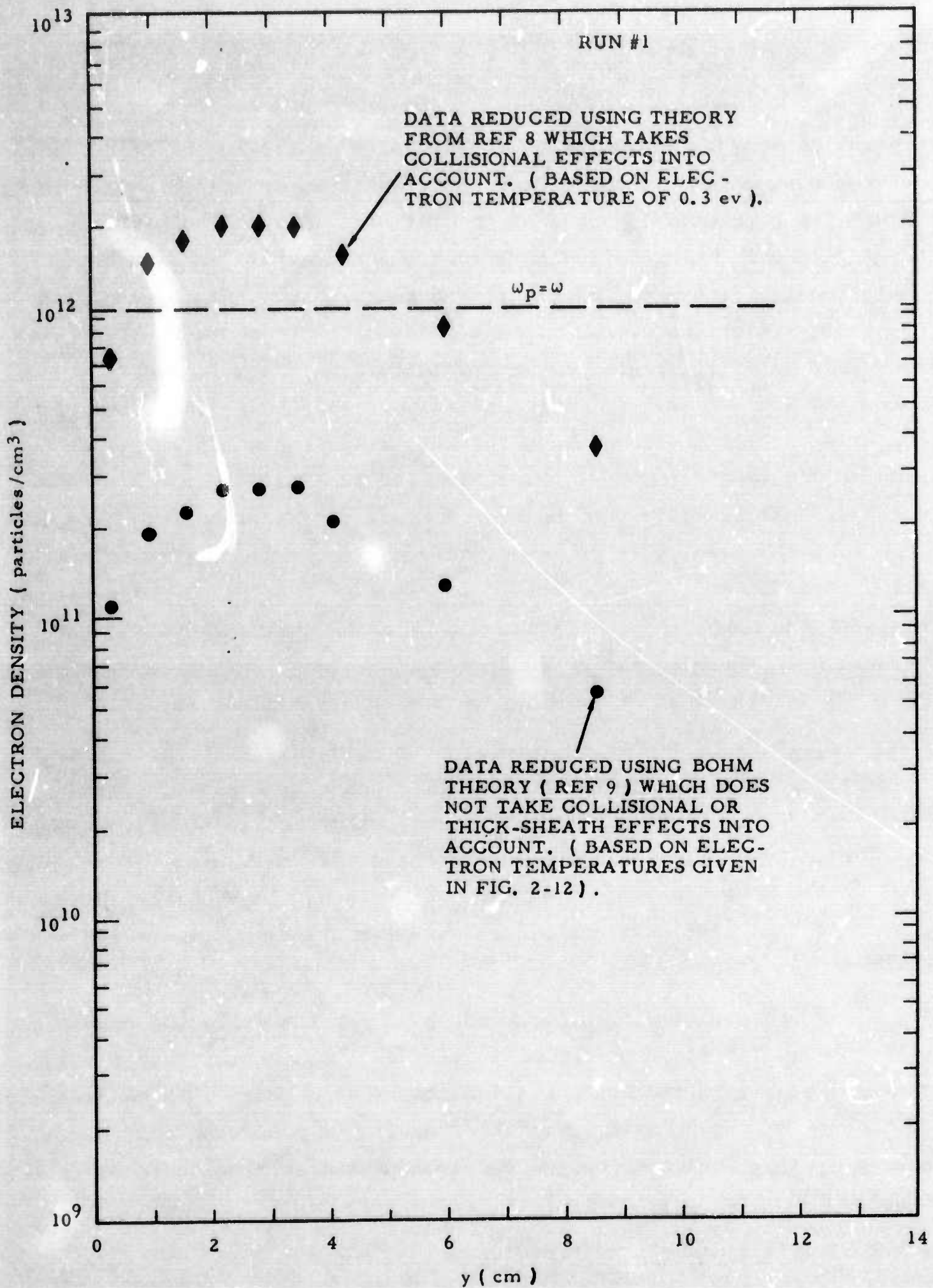


Figure 2-6. Comparison of Electron Density Obtained Using Various Data Reduction Theories



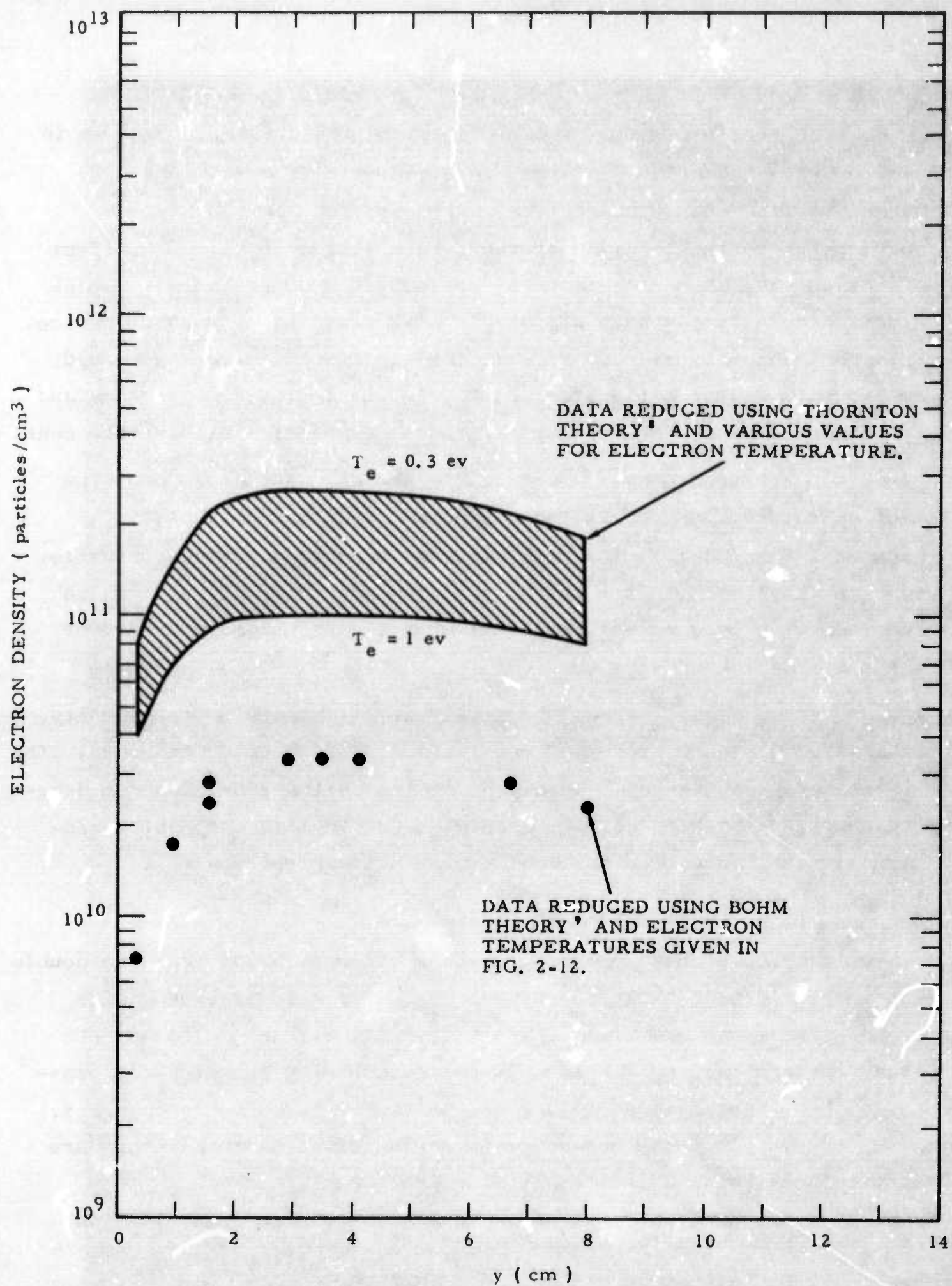


Figure 2-7. Influence of Electron Temperature on Experimental Electron Density Profiles

axial stations, for one particular operating condition, are shown in Figure 2-8. The axial distances were measured from the cone nose, back along the cone surface. The axial station where  $Z = 45$  cm corresponds to the location of the X-band slot antenna. The effect of moving back along the cone can be seen as a decrease in the peak electron density and a shift in this peak away from the cone surface. This behavior was observed for all the experimental runs and would be expected from consideration of the losses to the cone surface and the mixing of the boundary layer with the external flow over the cone.

Electron density profiles in the boundary layer over the slot aperture, for several operating conditions, are shown in Figures 2-9 and 2-10. The peak electron densities in these profiles cover a range such that  $n_p/n_\infty$  varies from approximately 0.3 to 1.4 and thereby provide a set of conditions of particular interest for the study of X-band slots.

Figure 2-11 shows the axial variation in electron density, at a fixed distance from the cone surface, for three of the runs. The linear decay on the log-linear plot indicates that the electron density obeys a simple power law decay although the gas composition apparently influences the particular constants in the power law.

### 2.5.3 Electron Temperature Results

It was noted previously (in Section 2.5.2.3) that the double electrostatic probe voltage-current characteristic can, under the proper circumstances, yield the electron temperature. Indeed, the electron temperature is necessary for determining the electron density either from the Bohm theory or the theory given in Reference 8.

Double probe measurements of the electron temperature are particularly vulnerable to the following:<sup>8</sup>

- Slight departures of the electron velocity distribution from Maxwellian.
- Contamination of the probe surface.

Double probe measurements of the electron temperature are also



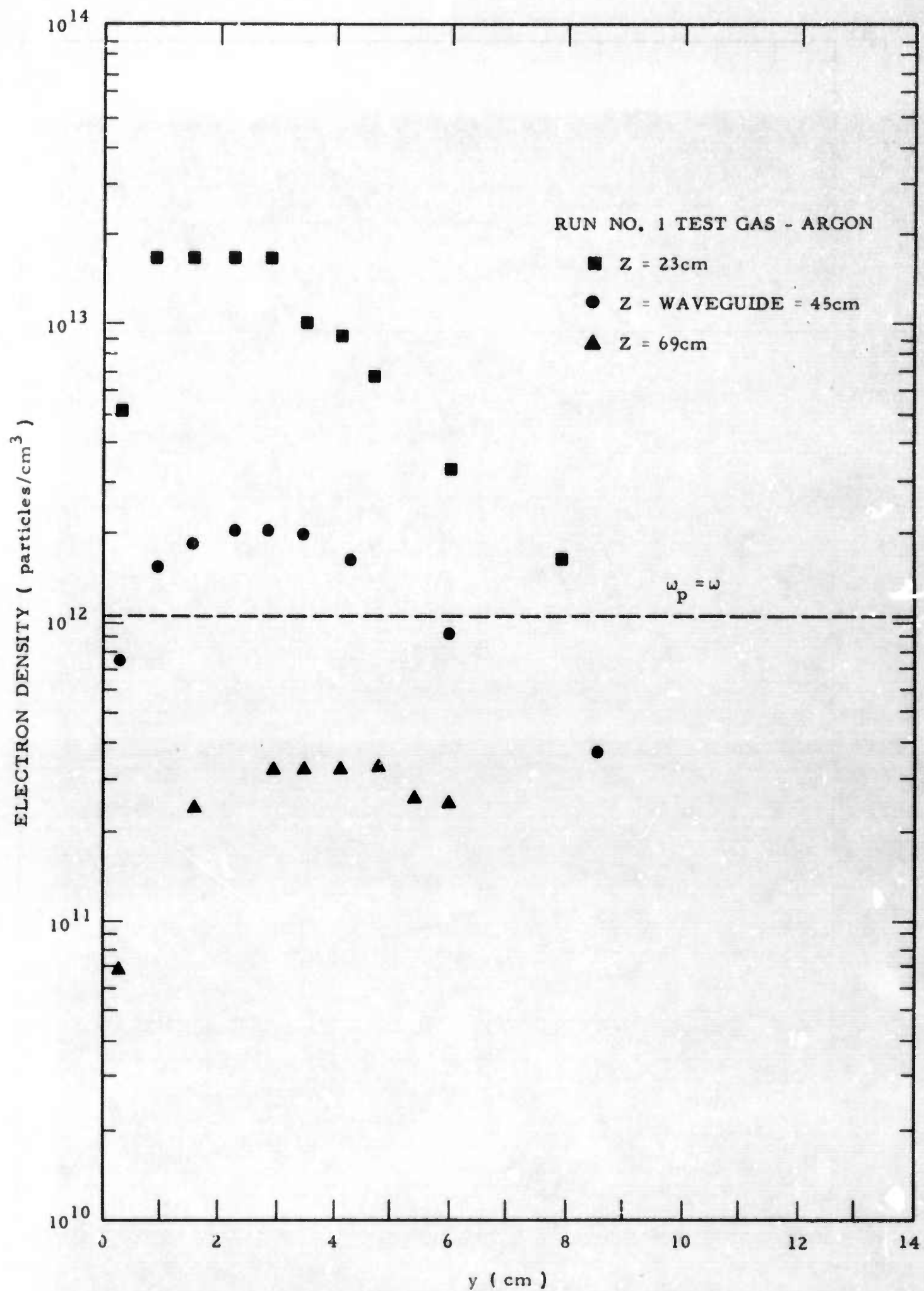


Figure 2-8. Electron Density Profiles at Various Axial Stations



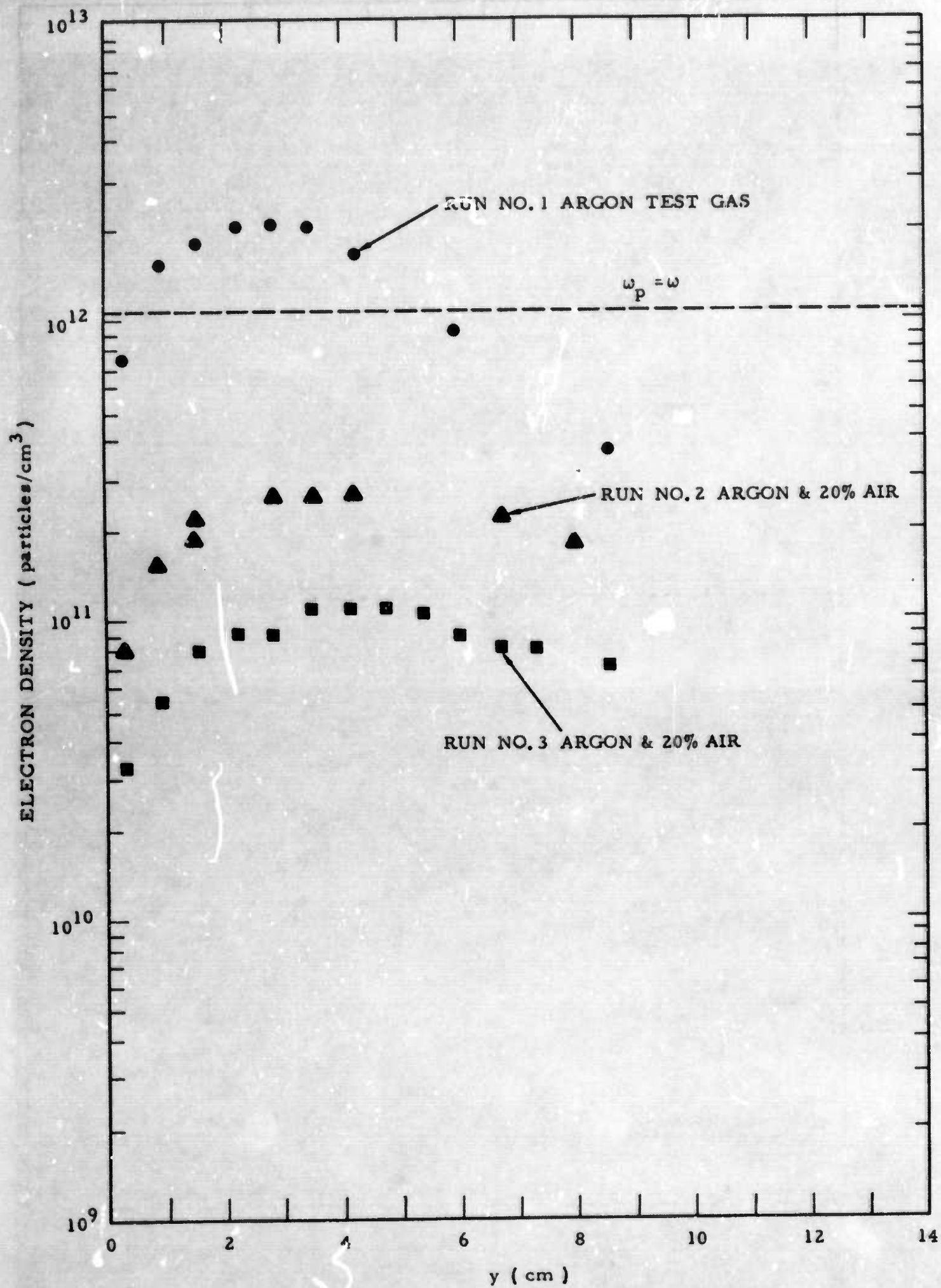


Figure 2-9. Electron Density Profiles over Microwave Slot Aperture

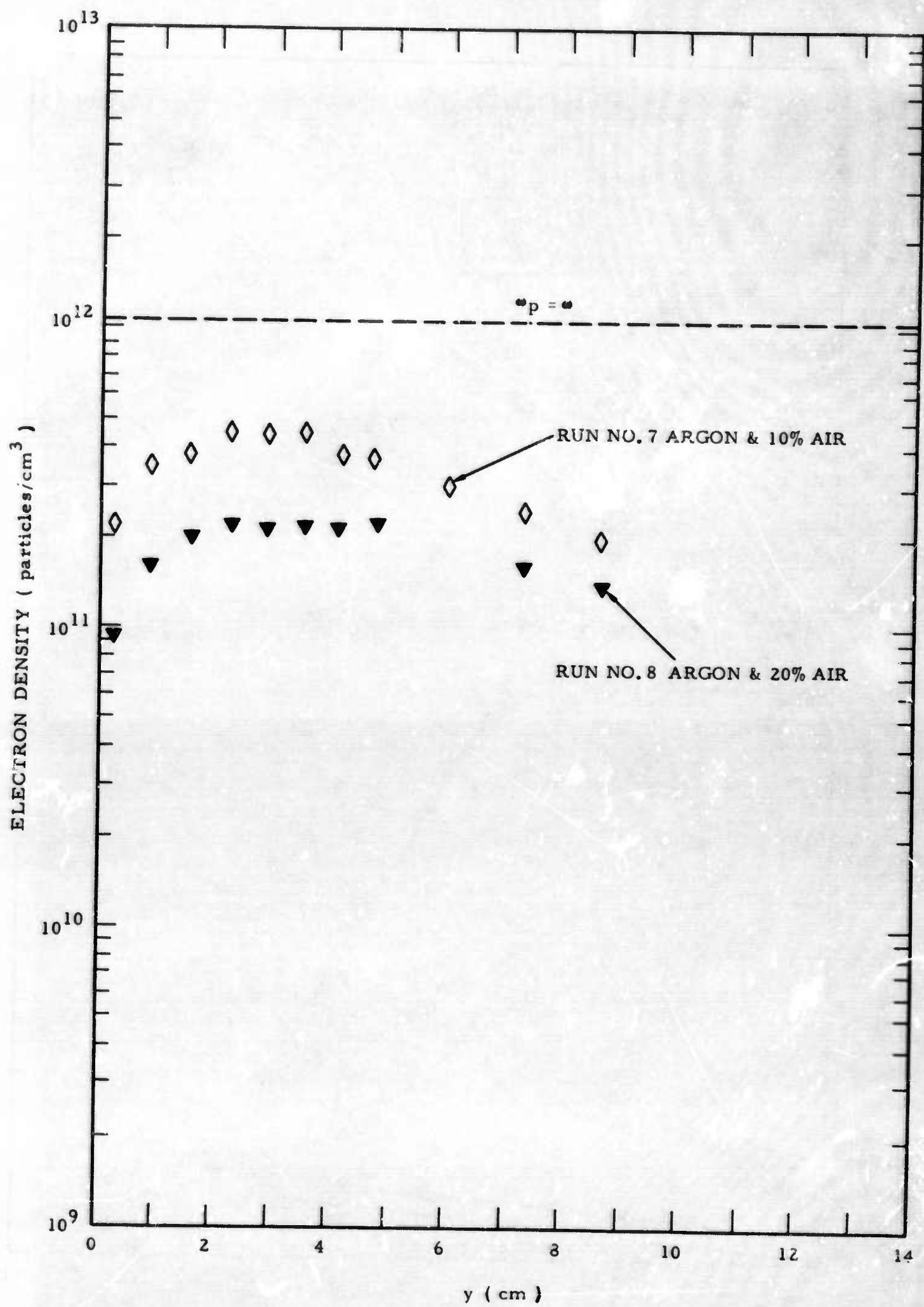


Figure 2-10. Electron Density Profiles over Microwave Slot Aperture



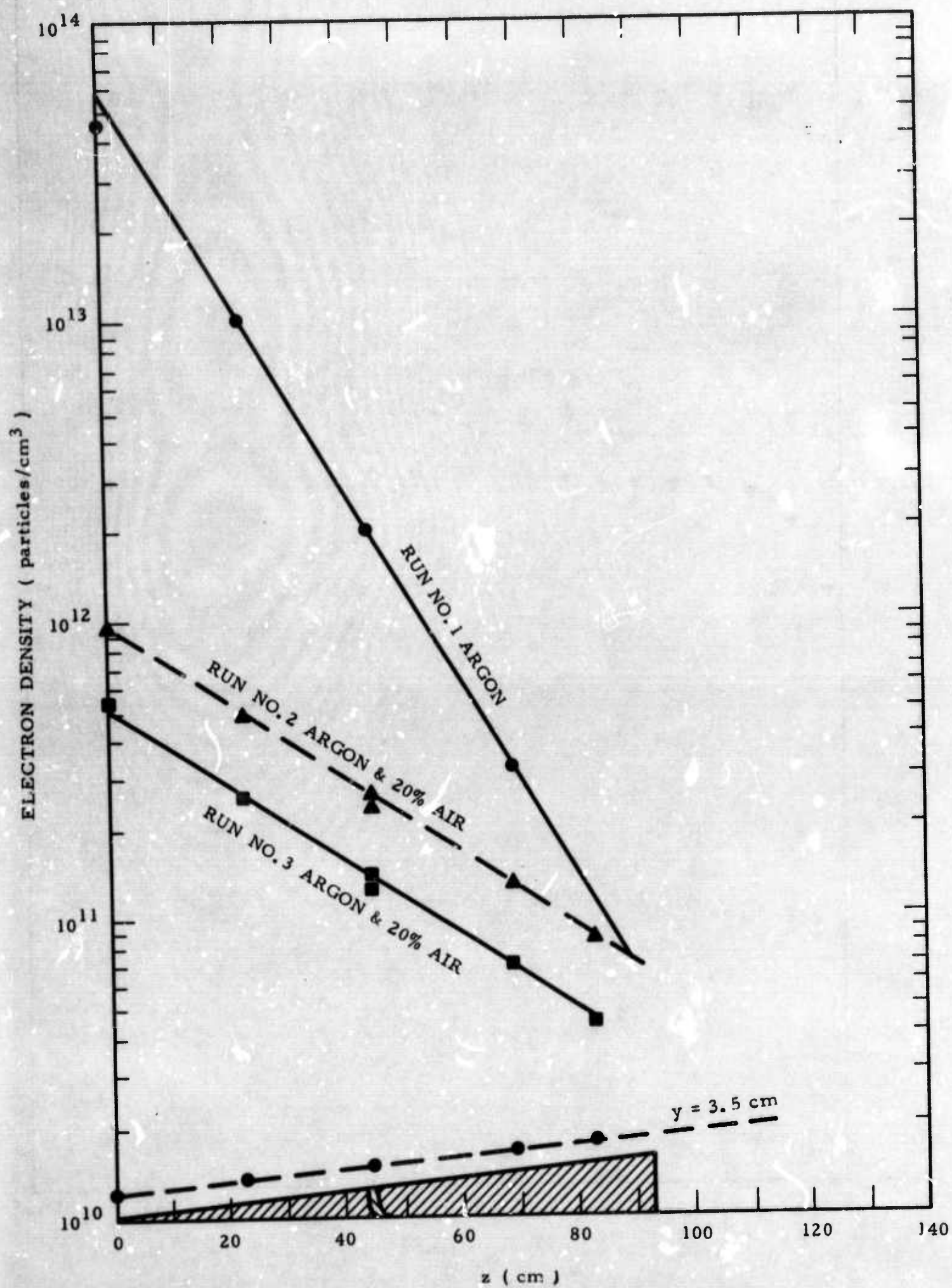


Figure 2-11. Axial Variation in Electron Density along Cone Surface



particularly vulnerable to slight departures of the electron velocity distribution from Maxwellian since the double probes, in effect, sample only a relatively small fraction of the electrons (those existing in the high energy tail of the distribution function) in making an electron temperature determination. Bradley<sup>11</sup> and Cozens<sup>12</sup> et al have considered the effects of collisions on the determination of the electron temperature from double probe characteristics and have concluded that collisional effects should offer no difficulties. Indeed, Cozens concluded that collisional effects increase the rate of energy transfer within the electron energy distribution and thus lead to a more meaningful identification of the temperature since, under these conditions, "in effect" the probe samples a greater fraction of the electron energy distribution.

Probe electrode surface contamination (such as that caused by ablation products) has been found to have a first order effect on the determination of electron temperature.<sup>13</sup> In particular, the existence of foreign material on the probe electrodes can influence the determination of the electron temperature in the following ways:

- The probe circuitry essentially measures the difference in the potential between the electron conduction bands in the two probe electrodes. Surface contamination essentially changes the electrode work function and thereby leads to erroneous voltage measurements. Since the contamination may evaporate due to surface bombardment, and since the bombardment current is dependent on the probe voltage, the contamination can result in the introduction of nonlinear phenomena which manifest themselves in the probe volt-ampere characteristic in such a way that electron temperature determinations are seriously affected.
- When an insulated layer of contamination develops over the probe surface the result is the same as adding a resistance in series with the probe circuit. Since the insulated layer may evaporate as a function of the applied voltage, difficult-to-account-for nonlinear phenomena are again introduced into the probe characteristic.

- The electron acceptance of the probe surface is sensitive to small insulator deposits. Evaporation of these deposits, with variations in the probe voltage, again introduces nonlinear phenomena which influence the apparent electron temperature.

The problems encountered in making probe measurements can perhaps best be illustrated by describing the results of a run in which a teflon overlay was attached to the cone surface and ablation was taking place. Almost immediately after the run began the double probe characteristics ceased to exhibit current saturation. At the conclusion of the run it was found, through examination with a sensitive ohmmeter, that the probe electrodes were completely electrically insulated even though no coating was visible to the naked eye.

Figure 2-12 shows a typical electron temperature profile as determined from the electrostatic probe data. The error bars of  $\pm 0.05$  ev are based only on an estimate of the ability to determine the slope of the voltage-current characteristic.

#### 2.5.4 Gas Temperature Results

The gas temperature was determined indirectly from the Mach number and stagnation temperature (see Figure 2-3). Using the measured impact and static pressures, the Mach number was calculated from the relationship<sup>14</sup>

$$p_I/p_s = \left[ 1 + \left( \frac{\gamma - 1}{2} \right) M^2 \right]^{\gamma/\gamma - 1} \quad \text{Eq. 2.2}$$

where  $p_I$  is impact pressure,  $p_s$  is static pressure and  $M$  is the Mach number. The ratio of specific heats,  $\gamma$ , was taken to be 1.667, and constant over the operating conditions of the present experiments, since over the range of argon/air mixtures used, this approximation introduces negligible error. Inasmuch as the operating pressures were sufficiently high, no corrections for viscous effects were made in the reduction of the impact and static pressure data.



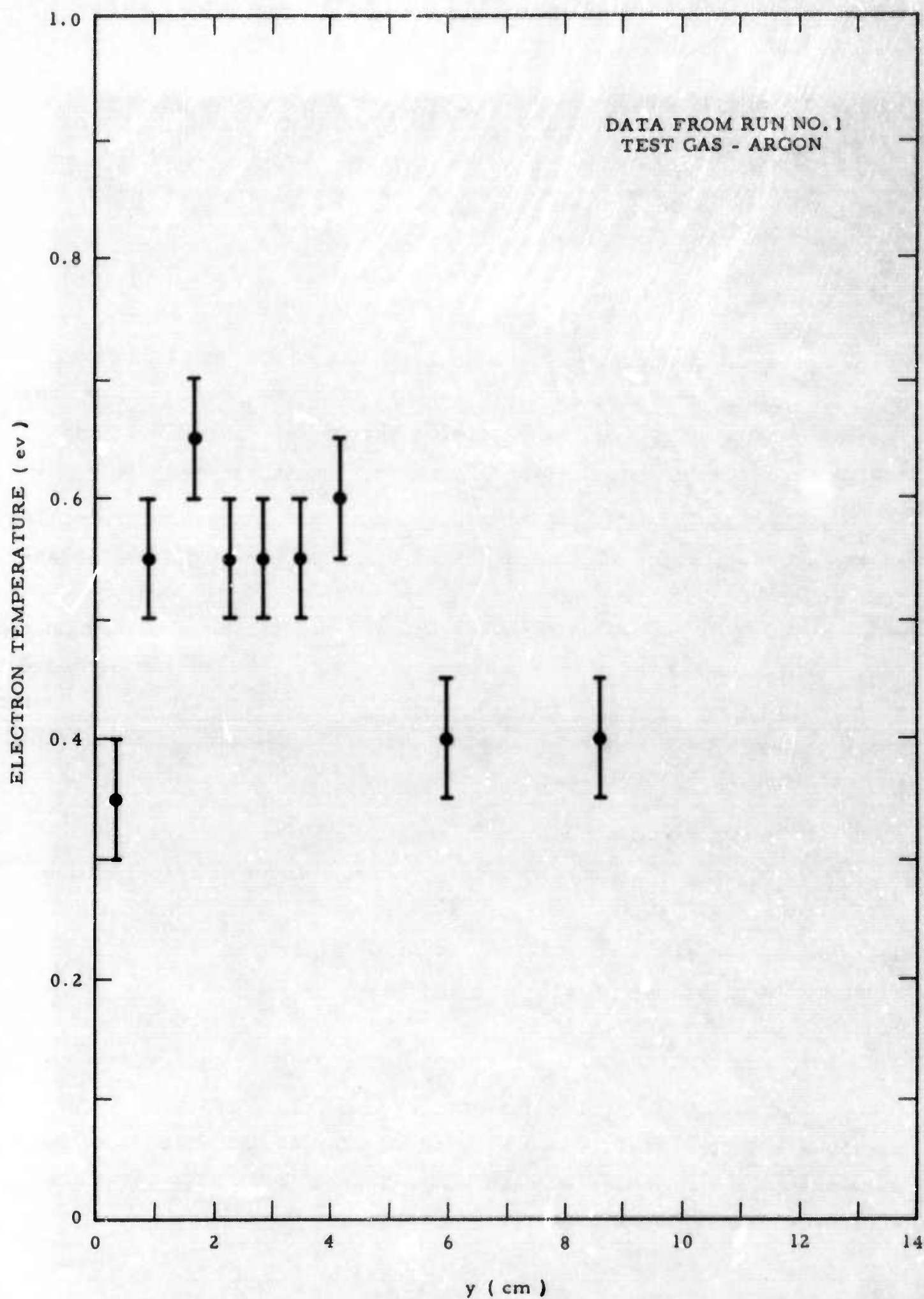


Figure 2-12. Typical Electron Temperature Profile over Microwave Slot Aperture



The calculated Mach number (always less than 1) was used in the relationship<sup>14</sup>

$$T_I/T_g = 1 + \left( \frac{\gamma - 1}{2} \right) M^2 \quad \text{Eq. 2.3}$$

where  $T_I$  is the temperature measured with the thermocouple sensor described in Section 2.3. It was assumed that the thermocouple sensing element came into equilibrium with the gas and therefore, that the temperatures measured with this probe were impact temperatures.

Figures 2-13 and 2-14 show typical gas temperature profiles in the boundary layer at various axial stations, and also the variation in the profile over the slot aperture as the test conditions were varied. It can be seen that these representative profiles do not indicate large gradients in the gas temperature. It should be noted that the temperatures indicated at  $y = 0$ , the cone surface, are measurements of the cone surface temperature with the thermocouple described in Section 2.2.

#### 2.5.5 Gas Density Results

The gas (number) density profiles over the slot aperture were calculated from the perfect gas law,  $p = N_A k T_g$ , using the measured static pressure and the gas temperature profiles of Figure 2-14. The results of these calculations are shown in Figure 2-15. The values of electron density and electron temperature are such that the electron partial pressure may be neglected.

The gas densities shown in Figure 2-15 correspond to an altitude of approximately 200 kilofeet. The gas densities for the high pressure runs enumerated in Table 2-1 correspond to altitudes of approximately 160 kilofeet.

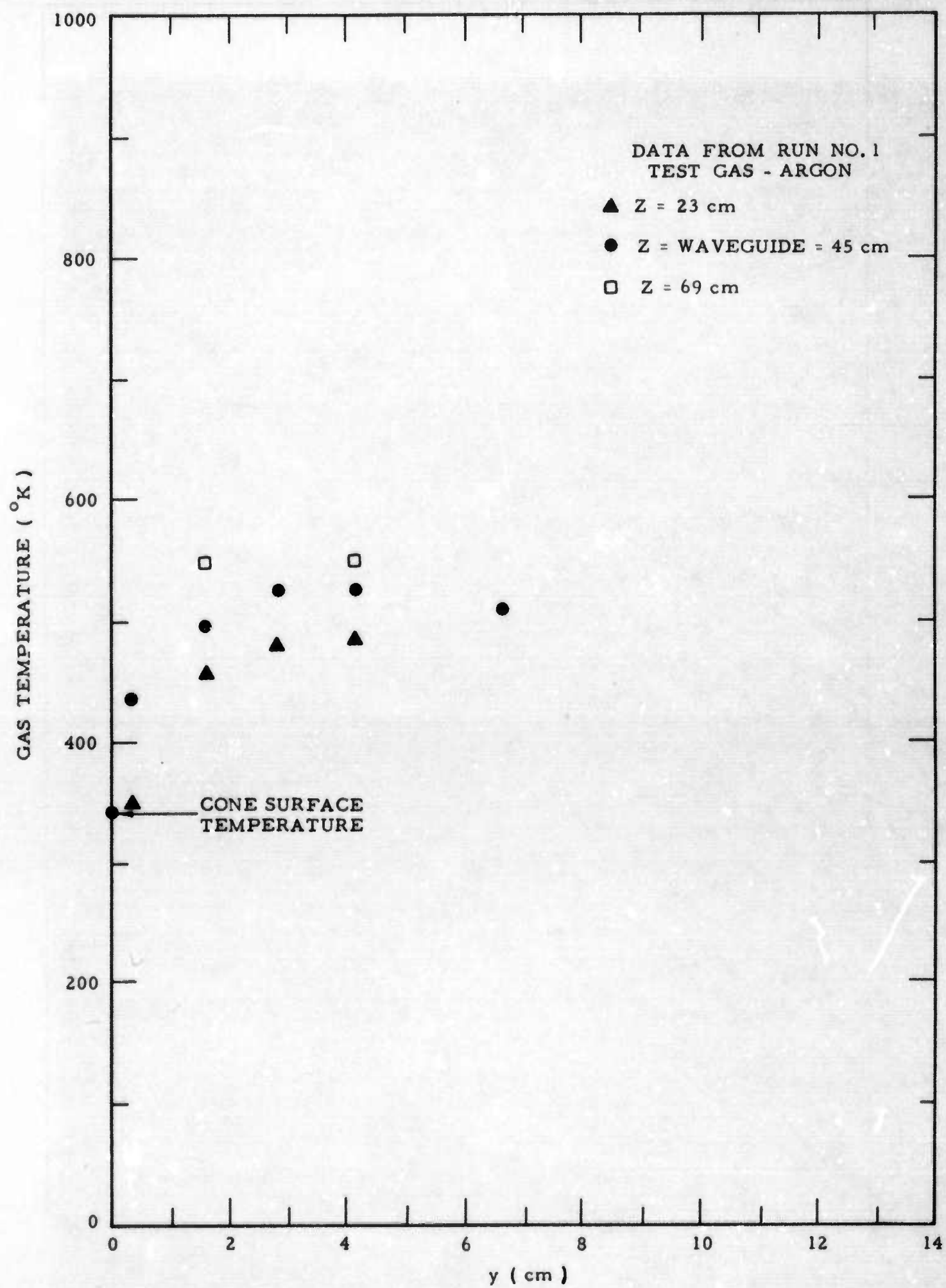


Figure 2-13. Gas Temperature Profiles at Various Axial Stations



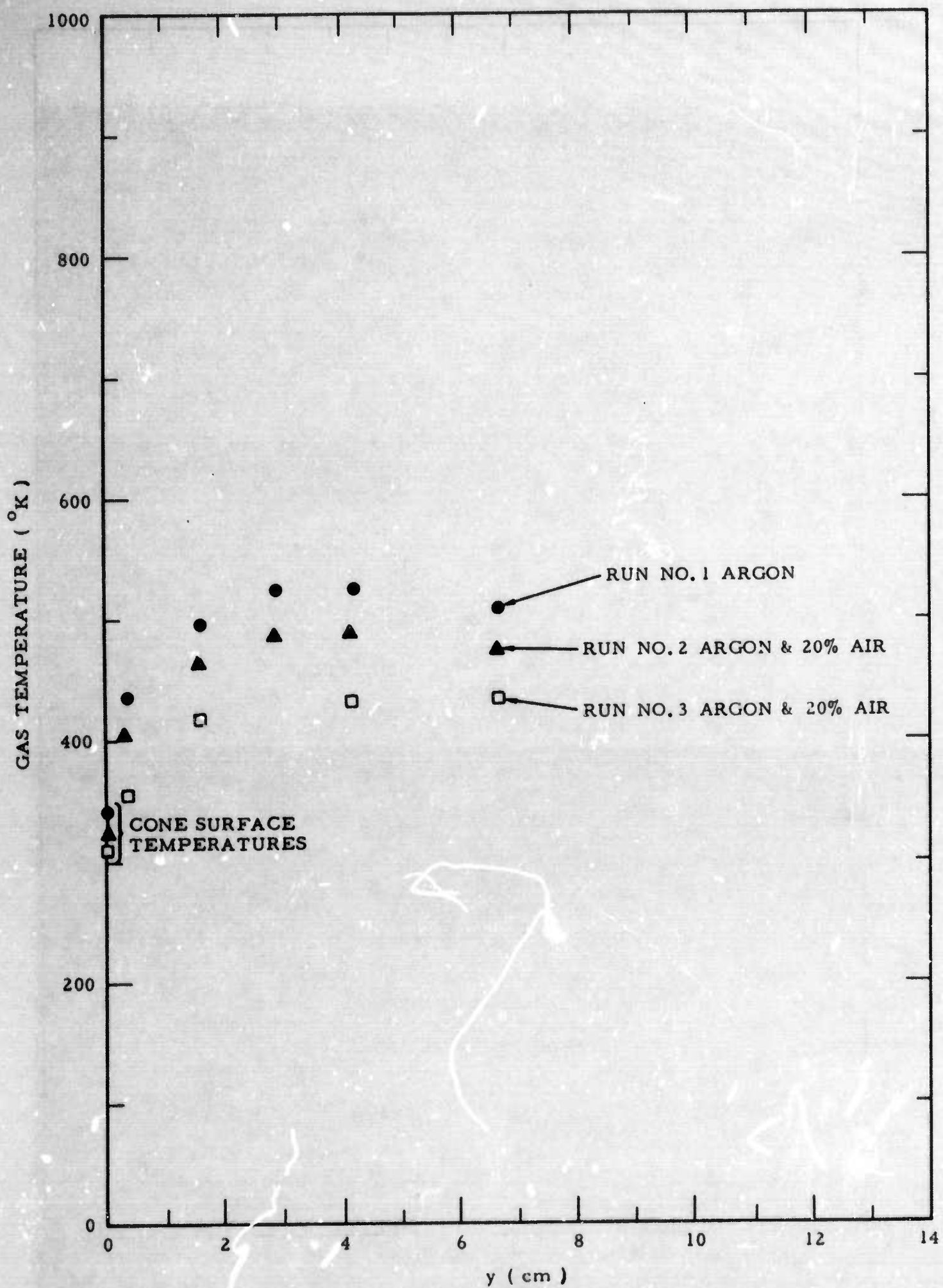


Figure 2-14. Gas Temperature Profiles over Microwave Slot Aperture



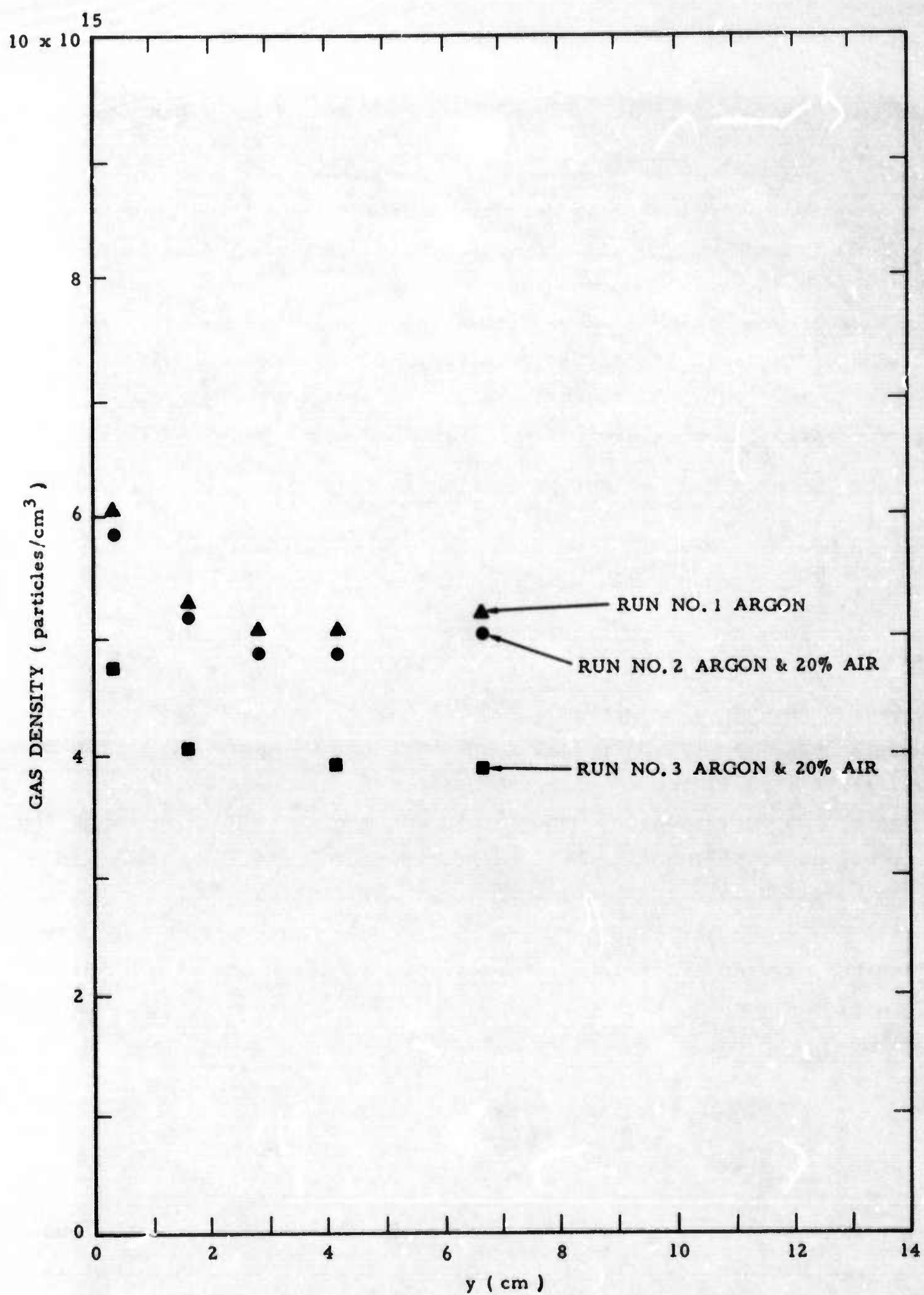


Figure 2-15. Gas Number Density Profiles over Microwave Slot Aperture

### 2.5.6 Gas Velocity Profiles

Boundary layer gas velocity profiles were calculated from the Mach number and the gas temperature profiles and the relationship  $M^2 = U^2 / \gamma R T_g$ . Figure 2-16 shows a typical velocity profile. For subsonic conditions such as those shown in Figure 2-16, where the random thermal velocity is greater than the directed bulk velocity, the influence of convective effects on electrostatic probe interpretation, and on microwave breakdown, can be neglected.

Figure 2-17 illustrates schematically the velocity profile variations in the flow over the cone.

### 2.6 ELECTRON COLLISION FREQUENCY

The electron collision frequency,  $\nu$ , like the electron density, is an important parameter in determining the breakdown and transmission characteristics of an antenna, since the parameter  $\nu/\omega$ , where  $\omega$  is the microwave frequency, is an index to the role of collisions in influencing the propagation of microwave energy. The electron collision frequency is a function of the densities of the various gas constituents, their respective total electron collision cross sections, and the electron energy distribution.

If the electrons are assumed to have a Maxwellian velocity distribution, the collision frequency for the electrons with a gas of species A, having number density,  $N_A$ , and a constant collision cross section  $Q_{eA}$ , is given by the relationship

$$\nu_{eA} = N_A Q_{eA} \left( \frac{8kT_e}{\pi m_e} \right)^{\frac{1}{2}} \quad \text{Eq. 2.4}$$

where  $k$  is the Boltzmann constant and  $m_e$  is the electron mass. Equation 2-4 provides a useful approximation for electron-neutral collisions. Spitzer<sup>15</sup> has derived a similar expression for the electron-ion

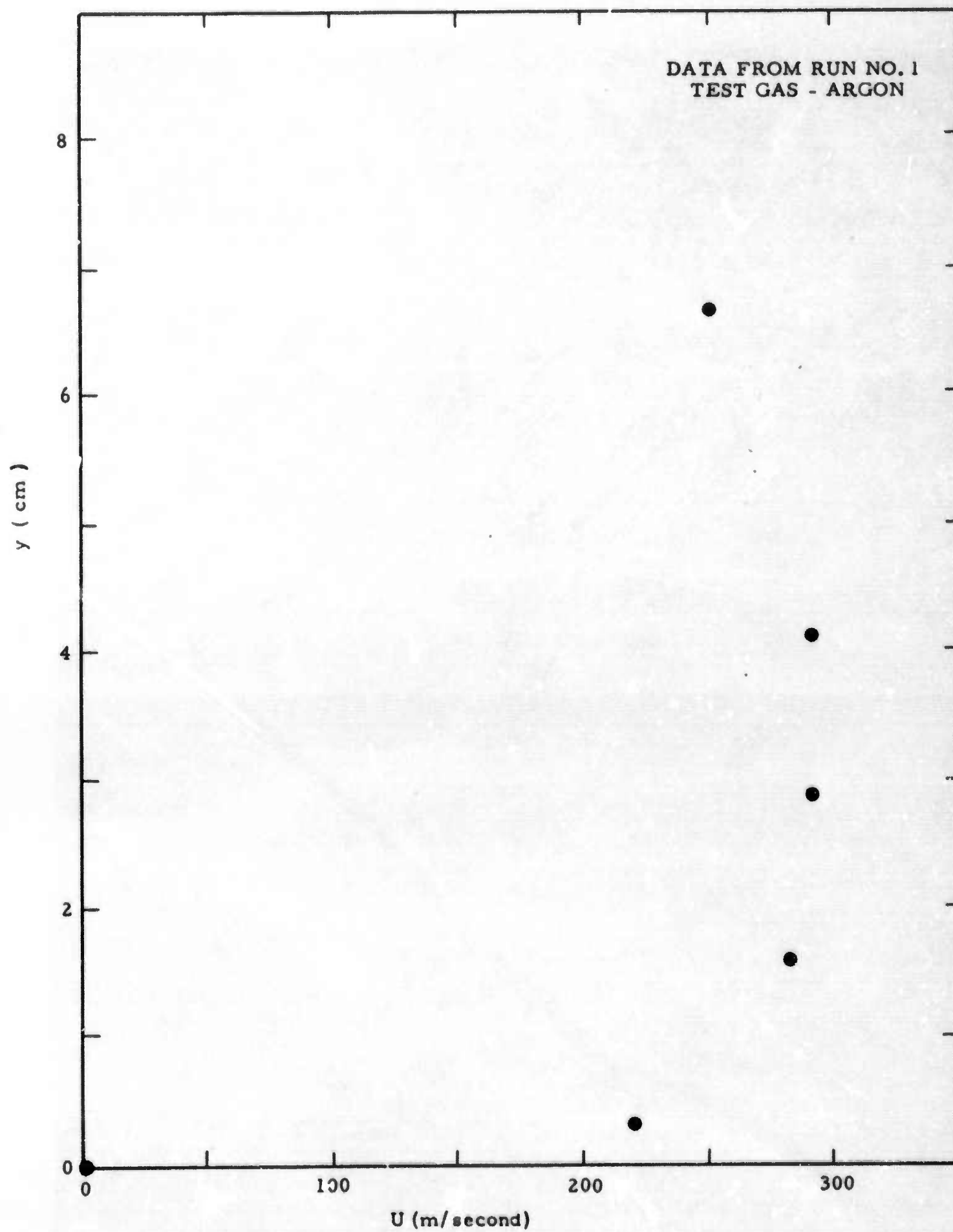


Figure 2-16. Gas Velocity Profile over Microwave Slot Aperture



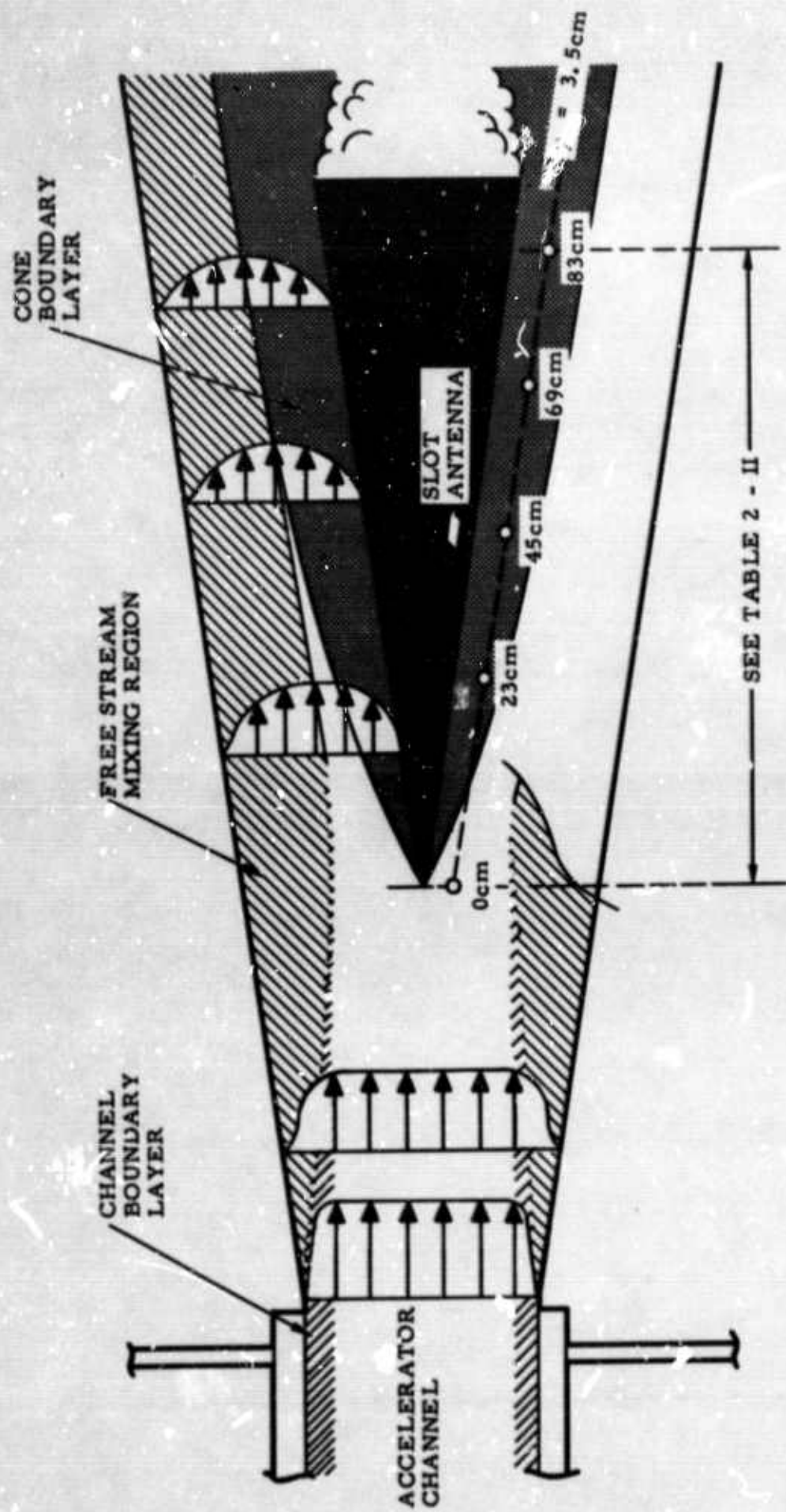


Figure 2-17. Flow Field over Microwave Test Cone

collision frequency, including the effect of the energy dependence of the Coulomb cross section. Spitzer's equation is

$$\nu_{ei} = 1.8 N_e T_e^{-3/2} \ln \Lambda \text{ sec}^{-1} \quad \text{Eq. 2.5}$$

where  $\Lambda$  is the mean value of the ratio of  $\lambda_D$ , the Debye shielding distance, to  $p_0$ , the impact parameter for  $90^\circ$  deflection scattering encounters.

Gas number density data, such as that shown in Figure 2-15, collision cross-sections obtained from Reference 16, and the electron temperatures and densities determined from the electrostatic probe measurements, were used to calculate the electron-neutral and electron-ion collision frequencies.

The results of these calculations indicate an electron neutral collision frequency of approximately  $5 \times 10^6 \text{ sec}^{-1}$ . For a microwave frequency of  $10^{10} \text{ Hz}$  (X-band) this yields a value of approximately  $10^{-4}$  for  $\nu/\omega$ . Electron-ion collision frequencies calculated using the Spitzer relationship were approximately two orders of magnitude larger than the electron-neutral collision frequency, thus yielding a value of  $\nu/\omega$  of approximately  $3 \times 10^{-3}$ . It was therefore concluded that the plasma can be treated with the usual "slightly" lossy approximation for the purposes of the microwave experiments.

## 2.7 SELECTION OF PLASMA CONDITIONS FOR MICROWAVE EXPERIMENTS

The objectives of the plasma microwave experiments are to determine the influence of the boundary layer plasma on the

- Breakdown
- Power Transfer
- Reflection Coefficient
- Pattern Distortion





for the X-Band slot antenna (see Section 3.1).

Since the major objective of the program is an investigation of antennas that are potential jammers for ECM systems, the primary interest is in the characteristics of the above phenomena in plasmas having electron densities near cut-off. For such plasmas, and for the boundary layer thicknesses encountered on slender cone ECM vehicles, collisional attenuation and other gas density effects are of secondary importance compared with the electron density. Thus,  $\frac{\omega_p}{\omega}$  is the primary parameter to be controlled over the slot antenna. Accordingly, the test conditions shown in Table 2-III were selected, from the eleven runs summarized in Table 2-I, for use in the microwave plasma experiments. These test conditions will be referred to as A,B,C,D and E for subsequent reference in this report.



TABLE 2-III  
EXPERIMENTAL CONDITIONS SELECTED FOR MICROWAVE ANTENNA TESTS

Run Identi- fication	Peak Electron Density ( $\text{cm}^{-3}$ )	Electron Density Profile	$\omega p/\omega$ 	Gas Density ( $\text{cm}^{-3}$ )	Temp. ( $^{\circ}\text{K}$ ) 	Ion Saturation Current(Nose Electrostatic Probe)( $\mu\text{amp}$ )
A	$2.0 \times 10^{12}$	Figure 2-9	1.4	$4.9 \times 10^{15}$	525	$1.4 \times 10^4$
B	$6.6 \times 10^{11}$	—	.79	$\sim 10^{16} *$	$\sim 500$	$1.0 \times 10^2$
C	$4.5 \times 10^{11}$	Figure 2-1C	.66	$4.7 \times 10^{15}$	514	$1.7 \times 10^3$
D	$2.6 \times 10^{11}$	Figure 2-9	.496	$5.0 \times 10^{15}$	485	$3.5 \times 10^2$
E	$1.1 \times 10^{11}$	Figure 2-9	.322	$3.9 \times 10^{15}$	435	$1.0 \times 10^2$

 1

Based on peak  $N_e$

 2

Peak gas temperature in B.L.

\*

Estimated from static and impact pressure sensors on cone.

**BLANK PAGE**

### 3. MICROWAVE SLOT ANTENNA TESTING

#### 3.1 INTRODUCTION

The objective of the microwave facet of the antenna test program was to determine the breakdown and transmission characteristics of a typical dielectric-filled slot antenna under ambient (cold air) and simulated re-entry conditions. Of particular interest were the:

- Power-handling capabilities
- Pattern of the radiated fields
- Input impedance

The geometry of a slot antenna located in a conducting plane which is covered by plasmas with various electron density distributions has received extensive attention in the literature. For the purposes of this program it was considered important that the antennas be compatible with the geometry of a conical re-entry vehicle. Therefore, the specific geometry chosen for study was a teflon-filled X-band slot aperture with the surface of the model acting as a conducting plane.

In considering the test objectives cited above, the following should be considered:

- The power handling capability of the slot antenna is dependent upon the magnitude of the peak electron density, and its spatial variation in the boundary layer, only insofar as these parameters determine (1) what absolute electron density increase is required to drive the ambient plasma to the critical electron density where  $\omega_p = \omega$ , and (2) whether the principal diffusion loss is free or ambipolar.



- The antenna input impedance and radiation pattern are a great deal more sensitive to the magnitude of the peak electron density, as well as to its spatial variation in the boundary layer.

In citing the above considerations, collisional effects were assumed to be of secondary importance for the electron densities and boundary layer thicknesses encountered on slender cone ECM vehicles.

The increased sensitivity of the input impedance and the far-field radiation pattern to the particular features of the electron density profile over the slot aperture, and the fact that observable effects are expected only when  $\omega_p / \omega > 0.1$ , provided the basis for the selection of the plasma test conditions discussed in Section 2.7.

The microwave tests consisted essentially of incorporating a teflon-filled X-band slot into the metal cone surface and performing initiate and extinguish breakdown power tests with both cold gas and plasma environments over the antenna. The tests were performed in a vacuum chamber lined with appropriate anechoic material (see Section 3.3.3.1). Incident and reflected power were measured during the tests and were used to calculate the power reflection coefficient and the voltage standing wave ratio (VSWR). Measurements of the far-field pattern of the slot antenna were made in an outdoor range, an indoor anechoic chamber, and in the anechoic lined vacuum chamber.

Considerable care must be exercised in making such measurements, both because of the errors that can arise from the losses in the long length of waveguide that connects the power source and the slot antenna, and because of the interference caused by reflection of electromagnetic energy from surrounding objects in the vacuum chamber. Therefore, the measurement techniques that were used in the microwave experiments are described in detail in Section 3.2, and a series of auxiliary experiments, that were conducted to verify the performance of the instrumentation and the slot antenna, are described in Section 3.3.

The X-band cold gas breakdown tests are described in Section 3.4 and the plasma experiments are described in Section 3.5.

A few experiments were conducted using a teflon overlay to simulate an ablating heat shield material. It was recognized at the outset of the present program that the ablation experiments would be quite qualitative in nature because of the characteristics of the plasma stream and the difficulty in documenting the nature and density of the ablating species. These tests were undertaken, however, to gain a better understanding of the problems associated with properly including and evaluating the effects of ablation in future programs. These experiments are described in Section 3.5.4.

### 3.2 MICROWAVE ELECTRICAL INSTRUMENTATION

#### 3.2.1 Power Source

The power source for the microwave experiments was a Raytheon QKH/366 pulsed magnetron with a frequency of 9.225 kMc and a peak power output of 75 Kw. The magnetron was driven at a 1000 cycle repetition rate with a pulse width of 1.0 microseconds. A power divider, (assembled from short-slot hybrids and existing 300 peak Kw loads), was used to vary the power fed to the slot antenna. This capability to accurately control the power was required in order to determine the "initiate" breakdown and "extinguish" breakdown power levels of the slot antenna. An isolator was inserted in the line between the magnetron output and the power divider to avoid magnetron damage due to reflected power.

#### 3.2.2 Power Measurement Circuit

The "initiate" and "extinguish" powers for the X-band slot antenna were determined with a power meter that was coupled to the main line through a calibrated directional coupler and attenuator. The peak power was determined from the average power indicated by the power meter by taking account of the pulse width and the pulse repetition rate. The experimental arrangement is illustrated



schematically in Figure 3-1.

### 3.2.3 Input Impedance Measurement Circuit

The antenna input impedance was measured using a reflectometer bridge<sup>17</sup> which was incorporated into the circuit as indicated in Figure 3-1. The reflectometer bridge was used to determine the phase and amplitude of the reflection coefficient. The bridge arrangement is shown in Figure 3-2.

The incident and reflected power systems shown in Figure 3-1 can also be used to determine the magnitude of the reflection coefficient.

The sensor for the power transmitted by the slot antenna was a DBG-520 horn mounted on a traversing mechanism as shown in Figure 3-3. The traversing mechanism, which must withstand relatively high temperatures, was constructed of non-metallic materials, such as glass-loaded teflon and phenolics, to minimize the perturbation to the radiation field. The metallic drive motors and chains and sprockets were located at the top of the vacuum chamber behind the anechoic material, as indicated in Figures 3.3 and 3.4.

The receiving horn was located in the far field of the slot antenna. The detector was a thermistor attached to the horn and protected from low pressure effects<sup>2</sup> by a vacuum seal. The received power was read directly on a Hewlett-Packard 430C power meter.

E-plane radiation pattern measurements were made by traversing the receiving horn axially along a beam located above, and parallel to, the test model. The receiving horn was manipulated so as to point always toward the slot antenna. This orientation was accomplished through the use of a tilting capability that was built into the traversing mechanism.

Measurements of the H-plane radiation patterns were made by rotating the cone and slot antenna about the cone axis with the





D : CRYSTAL DETECTOR  
 DC : H. P. x 752D DIRECTIONAL COUPLER  
 O : OSCILLOSCOPE  
 PA : H. P. x 382A PRECISION ATTENUATOR  
 PS : H. P. x 885A PHASE SHIFTER  
 T : TERMINATION  
 MT : MAGIC TEE

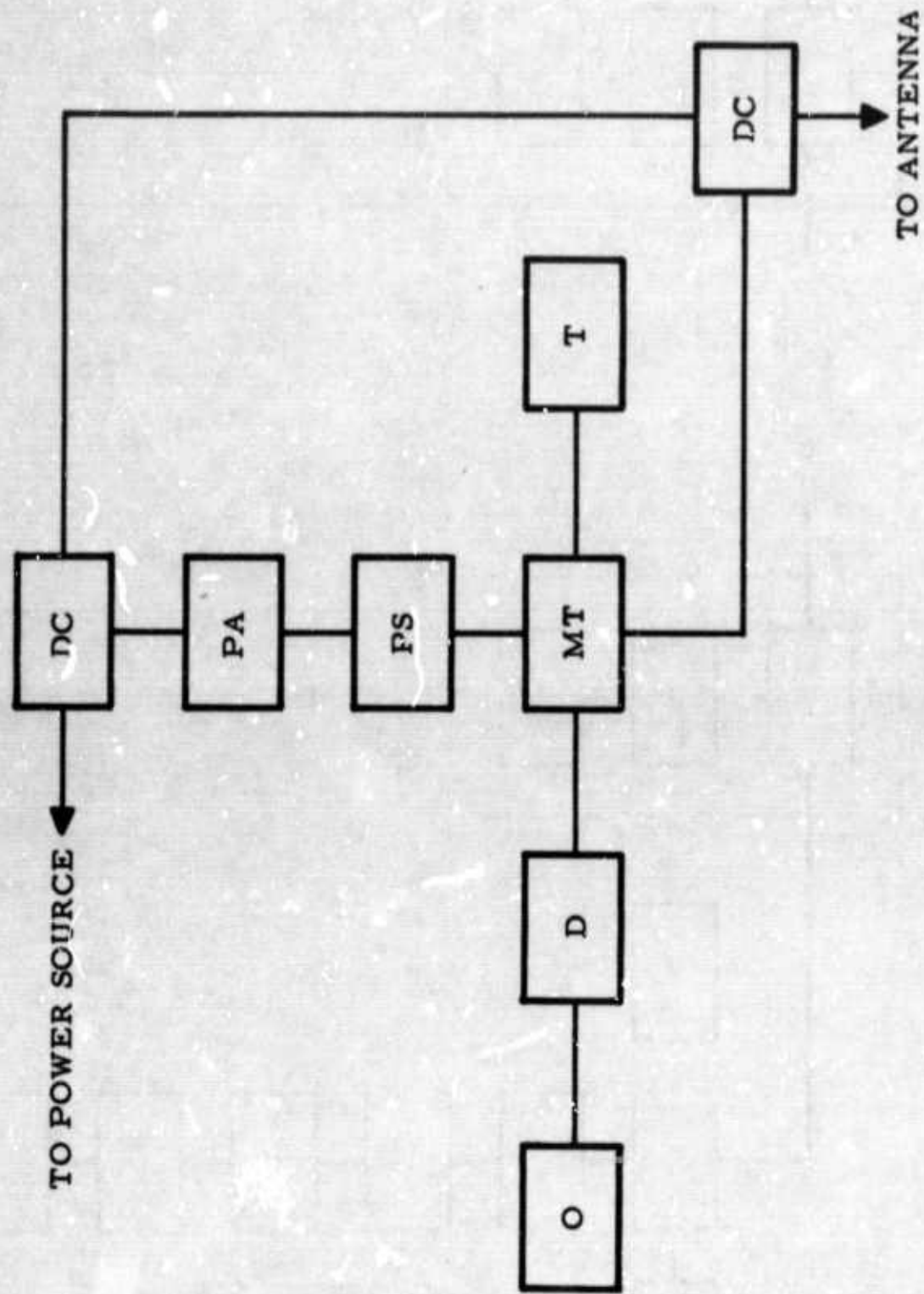


Figure 3-2. Schematic of Reflectometer Bridge Arrangement

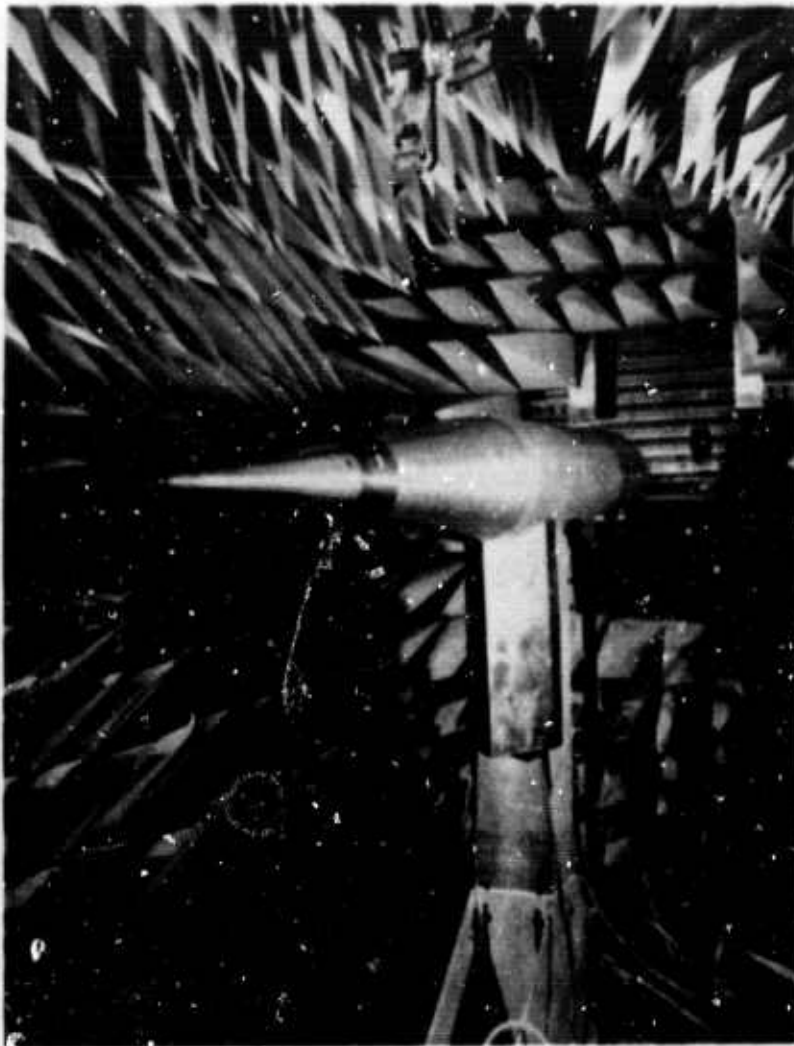


Figure 3-3. Experimental Arrangement of Test Cone in Vacuum Chamber



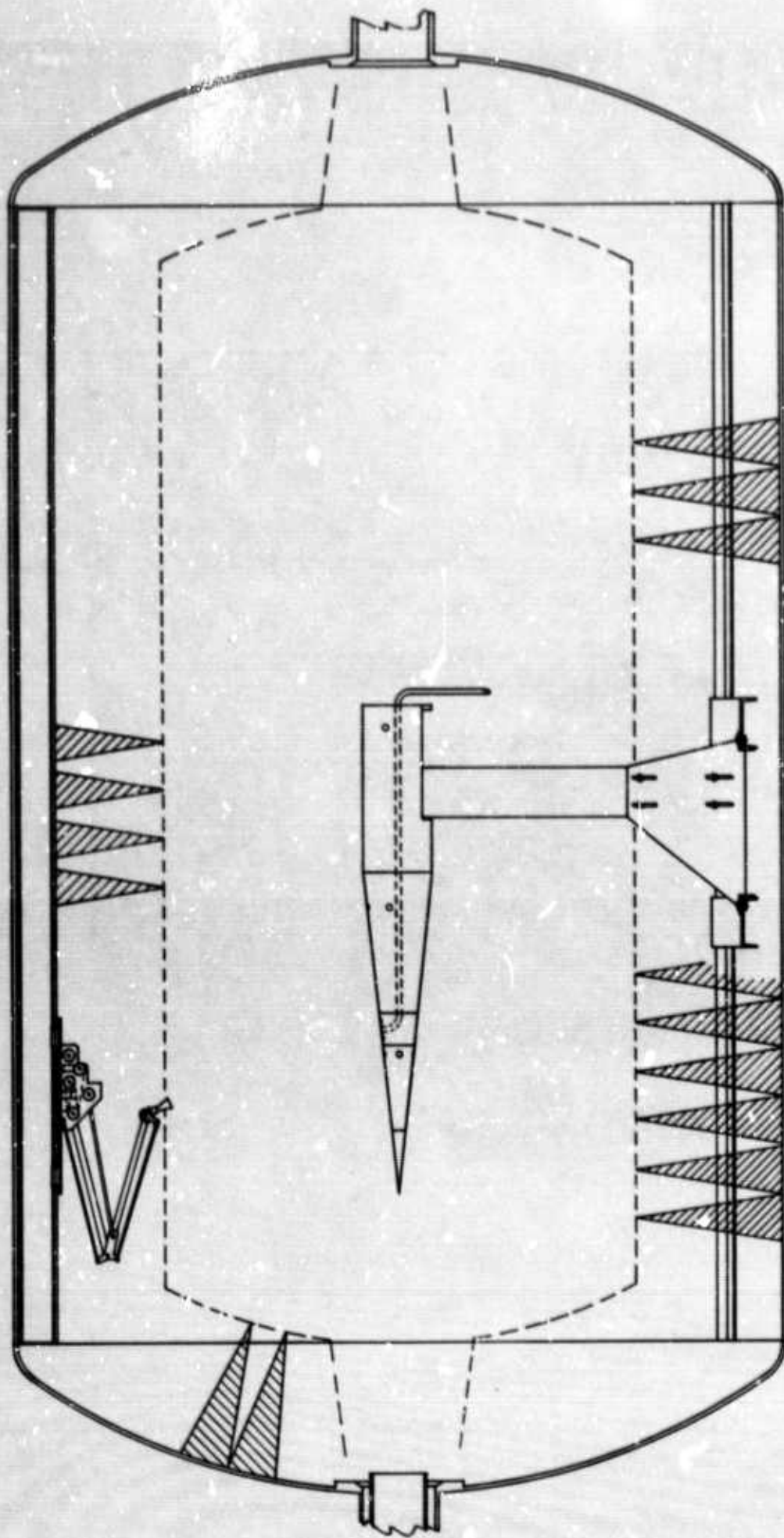


Figure 3-4. Test Chamber and Model Layout

receiving horn located at a particular axial station. Although measurements were taken at a number of axial stations, the majority of measurements were taken in the principal H-plane.

### 3.3 PRELIMINARY EXPERIMENTS

#### 3.3.1 Introduction

Auxiliary tests were conducted prior to the microwave breakdown experiments in order to calibrate and verify the performance of the microwave electrical instrumentation and to evaluate the antenna pattern measurement techniques.

Auxiliary electrical instrumentation tests included:

- Evaluation of the losses in the long length of waveguide between the magnetron and the slot antenna.
- Calibration of directional couplers and other microwave instrumentation.
- Determination of a phase reference for the antenna input impedance measurements.

Auxiliary antenna performance measurements were made to delineate potential problem areas and to verify that the antenna pattern data acquisition techniques were sufficiently accurate. The tests included:

- Evaluation and selection of an anechoic material.
- Measurements of the slot antenna radiation pattern under a variety of environmental conditions.

#### 3.3.2 Auxiliary Electrical Instrumentation Tests

The microwave instrumentation, such as directional couplers, was calibrated using well established methods.<sup>18,19</sup> Therefore no description of these calibrations is included here.

The power source was connected to the slot antenna, located on the cone surface, by approximately 30 feet of RG-52/U waveguide. Because the incident power is measured at the magnetron

rather than at the slot, the losses in the waveguide system (waveguide lengths and various connecting bends) must be taken into account in interpreting the "initiate" and "extinguish" breakdown data.

The waveguide losses were determined by using a directional coupler and average power meter to compare the incident power measured at the magnetron with that measured just ahead of the slot. The waveguide was terminated with a high power load for this experiment. The power measured at the slot was found to be 0.6 of the power measured at the magnetron. This corresponded to an attenuation of 2.2 db, and agrees quite well with the predicted value based on the waveguide length, material, and operating frequency.

The measurement of the antenna input impedance was based on a measurement of the phase and amplitude of the reflection coefficient. Therefore a series of tests, using aluminum foil tightly covering the slot aperture, was made to calibrate the reflectometer bridge. The specific purposes of these experiments were to:

- Simulate a reflection coefficient of unity magnitude.
- Determine a phase reference for the bridge.
- Define the sense of phase angle rotation.

For a reflectometer bridge such as the one shown in Figure 3-2, the response can best be related to the processes occurring at the slot aperture-plasma boundary by experimental methods.

The reflection coefficient was determined, for the condition where the slot was tightly covered with aluminum foil, by measuring the incident and reflected power using the arrangement shown in Figure 3-1. It will be recalled that the reflection coefficient must be corrected for the attenuation of both the incident power and the reflected signal due to the long length of waveguide. When this correction was included, the voltage reflection coefficient was 0.92.



With the aluminum foil tightly covering the slot, the variable phase shifter in the reflectometer bridge (shown in Figure 3-2) was adjusted for a minimum output as indicated by the crystal detector on the oscilloscope readout. In order to present the phase angle in the usual polar representation, wherein the rotation can either be toward the load (the slot antenna), or toward the generator (the magnetron), the aluminum foil was moved away from the slot and the bridge output was readjusted for a minimum. The sense of the readjustment was noted and this was used as the convention for rotation of the reflection coefficient toward the load.

The measurement of the phase angle of the reflection coefficient of an antenna, separated from the measurement apparatus by a long length of waveguide, is particularly vulnerable to errors. Of particular importance is the change in the physical, and therefore the electrical, length of the waveguide due to thermal expansion. For example, a  $10^{\circ}\text{C}$  temperature change will cause a length of X-band waveguide approximately 30 feet long to introduce a phase shift of approximately  $25^{\circ}$ . This temperature change is typical of that encountered in the laboratory, particularly when the phase reference is chosen under cool ambient conditions and the antenna measurements are conducted under relatively high temperature plasma conditions.

### 3.3.3 Antenna Far-Field Pattern Considerations

#### 3.3.3.1 Anechoic Material Evaluation

When making radiation pattern measurements in a vacuum chamber the walls of the vacuum chamber must be lined with anechoic materials to avoid the interference caused by wall reflections of electromagnetic energy.

Selection of an anechoic material was made after evaluation of the products of three manufacturers. The evaluation consisted of determining the compatibility of the materials with the chamber heating produced by the plasma beam. On the basis of these tests, Emerson

Cuming HPY-18 and HPY-24 were selected for their self-extinguishing characteristics in the event of deposition of hot ablation products or arcing due to electrical malfunctions. The main disadvantage of the material is the large surface area which can absorb atmospheric water vapor and result in longer pump-down times for the vacuum chamber. The placement of the anechoic material around the chamber is indicated in Figures 3.3 and 3.4.

During the evaluation process, only five to ten units of the anechoic material were tested at a time. However, when the interior of the vacuum chamber was completely lined with the anechoic material, the outgassing of the absorbed water vapor increased the time required to reach the system base pressure ( $\sim 0.002$  Torr) by approximately 24 hours. This is undesirable for expeditious antenna testing, particularly when adjustments to the system, that require entry into the vacuum chamber, are necessary. Therefore, it is recommended that future testing programs incorporate closed cell polyurethane foam anechoic materials, or the recently developed high temperature ferrite loaded materials such as Emerson & Cuming NZ-1.

#### 3.3.3.2 Preliminary Antenna Pattern Measurements

Preliminary antenna pattern measurements were made with a variety of configurations to verify that the data acquisition techniques were sufficiently accurate, and that reliable measurements could be made in the anechoic-material lined vacuum chamber where reflections from the metal chamber walls might be expected to be greatest.

The majority of these measurements have been previously reported<sup>2,3</sup> and will therefore be only summarized here. Basically the measurements consisted of:

- a. Measurements of the E and H-plane patterns of an open ended slot antenna in an outdoor range.<sup>2</sup>

- b. Measurements of the E and H-plane patterns of a cone-mounted teflon filled slot antenna in an outdoor range.<sup>2</sup>
- c. Measurements of the E and H-plane patterns of a cone-mounted teflon filled slot in an indoor anechoic chamber having the same configuration as the vacuum chamber used in the testing program.<sup>3</sup> (The influence of fixed metal objects located within the test chamber were ascertained in these tests).
- d. Measurements of the E and H-plane patterns of a cone-mounted teflon filled slot antenna in the anechoic lined vacuum chamber.

Measurements a-c (described previously)<sup>2,3</sup> indicated that the anechoic material would be quite effective in eliminating reflections of electromagnetic energy from the metal test chamber walls. Measurements listed in item d. were performed subsequent to the other tests and verified that reflections from the test chamber walls would not complicate data acquisition and interpretation, and that antenna pattern measurements in the vacuum chamber could be made with confidence.

### 3.4 COLD GAS BREAKDOWN EXPERIMENTS

#### 3.4.1 Introduction

One of the primary objectives of the microwave antenna test program was to determine the cold air breakdown characteristics of the X-band slot antenna. Therefore a series of measurements was made of the breakdown characteristics (i.e., the initiate and extinguish power as a function of the ambient pressure) of the X-band slot antenna. The tests were conducted at 9.225 kMc using the experimental arrangement described in Figure 3-1. The tests were conducted in the anechoic-lined vacuum chamber using air, argon and argon/20% (by weight) air mixtures. A slight gas flow was maintained during the tests, (i.e., after the chamber had been flushed several times with the desired test gas the pumping system was used to adjust the desired ambient pressure). Breakdown was defined by the simultaneous appearance of luminosity



and an abrupt change in reflected power.

#### 3.4.2 Initiate and Extinguish Breakdown Power Levels

The experimental results of the cold air breakdown studies are shown in Figure 3-5. It should be noted that the pressure scale is really a density scale based on an ambient temperature of  $300^{\circ}\text{K}$ . The density range covered represents an equivalent altitude change of from approximately 70 to 200 kilofeet. Also shown, for comparison, are the experimental results of Scharfman.<sup>20</sup> His tests incorporated a polonium source to ensure repeatable measurements.

Ordinarily, in a pulse experiment, the difference between the initiating and extinguish power level is an indication of the residue of electrons left from the previous breakdown pulse. If the conditions are such that the electron density remaining from the previous breakdown pulse is negligible, then there will be a negligible difference between the initiating and extinguish levels.

As noted previously, the experiments in the present program did not include the use of a radioactive source to supply initial electrons. However, the loss of residual charges is by free diffusion and it is well known that such charges can persist for an extended period of time after a plasma discharge has occurred in a vessel of significant size. Similar observations were made in the present experiments. In particular, when comparing experimental data obtained at a common ambient pressure, it was observed that the power required for breakdown was frequently increased by a factor of two, if the time lapse between successive breakdowns was increased from several minutes to several days.

Because of the rapid rise time of the microwave pulse, the response of the plasma can be thought of as lagging behind the stimulus of the electric field. Thus, it would be expected that the observed initiate breakdown power levels represent a maximum, and that the actual breakdown power (defined as the onset of nonlinear effects)

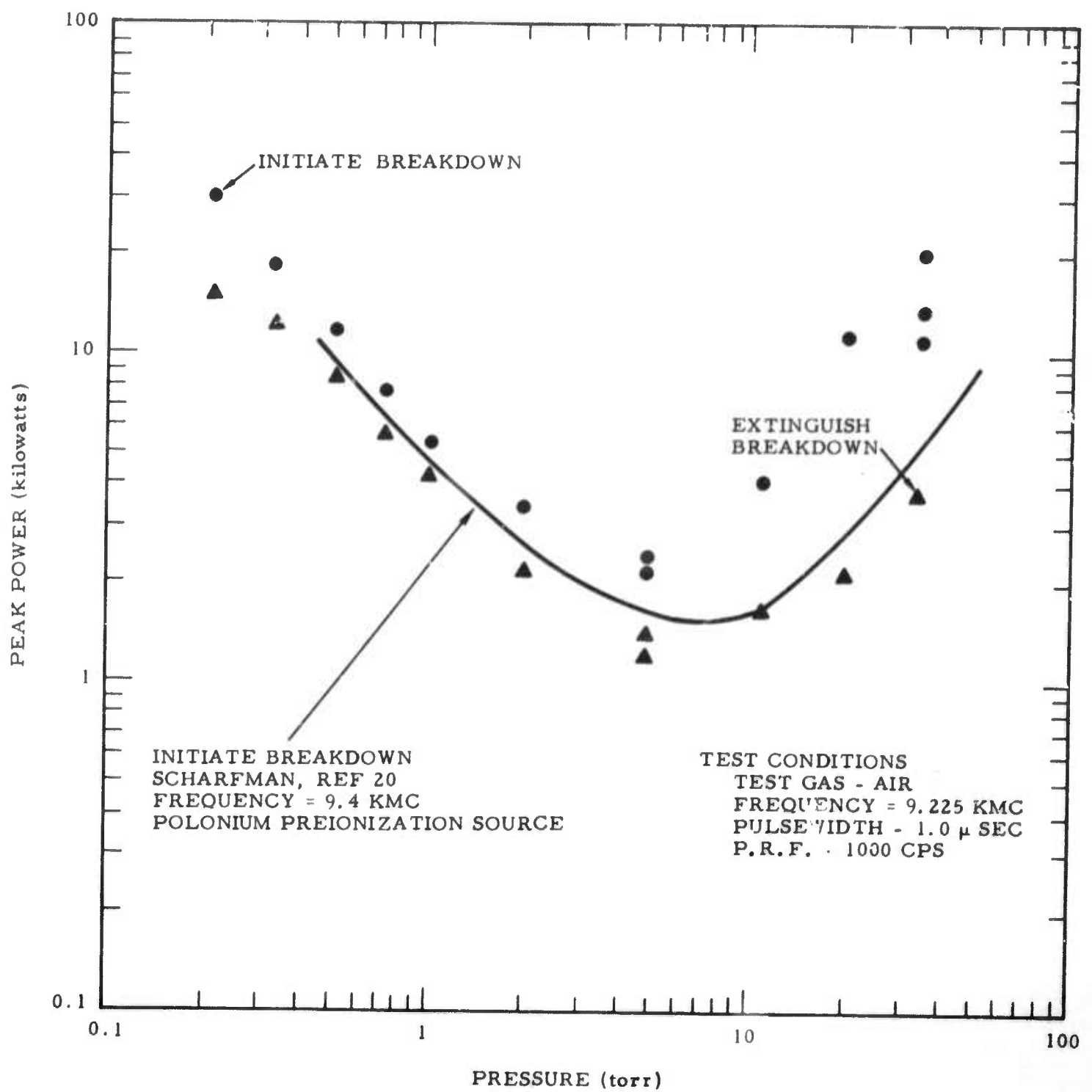


Figure 3-5. Results of Cold Air Breakdown Studies

may be lower in value. Conversely, the measured extinguish power levels represent minima and the actual values will tend to be greater.

Figure 3-6 shows the initiate and extinguish breakdown power levels for pure argon gas, and Figure 3-7 compares the initiate breakdown power levels for the three gas mixtures used in the present program. It will be noted that while air requires higher initiate breakdown power levels than argon, the addition of 20% air to argon gas does not significantly alter the breakdown characteristics.

#### 3.4.3 Reflected Power Measurements

The slot antenna power reflection coefficient was measured before, and during, the plasma breakdown using the experimental arrangements shown in Figures 3-1 and 3-2.

Figure 3-8 shows the cold air voltage reflection coefficient amplitude as a function of the ambient pressure in the vacuum chamber. Note that several of the data points are numbered sequentially for future reference in Figure 3-9. Figure 3-9 shows the phase and amplitude of the voltage reflection coefficient for the selected points denoted in Figure 3-8. The scatter in the reflection coefficient phase angle is believed to be due to the changing waveguide length and therefore the changing phase reference discussed previously in Section 3.2.2. The cold air voltage reflection coefficient is observed in Figure 3-8 to increase monotonically with decreasing pressure. However, in the argon experiments, the reflection coefficient was observed to remain relatively constant, at a value ( $\sim 0.76$ ) which corresponded to the maximum observed reflection coefficient for the air experiments.

The cold air antenna input impedance did not exhibit any pressure or power dependence (see Figure 3-9). Similar results were obtained with the other cold gas mixtures.



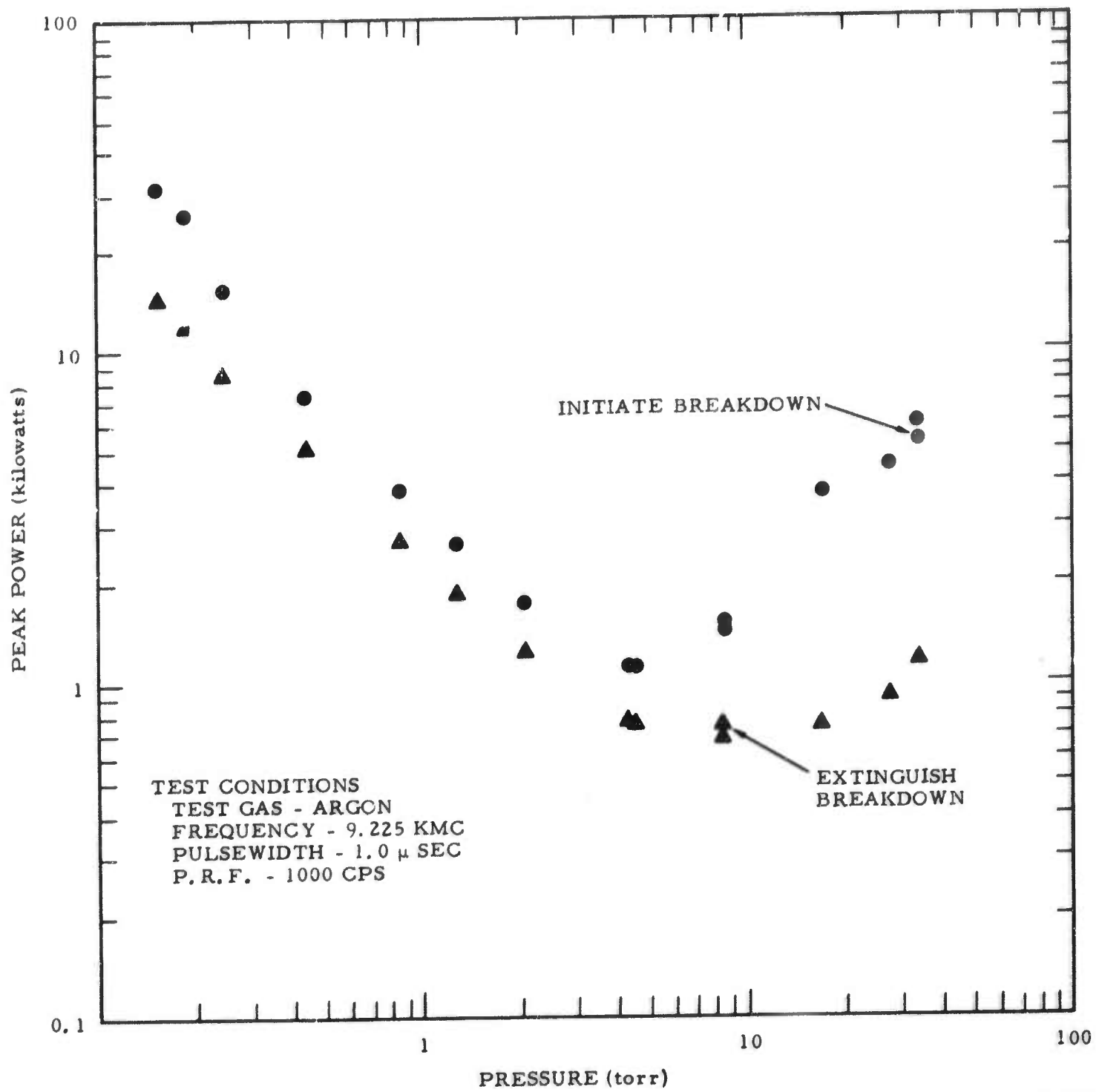


Figure 3-6. Results of Cold Argon Breakdown Studies

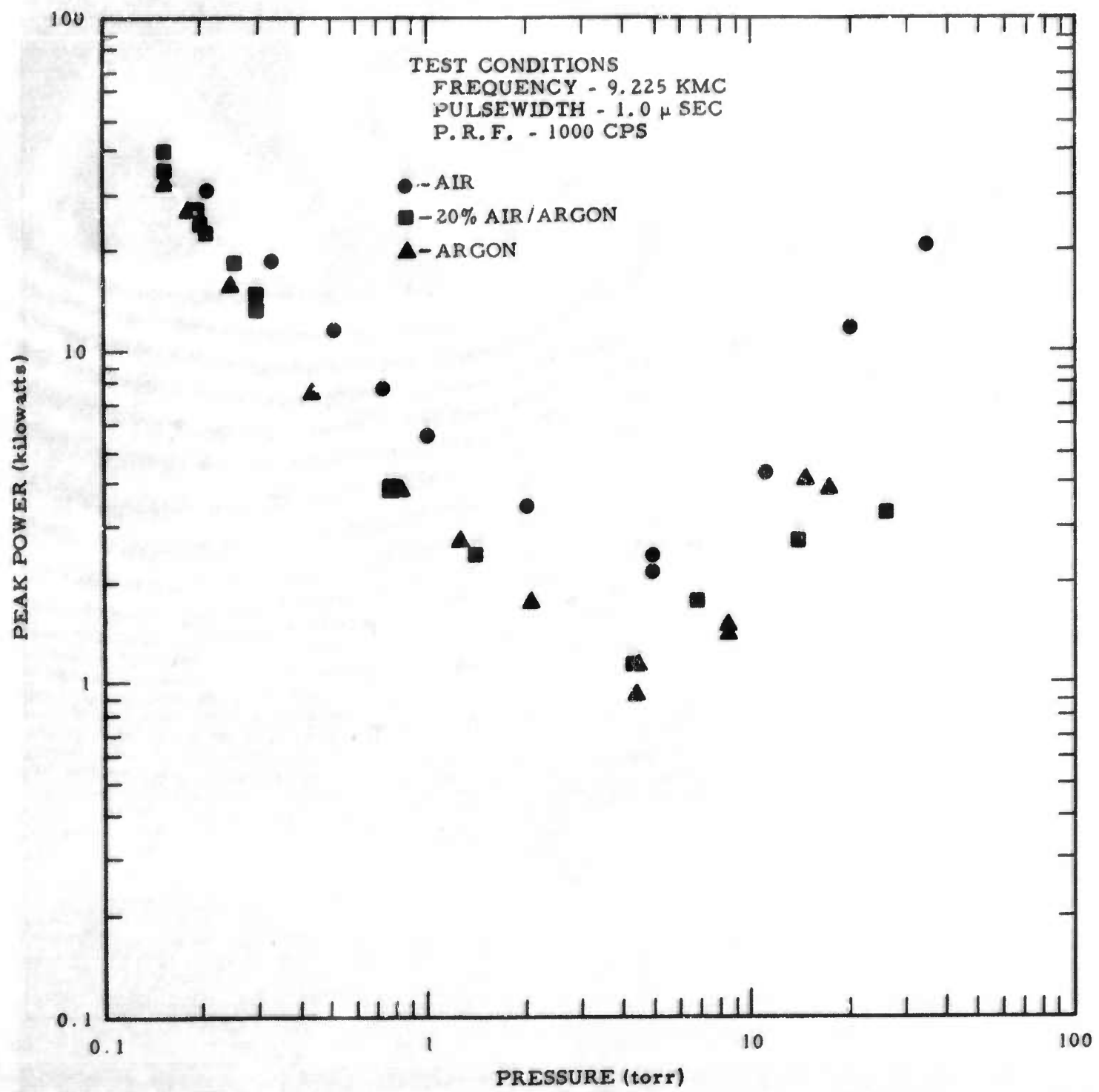


Figure 3-7. Comparison of Breakdown Results for Several Gas Mixtures

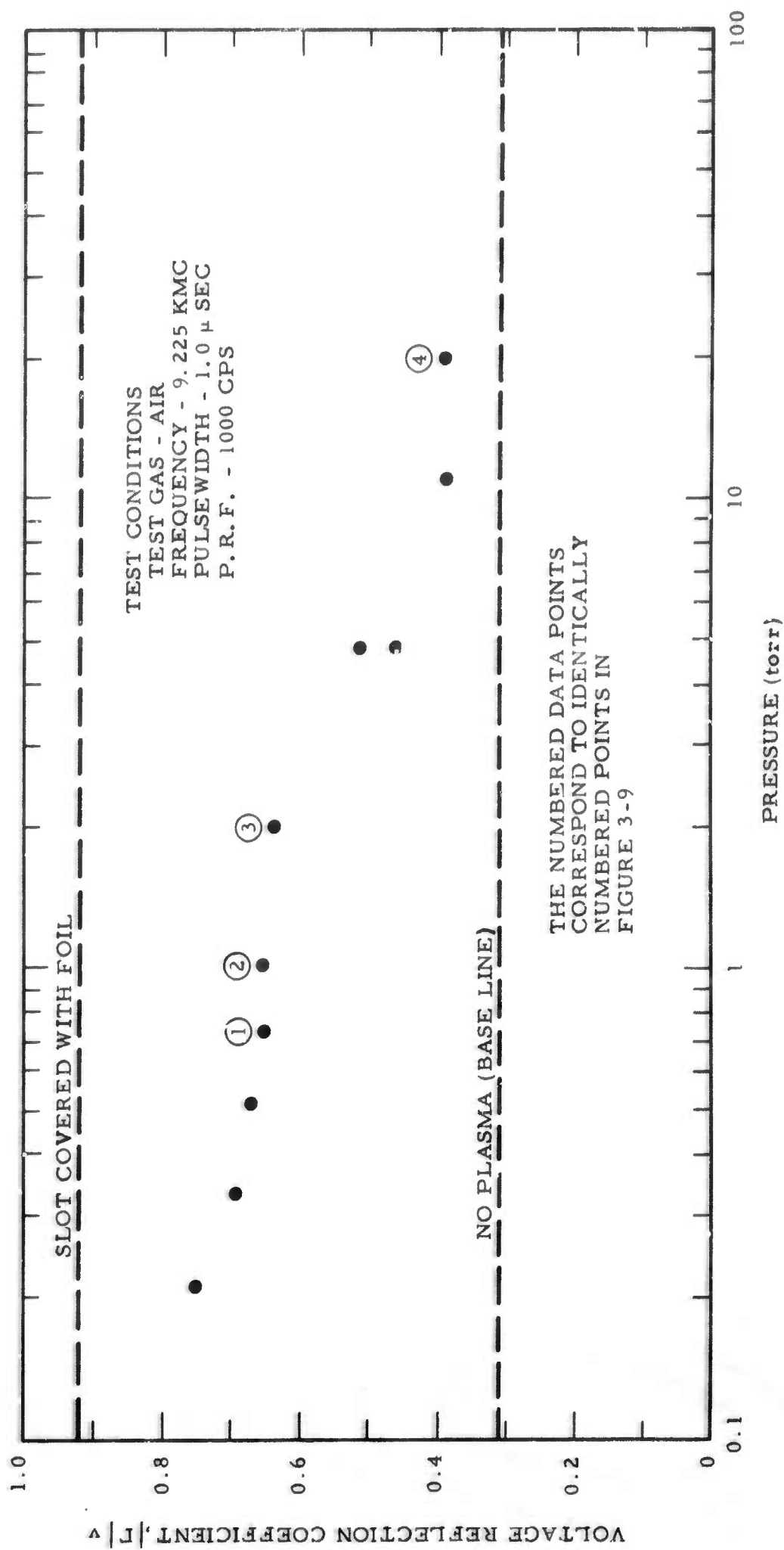


Figure 3-8. Reflection of Coefficient Amplitude in Cold Air Experiments



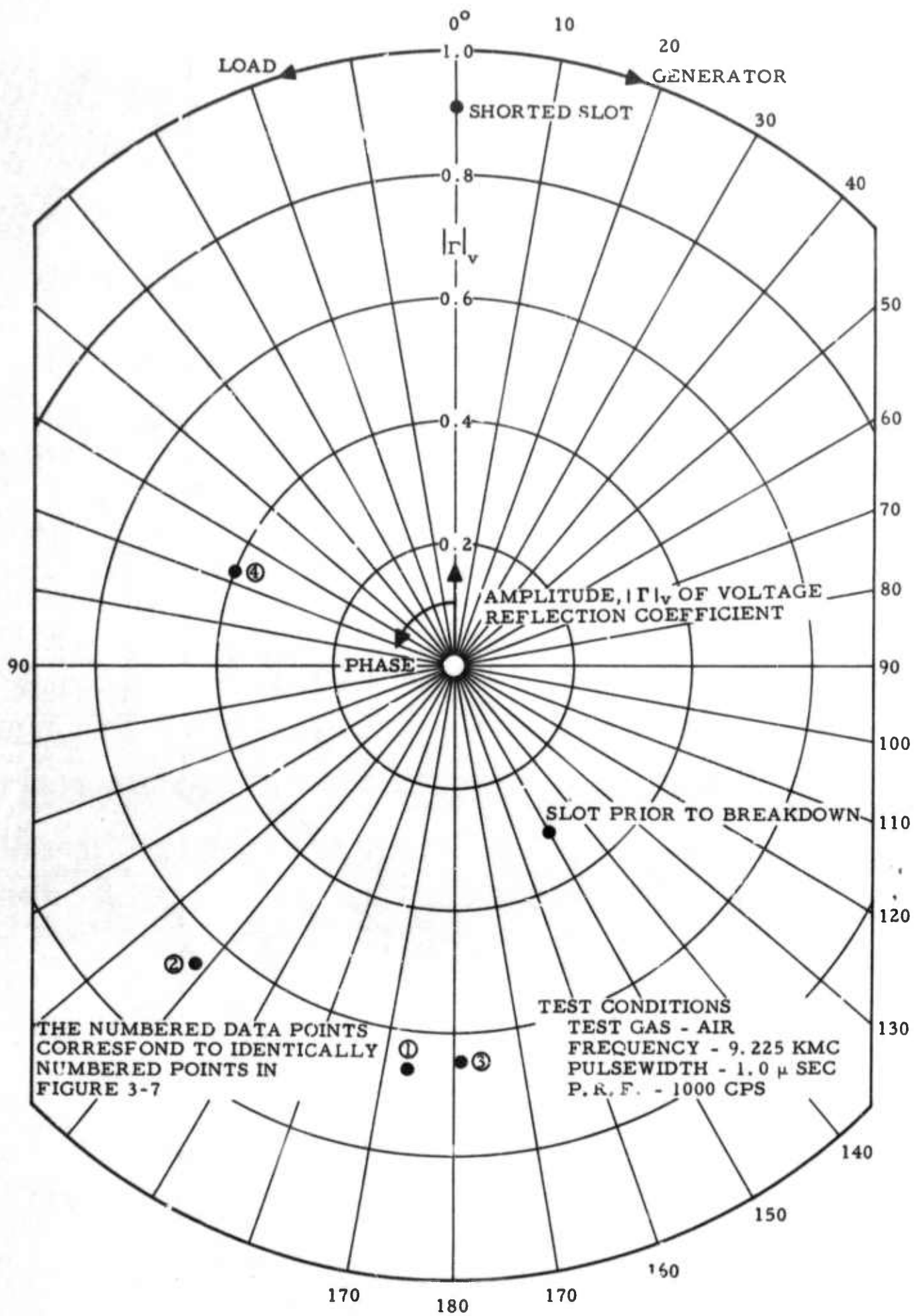


Figure 3-9. Phase and Amplitude of Reflection Coefficient in Cold Air Experiments

### 3.5 X-BAND SLOT ANTENNA-PLASMA LAYER EXPERIMENTS

#### 3.5.1 Introduction

In this section some of the characteristics of the interaction between the electromagnetic fields from the slot antenna, and the plasma flows described in Chapter 2, are discussed. The particular measurements included:

- Initiate breakdown power
- Extinguish breakdown power
- Reflected power
- Power received at a station outside the plasma beam
- Phase of the reflection coefficient
- H-plane power patterns
- E-plane power patterns

Table 3-I summarizes the particular microwave measurements that were made in the various plasma conditions.

#### 3.5.2 Experimental Procedure

The basic experimental approach was to preset the plasma tunnel to an operating condition corresponding to one of the test runs discussed in Chapter 2. The plasma instrumentation located on the test cone was used as an index for adjustment of the plasma tunnel.

When the desired plasma conditions had been achieved, the receiving horn for monitoring the power transmitted through the plasma was positioned at a fixed station along the normal to the plane containing the slot antenna. The power to the slot was varied and the received, reflected and incident power were monitored. At selected points the phase angle on the reflection coefficient was also measured.

The initiate breakdown power level was deduced from the appearance of a distortion of the pulse waveform observed by the

detector monitoring the impedance bridge unbalance. In addition to the distortion of the pulse shape, nonlinear attenuation of the signal transmitted through the plasma was found to be a good indicator of the onset of breakdown. Occasionally, it was possible to detect the breakdown plasma visually as enhanced luminosity over the slot aperture. However, the luminosity did not prove to be a reliable indicator.

Far-field H-plane pattern measurements were made by rotating the cone about its axis with the receiving horn positioned at a fixed station directly above the slot antenna. E-plane patterns were made by traversing the receiving horn along an I-beam located directly above, and parallel with, the axis of the plasma tunnel and the test cone.

### 3.5.3 Experimental Results

#### 3.5.3.1 Transmitted and Reflected Power

We define the transmitted power as the power received by a horn located at a fixed position outside the plasma beam. (Corrections for the microwave energy that is reflected, scattered, and/or absorbed by the plasma are not included).

Transmitted and reflected power experiments were conducted at each of the "calibrated" plasma conditions described in Chapter 2, i.e., conditions A,B,C,D, and E in Table 2-III. The microwave measurements that were made in each of the experiments are summarized in Table 3-I.

Run A in Table 3-I corresponds to a pure argon test in which the peak electron density over the slot aperture was above cutoff ( $\omega_p/\omega > 1$ ). During the course of the "condition A" experiments, two additional runs were made at lower electron densities. For future reference these runs will be identified as follows:



TABLE 3-I

SUMMARY OF MICROWAVE MEASUREMENTS  
MADE DURING PLASMA TUNNEL TESTS<sup>‡</sup>

Run No.	$\omega_p/\omega$ <sup>*</sup>	P <sub>BD</sub>	P <sub>Ext</sub>	P <sub>R</sub>	P <sub>t</sub>	$\Delta\phi$ <sup>**</sup>	P <sub>H</sub> ( $\theta$ )	P <sub>E</sub> ( $\theta$ )	Remarks
A	1.4	x		x		x			P <sub>t</sub> measured for various "under-dense" beams as described in text.
B	0.79	x		x	x		x		
C	0.66	x	x	x	x	x	x		
D	.496	x	x	x	x	x	x	x	
E	.322	x	x	x	x	x	x	x	
10				x	x		x		Teflon ablation
11		x	x	x	x	x	x	x	Teflon ablation

<sup>‡</sup> See Section 2.7.

<sup>\*</sup> Based on peak value of N<sub>e</sub> in boundary layer profile over slot antenna.

<sup>\*\*</sup> Phase shift required to rebalance impedance measuring bridge.

P = Measured microwave power

Subscripts:

BD - Breakdown  
Ext - Extinguish  
R - Reflected  
t - Transmitted  
H - Pertains to H-plane pattern  
E - Pertains to E-plane pattern

- Run A-1 An experiment conducted at overdense plasma conditions specified as Run A in Table 2-III.
- Run A-2 An experiment conducted at the same accelerator operating conditions as for Run A-1. However, because of the presence of water vapor from the anechoic material, the electron density was reduced.
- Run A-3 An experiment conducted at the same accelerator operating conditions as for Run A-1. However, an increased level of water vapor contamination resulted in an electron density that was less than in Run A-2.

Figure 3-10 shows the transmitted power, ( $P_t$ ), as a function of the power incident on the slot antenna, ( $P_i$ ), for the A-2 and A-3 runs. It can readily be seen that the increased ambient electron density for the A-2 plasma lowers the power level at which breakdown occurs.

Figure 3-11 shows the variation in transmitted power, ( $P_t$ ), and reflected power, ( $P_R$ ), as a function of  $P_i$  for the A-3 beam. The onset of nonlinearities appears simultaneously in both measurements.

The reflected power characteristics of the three "class A" plasmas are compared in Figure 3-12. The reflection coefficient for the A-1 beam was essentially constant and slightly less in magnitude than the reflection coefficient of the aluminum-foil covered slot. The observation that the reflection coefficient with an overdense plasma electron density present over the slot was less than that with a metal cover is not surprising, inasmuch as the plasma will absorb some power. This in turn appears as a reduced amount of reflected power.

It is of interest to examine the antenna input impedance as a function of power incident on the slot antenna for the "overdense" plasma layer. Figure 3-13 shows the reflection coefficient variation where the labeled points correspond to the appropriate labeled points in Figure 3-12. It is seen that, although the magnitude of the reflection coefficient is essentially constant, the phase angle

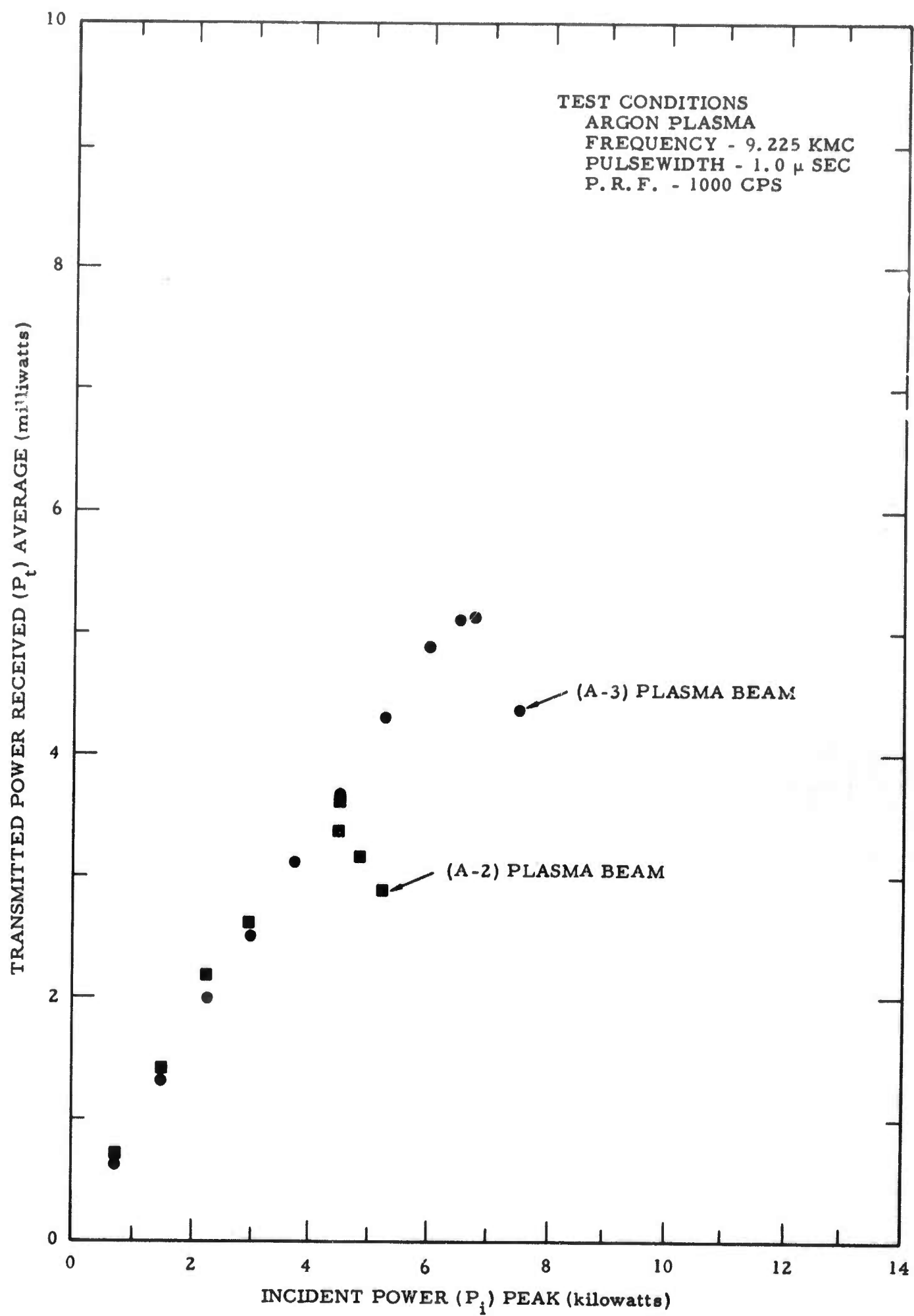


Figure 3-10. Power Transmitted During Plasma Experiments



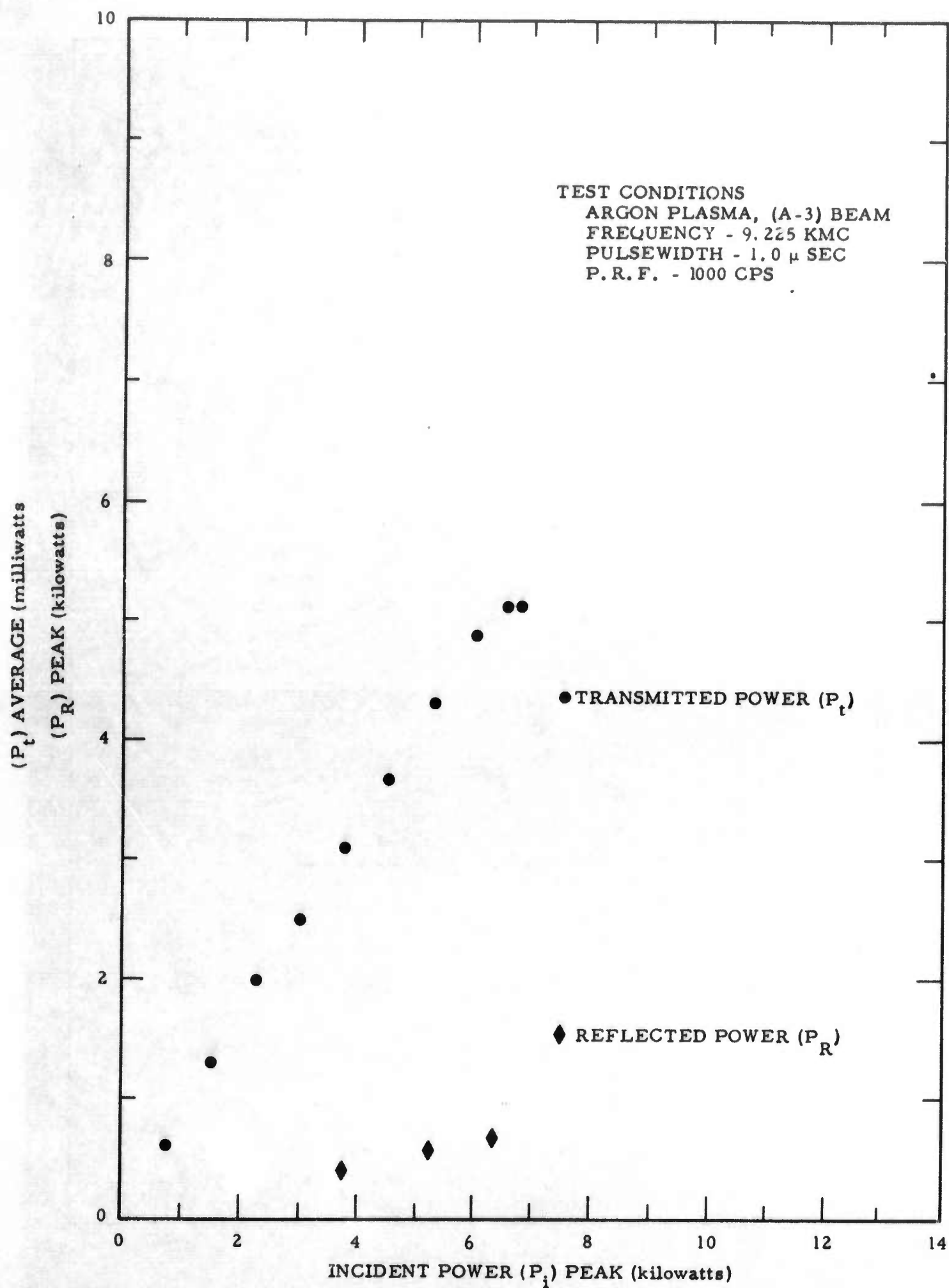


Figure 3-11. Power Transmitted and Reflected During Plasma Experiment

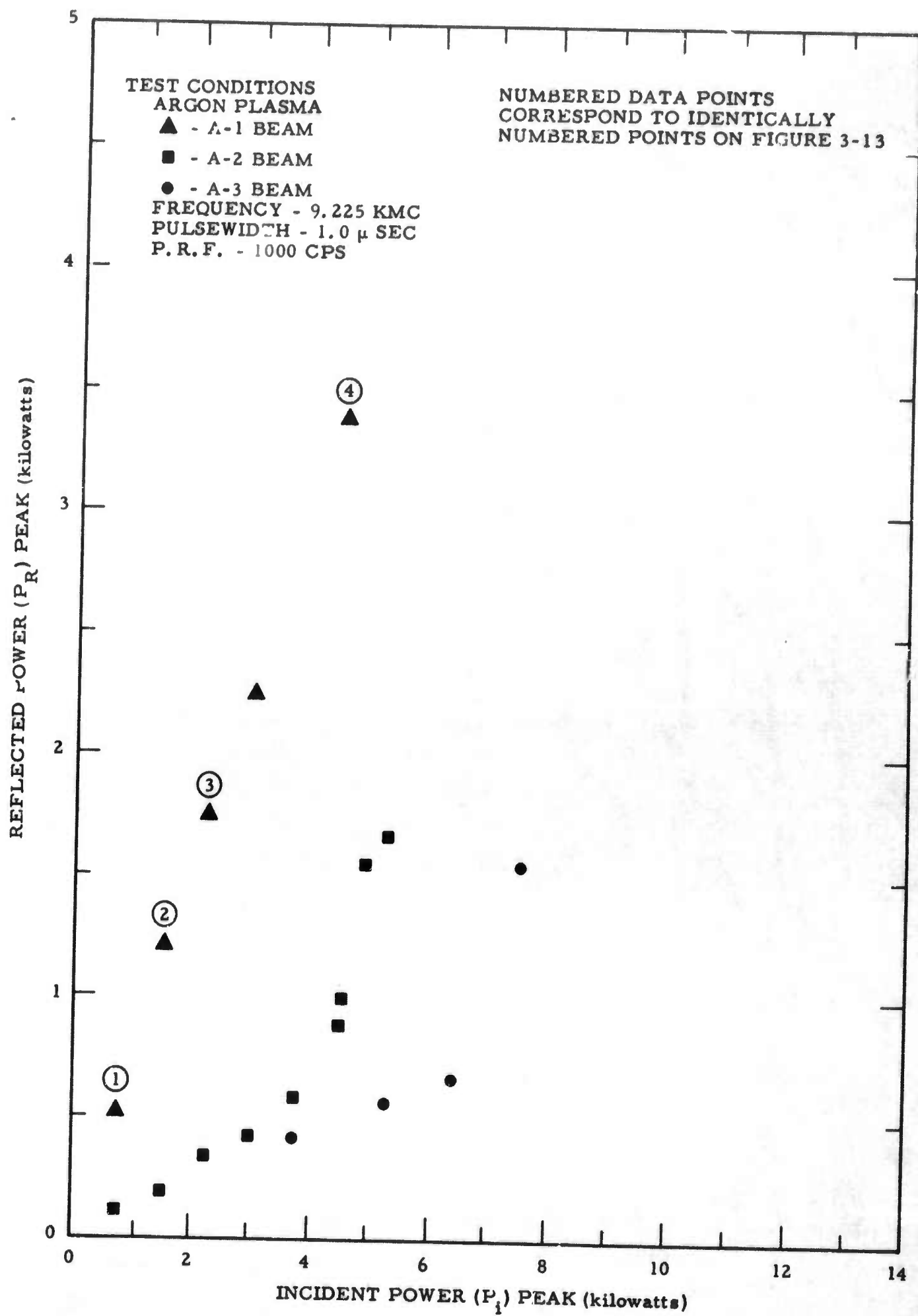


Figure 3-12. Reflected Power Characteristics

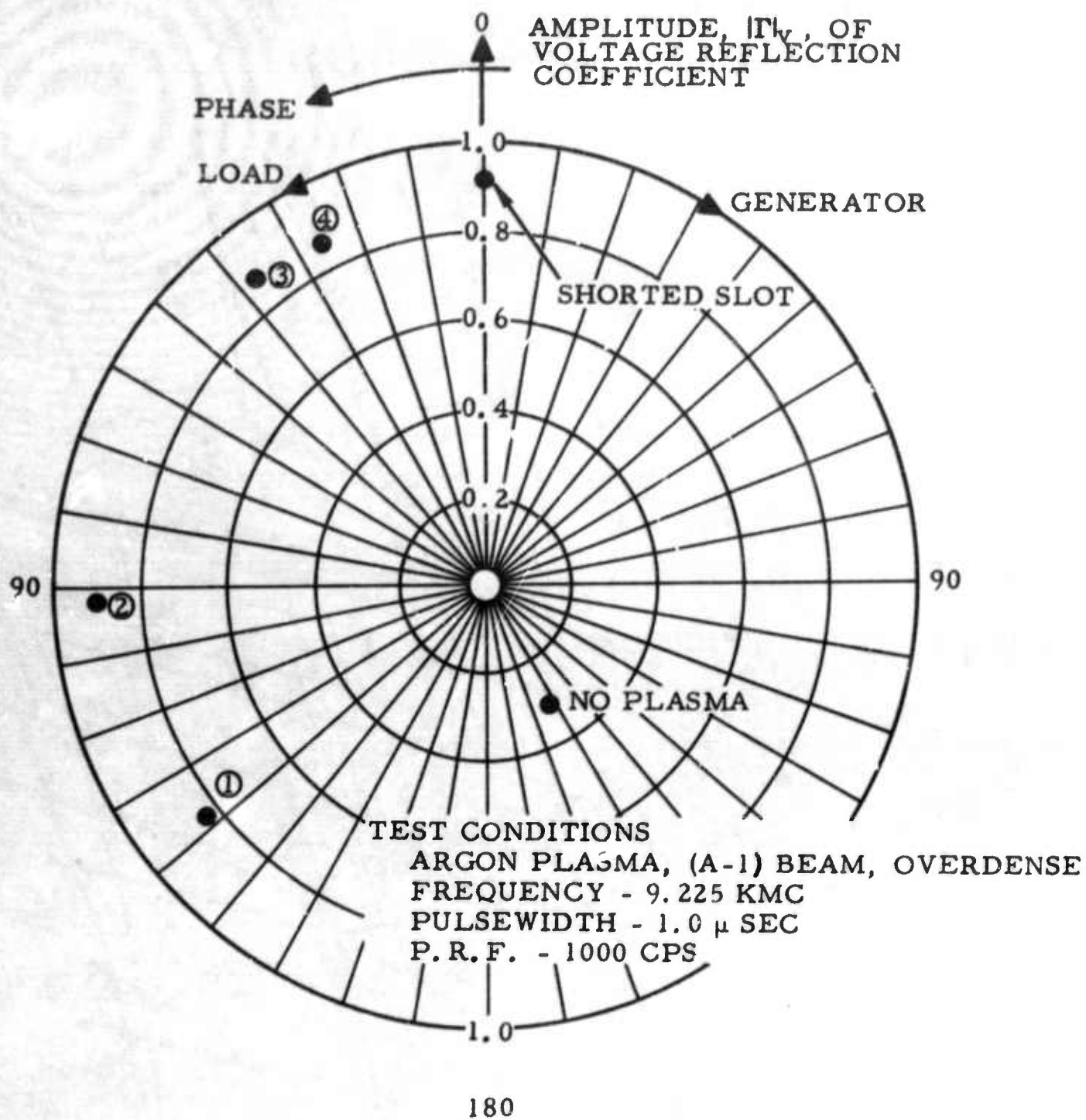


Figure 3-13. Variation of Antenna Input Impedance for Overdense Plasma Layer



rotates progressively toward the generator as the input power to the slot is increased. Since the peak electron density over the slot is greater than the cutoff value, and the electron density adjacent to the cone surface is significantly lower, it would appear that the major effect of increasing the power to the slot is to increase the localized electron density adjacent to the cone surface. Thus, it appears that raising the input power essentially moves the effective boundary of the overdense layer progressively closer to the slot aperture. This is equivalent to moving a metal plate toward the slot and appears as a rotation of the phase angle toward the generator (see Section 3.3.2).

The transmitted and reflected power are plotted as a function of the power incident on the slot antenna in Figures 3-14, 3-15 and 3-16 for three runs corresponding to plasma conditions D, C, and B; i.e., conditions in which the peak electron density in the boundary layer over the aperture is successively greater. Figure 3-17 summarizes the transmitted power variation with the incident power for the various operating conditions.

Figure 3-18 shows a plot of the peak power transmitted, as identified in Figure 3-17, as a function of  $(\omega_p / \omega)^2$  for the microwave tests that were conducted at the predetermined conditions described in Chapter 2; i.e., runs B, C, D and E. It is seen that the peak power transmitted through the plasma layer correlates quite well with the reciprocal of the peak value of the electron density over the slot antenna, (i.e., with the reciprocal of the ratio of the plasma frequency squared to the rf frequency squared). On the basis of this figure the peak electron density over the slot antenna for runs A-2 and A-3 can be estimated. In particular, the electron density for run A-3 is estimated to be about  $4.6 \times 10^{11} \text{ cm}^{-3}$ , and the density for run A-2 to be about  $6.5 \times 10^{11} \text{ cm}^{-3}$ .

Results similar to Figures 3-14 through 3-17 were obtained for the runs where teflon ablation products were present; however,

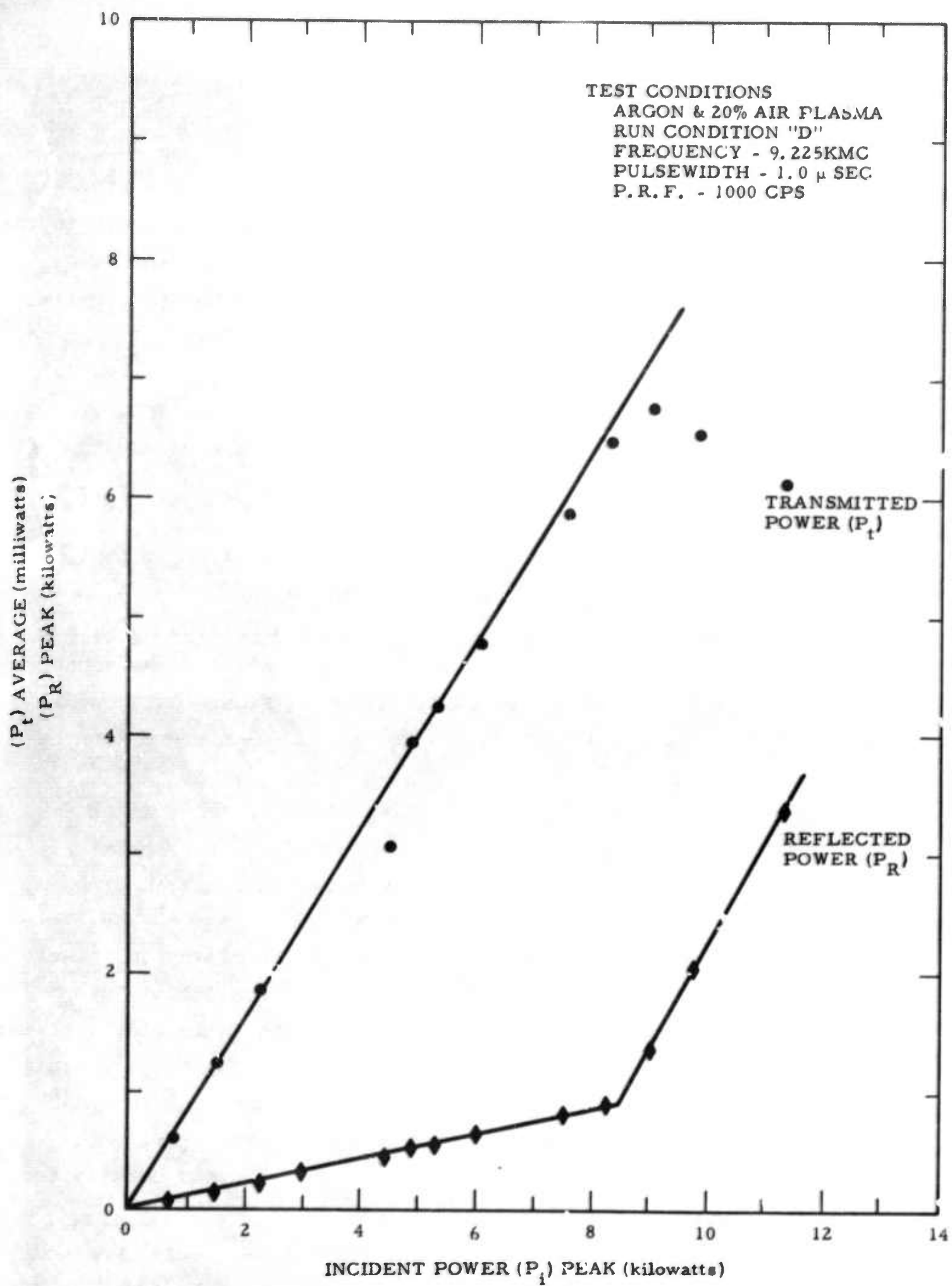


Figure 3-14. Power Transmitted and Reflected During Plasma Experiment

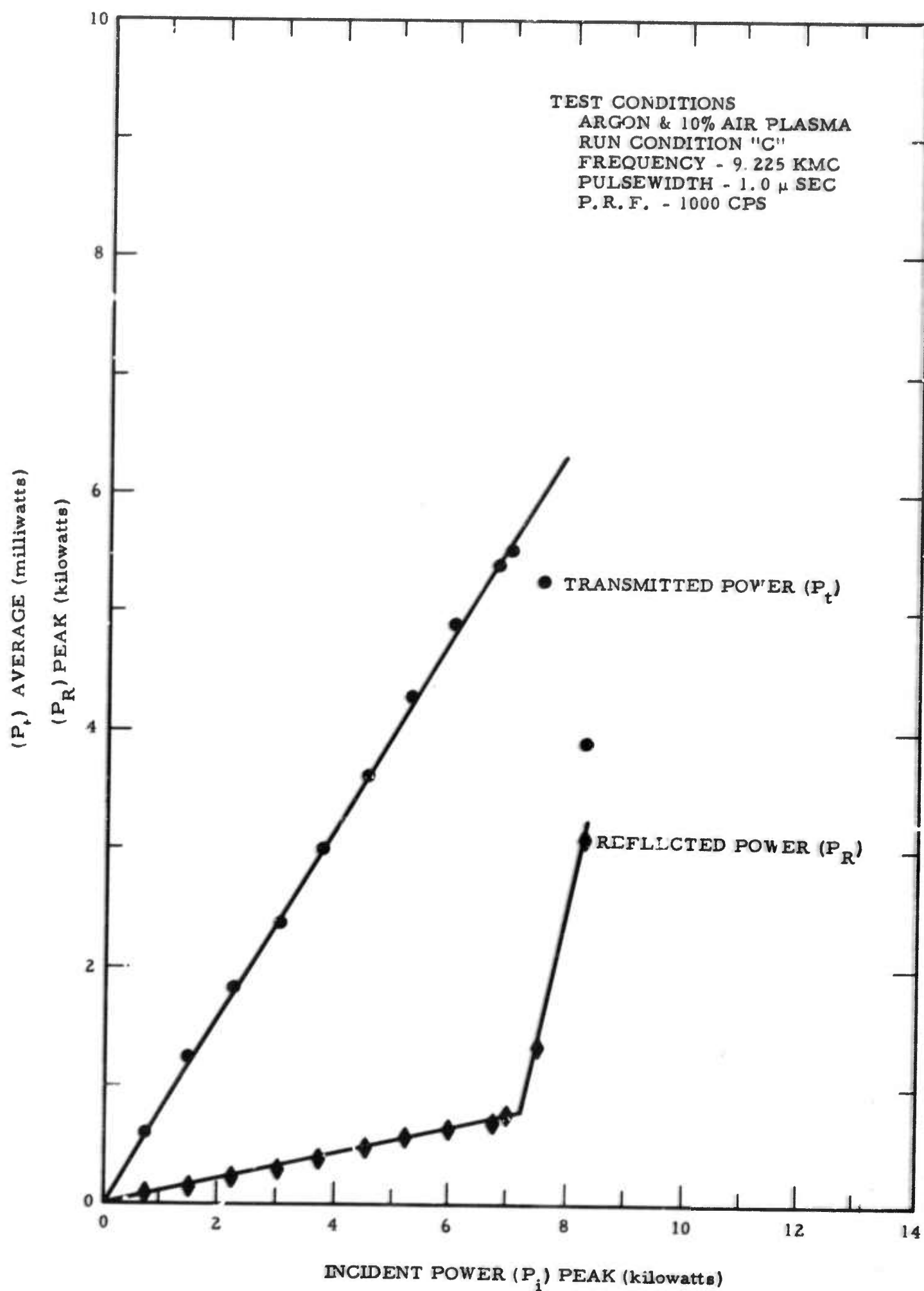


Figure 3-15. Power Transmitted and Reflected During Plasma Experiment



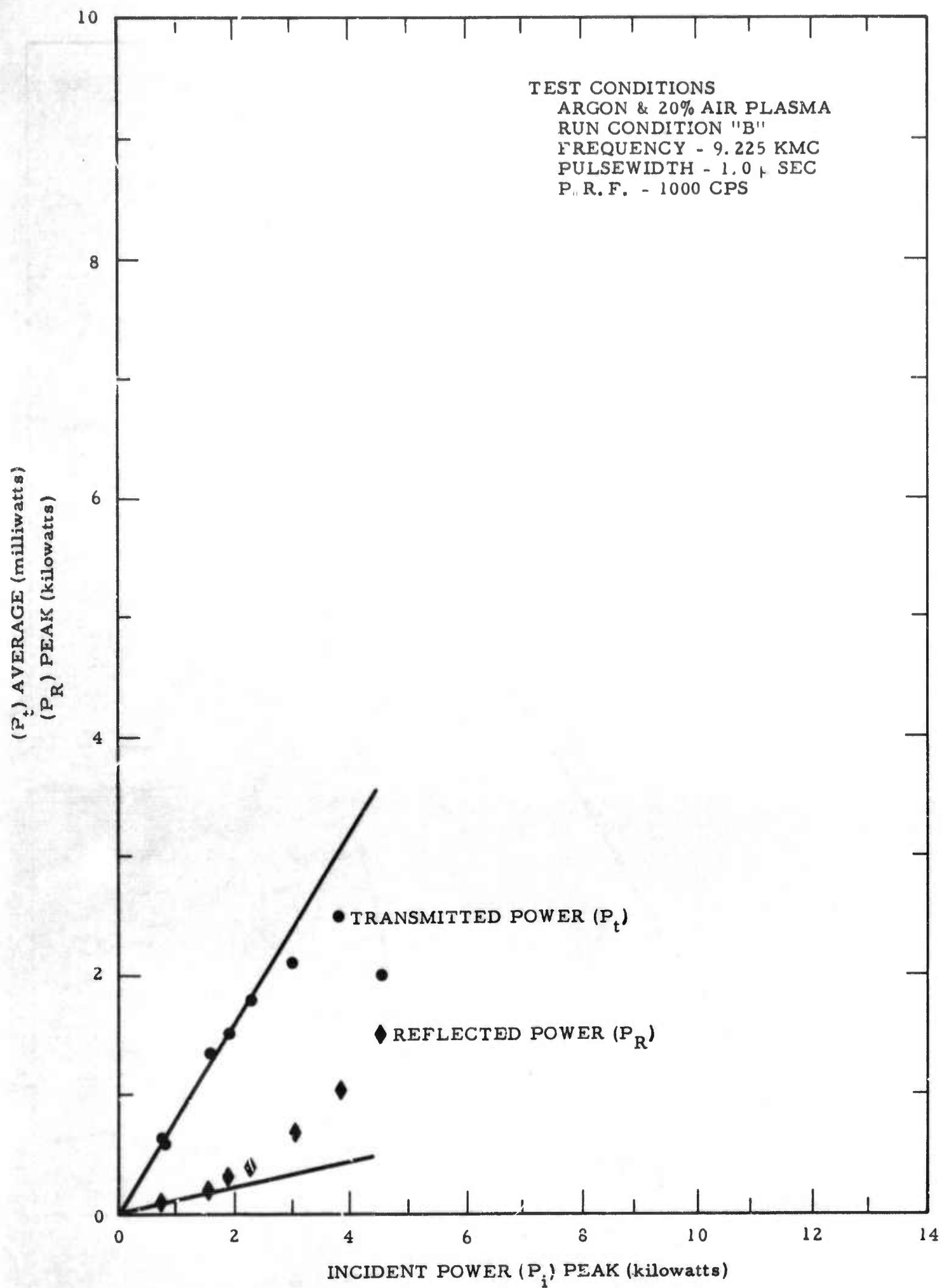


Figure 3-16. Power Transmitted and Reflected During Plasma Experiment

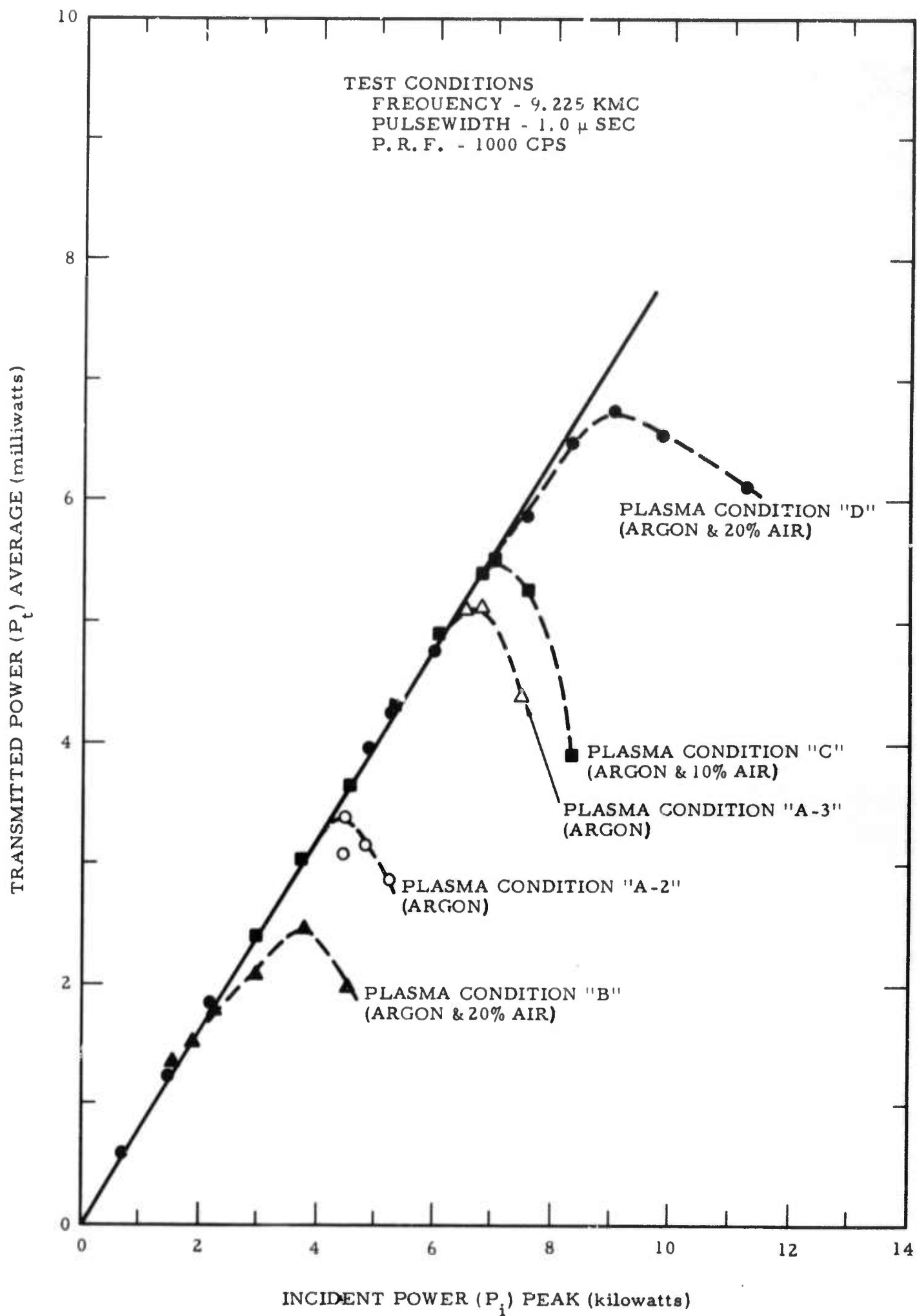


Figure 3-17. Power Transmitted During Plasma Experiments

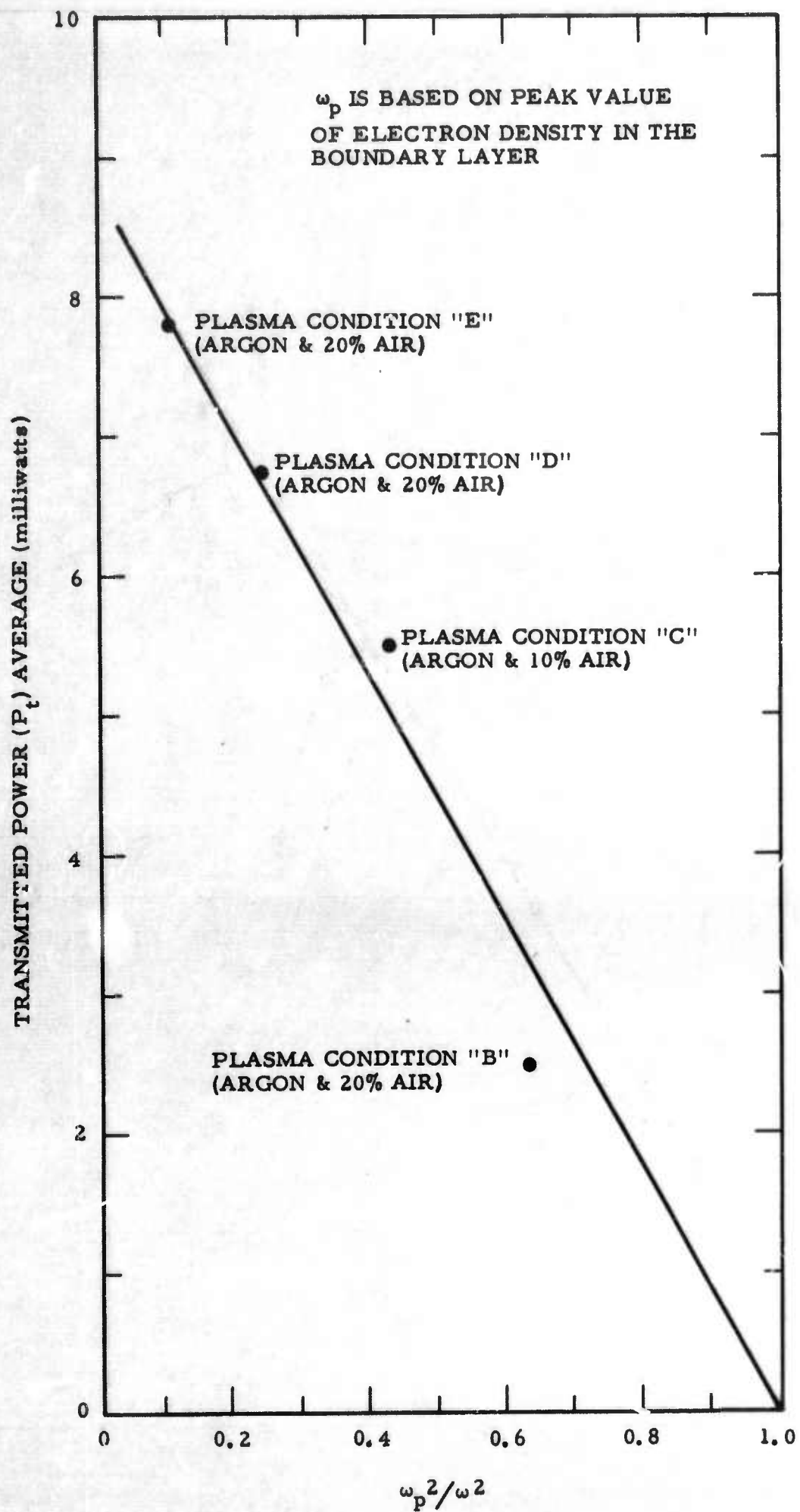


Figure 3-18. Peak Power Transmitted During Plasma Experiments



the presentation of those data will be deferred to Section 3.5.4, where they can be explained in the proper context.

#### 3.5.3.2 Plasma Enhanced Breakdown

The effect of the ambient plasma layer is to lower the power level for initiating breakdown. The effect of this "preionization" can be seen in Figure 3-19, where the initiate breakdown power-pressure variation of Figure 3-7 for cold argon and argon/20% air is replotted, with the measured breakdown power levels for various ambient electron densities superimposed.

It should be noted again that the pressure scale is really a density scale based on an ambient temperature of  $300^{\circ}\text{K}$ . The plasma breakdown data are based on the actual density at the peak temperature in the boundary layer, as determined from the gas dynamic measurements described in Section 2.5.4. The plasma data taken at a pressure of 0.25 Torr, (corrected to the actual density), clearly show that the effect of increasing the electron density is to progressively lower the breakdown power level. The observed decrease in power level varied from approximately 6 to 10 db.

The initiate-breakdown data quite frequently exhibited the "flicker" behavior reported previously by Covert.<sup>21,22</sup> The extinguish power levels were extremely difficult to discern either visually, or with the microwave instrumentation. In general, however, less than 3% difference in the initiate and extinguish breakdown power was observed. Therefore, because this uncertainty is within the experimental error in the power measuring equipment, specific data are omitted.

#### 3.5.3.3 Input Impedance Measurements and Antenna Pattern

Considerable difficulty was encountered in the measurements of the phase angle of the reflection coefficient that were attempted during the plasma tests. In particular, it was found that:

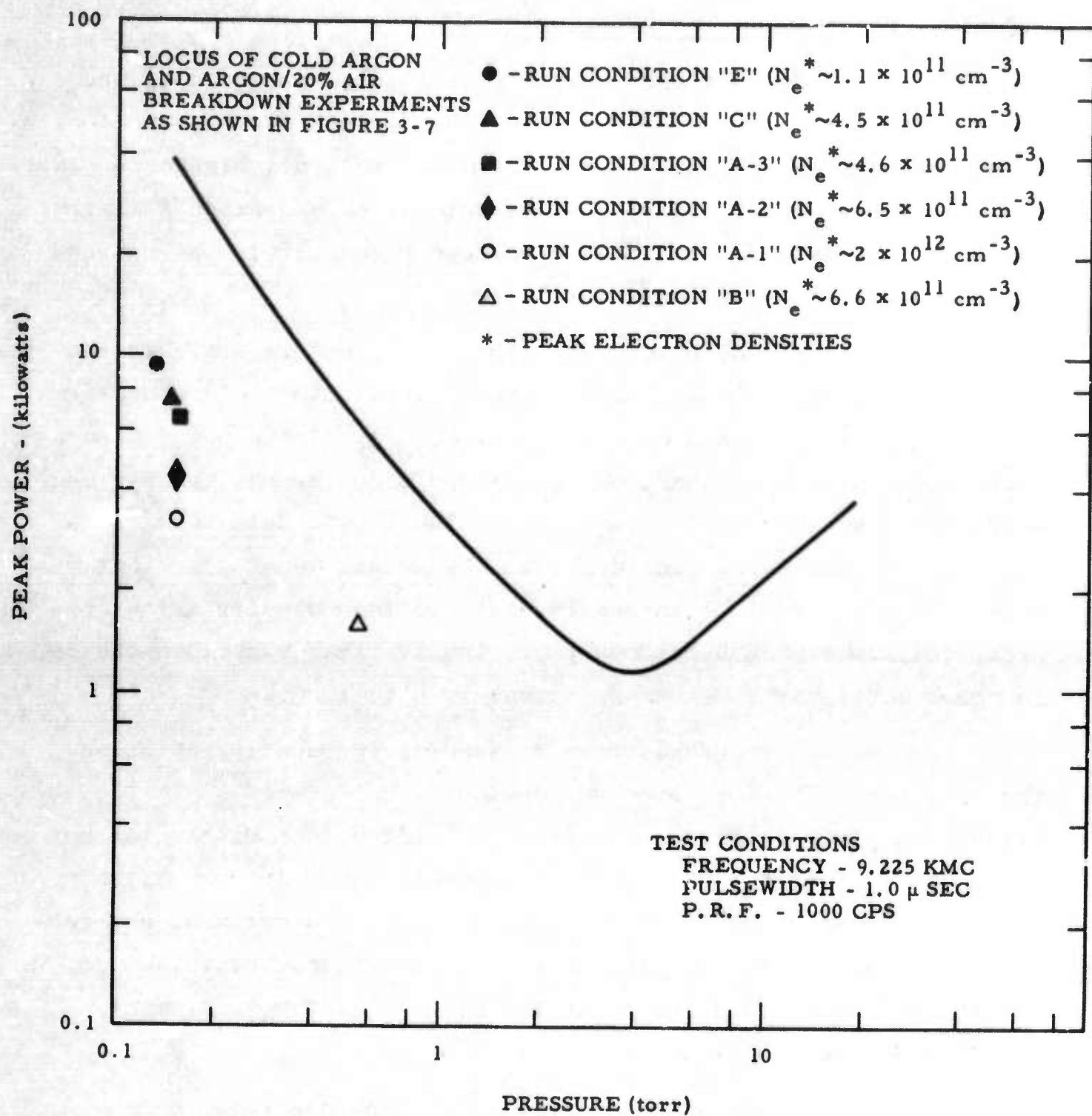


Figure 3-19. Effect of Ambient Plasma on Breakdown Power Level

- a. The phase reference for the reflectometer bridge drifted both on a long and short term basis.
- b. The bridge arrangement was difficult to rebalance.

The difficulty described in item a. above is believed to be primarily due to variations in the ambient temperature and to localized heating of the test cone during the plasma tests. This difficulty was discussed previously in Section 3.3.2. The difficulty in balancing the bridge (item b.) resulted both because of the relative insensitivity of the particular phase shifter that was incorporated into the system, and continuous changes in the null, or balance point, due to temperature effects.

Therefore, although some data are presented (see Figure 3-13), it is believed that the uncertainty of the antenna impedance measurements makes a critical comparison of theory and experiment unwarranted.

Antenna pattern measurements were made in the anechoic lined vacuum chamber under a variety of plasma conditions. Under no circumstances was pattern distortion due to the plasma observed (within the experimental error of the measurements) prior to the onset of breakdown. After breakdown had occurred, the transmitted signal was observed to increase, as shown previously in Figure 3-17, and antenna patterns were not taken.

The absence of pattern distortion prior to breakdown is not surprising when one considers the range of electron densities used in the present program. Indeed, it can also be shown, using the results of Heald and Wharton,<sup>23</sup> that for the electron densities, collision frequencies, and plasma thicknesses, encountered in the plasma boundary layer over the slot antenna, the plane wave attenuation should be no more than 1 db, (i.e., ~20% attenuation) of the received signal. The maximum observed decrease in signal was approximately 10% and the accuracy of the power meter is only 5%, thus pattern distortion was not expected.



Taylor<sup>24</sup> has observed attenuation and distortion in his measurements of the field pattern from a teflon-filled slot covered by plasma layers having varying properties. However, the experimental conditions differed in the following important aspects:

- The plasma layers were significantly thinner and consequently had much steeper gradients.
- The peak electron density in the profile was generally closer to cutoff than in the present work.
- Many of the patterns were taken under conditions such that the plasma layer was centered approximately  $1/2$  wavelength off the face of the slot.
- The slot dimension parallel to the E-plane was reduced to 0.2 cm. to produce high near-fields around the aperture.
- The reflections from the plasma container were felt to affect the fine structure observed in the measured patterns.
- The electron densities were determined from electrostatic probe data and corrections for collisional effects, which should be quite important for the pressures used (0.5 to 0.7 Torr), were not included.

Because of these significant differences between the two experiments, direct comparisons are not possible.

#### 3.5.4 Ablation Tests

During re-entry, ablation effects can be expected to have three influences on the breakdown and transmission characteristics of an ECM antenna:

- Increase the electron density because of the introduction of low ionization potential species, or metastable states that promote two-step ionization process; or decrease the electron density, because of the introduction of electronegative species that promote electron attachment, or because of a simple cooling which results in a reduction of the heavy particle temperature.
- Change in the boundary layer electron density profile, since the ablation products are introduced into that portion of the boundary layer that is closest to the body.

- Increase in the electron-neutral collision frequency, and thus in the tendency for collisional attenuation to occur.

The net increase or decrease in electron density, by the processes cited in the first point above, will depend on the nature of the ablation material. For ablation materials such as teflon, a net decrease in electron density is to be anticipated.

The laboratory situation is considerably different from the re-entry case. The nature of the plasma beam produced by the Litton traveling wave accelerator is best characterized as an afterglow plasma; i.e., the electron density is considerably greater than the value predicted by evaluation of the Saha equation at the electron temperature and gas density, and recombination is a significant loss mechanism. The ionization that does occur in the beam is primarily the result of multistep processes involving metastable species. In such a plasma the introduction of ablation products can be expected to result in a destruction of metastables in the parent flow, attachment, and cooling. Thus, the anticipated result is a reduction in the electron density. Laboratory ablation from the cone surface should also result in a change in the electron density profile and the electron-neutral collision frequency. Therefore, preliminary ablation experiments were conducted in the laboratory plasma for the purpose of gaining a better understanding of the problems associated with properly including and evaluating the effects of ablation in future laboratory programs.

Teflon was used as the ablation material. The ablation overlay consisted simply of DuPont FEP heat-shrinkable teflon roll covers which were attached over approximately five inches of the cone surface beginning just behind the boron nitride nose tip (see Figures 2-1 and 3-20).

The experiments were conducted with an overdense argon plasma (condition A in Table 2-III). No attempt was made to make a

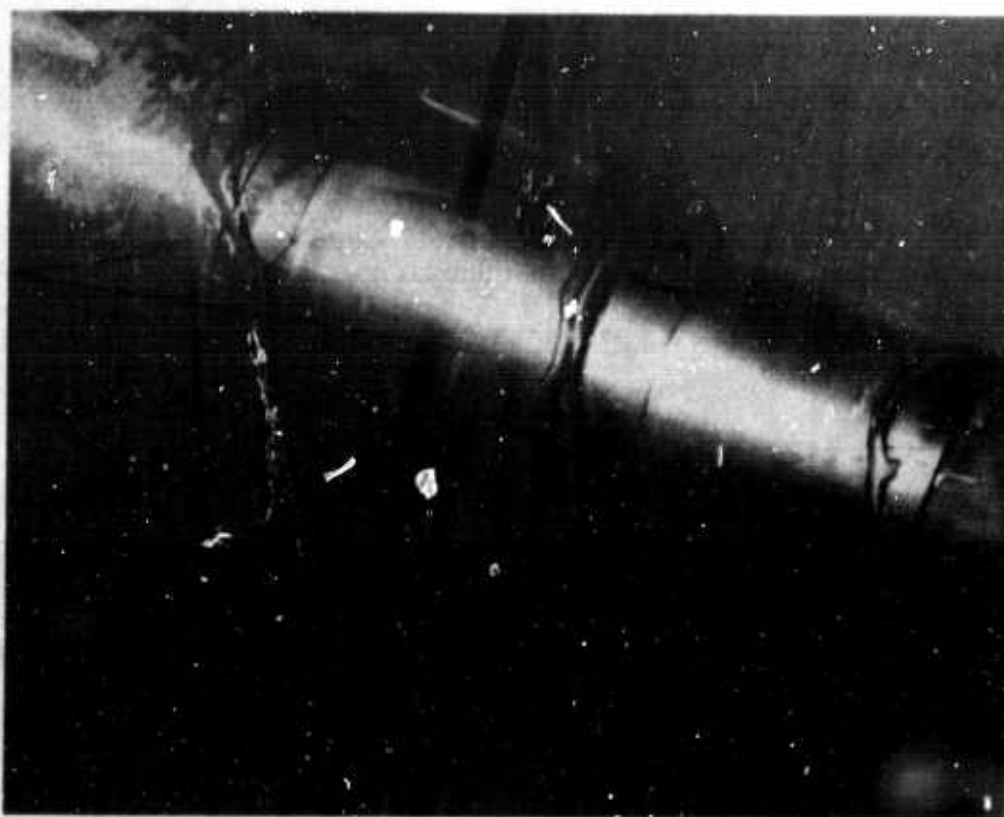


Figure 3-20. Ablated Teflon-covered Cone Tip



quantitative determination of the products of ablation (such a determination would require extensive optical and mass spectroscopy). Visually, the first indication of the ablation effects was a bluish glow which originated at the leading edge of the teflon overlay. The subsequent addition of air, or operation on argon/air mixtures, resulted in a change of the bluish color to an orange glow. Qualitative optical spectroscopic observations indicated the presence of CN bands in addition to the usual argon and hydrogen spectra. When air was added the air spectra were also visible.

The ablation products quenched the electron density sufficiently to allow propagation through the plasma layer. Figure 3-21 shows the measured transmitted and reflected power during ablation. After the cessation of ablation, the transmitted power was cut off and the reflected power exhibited behavior identical to that observed for the A-1 microwave tests described in Section 3.5.3. If we assume that the peak transmitted power in Figure 3-21 can be related to the plasma frequency using Figure 3-18, the peak electron density during ablation is concluded to have been approximately  $7 \times 10^{11}/\text{cm}^{-3}$ . Thus it would appear that the ablation products reduced the electron density from about  $2 \times 10^{12}/\text{cm}^{-3}$  to about  $7 \times 10^{11}/\text{cm}^{-3}$ .

Although the initial argon beam was very steady, the initiation of ablation was accompanied by the appearance of fluctuations which manifest themselves both in the luminosity and in the transmitted microwave signal. It is recommended that, in future laboratory investigations, particular effort be directed toward minimizing these fluctuations and documenting the nature of the ablation products. This documentation is essential, since the laboratory tests obviously do not duplicate the chemistry in the real re-entry situation.

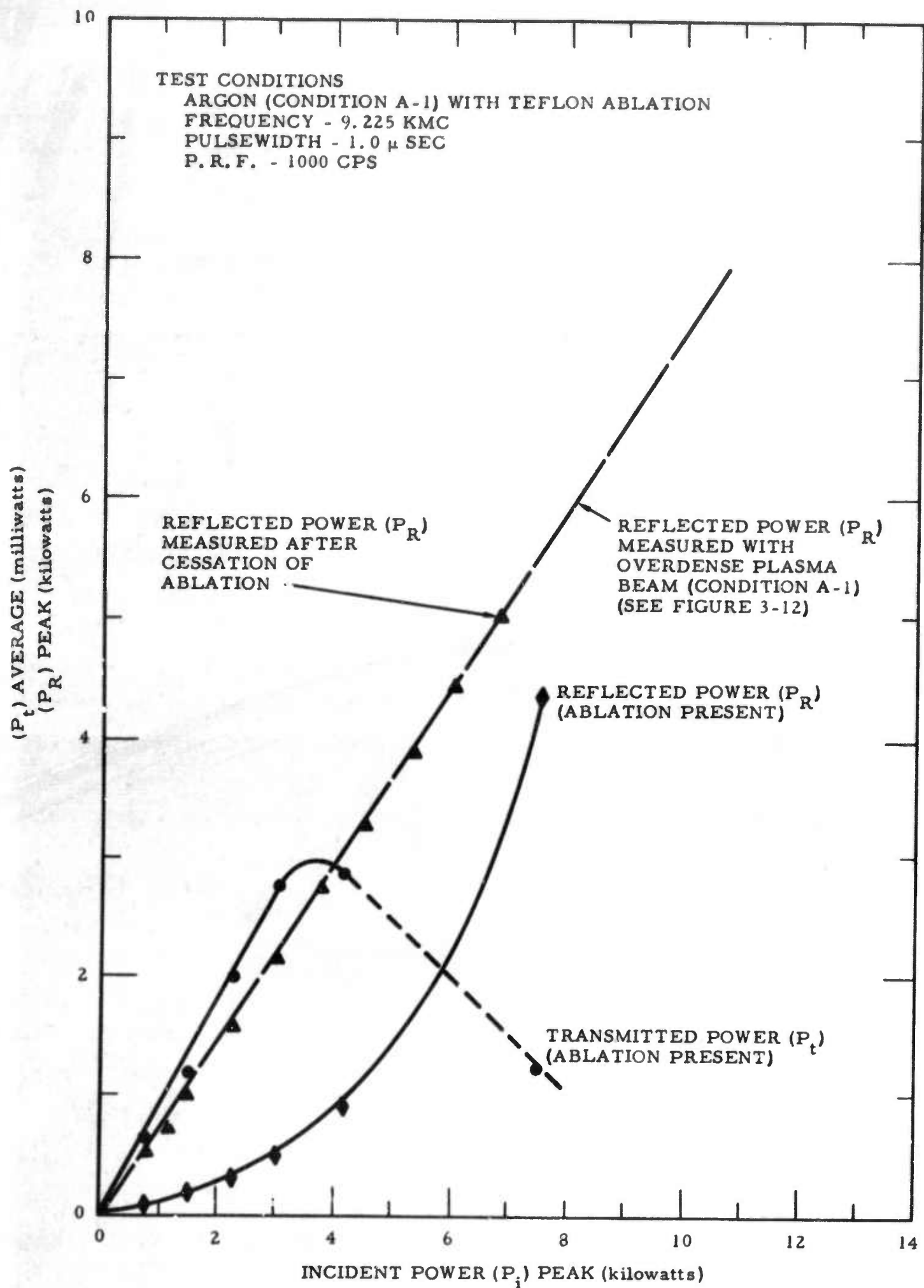


Figure 3-21. Power Transmitted and Reflected During Ablation Experiments

#### 4. MICROWAVE EXPERIMENTS, SUMMARY AND CONCLUSIONS

##### 4.1 INTRODUCTION

Chapter 3 of this report has described an investigation of the antenna characteristics of an X-band slot aperture located in a ground plane formed by a conical re-entry type vehicle. Measurements were made of the initiate and extinguish breakdown power levels, as a function of the cold gas ambient pressure, for a fixed frequency of 9.225 kMc, with a pulse width of  $\sim 1.0 \mu\text{sec}$ , and a pulse repetition frequency of 1000 cps. The breakdown power levels were also measured with plasma layers covering the slot aperture. The variations of the antenna reflection coefficient (phase as well as amplitude) were measured in all the tests. The effects of the plasma layers on the far-field radiation pattern were also investigated.

In addition, during the course of this investigation, a great deal of the previous literature was surveyed so that results of the present investigation could be maintained in proper perspective. Two general conclusions, and a recommendation, can be made as a result of the literature review. The conclusions, which relate to the current state-of-the-art concerning the antenna characteristics of X-band slot apertures, are:

- Current analytical work concentrates primarily on investigating the relative influence of the various parameters that define the problem. This limitation in the approach is a consequence of the fact that the analytical formulations for both the electromagnetic field, and the diffusion controlled plasma, involve boundary value problems and the geometry is, in general, complex.



- Current experimental work, which also concentrates on the relative influence of various parameters, is characterized by complex geometries and a failure to provide a complete description of many of the important experimental parameters. These difficulties are due, in part, to the problems of generating a plasma with a simple geometry, and to the difficulties in making plasma measurements.

Thus, it is concluded that both the analytical work and the experimental work are proceeding along parallel lines, but that the problems of geometry, and of making reliable plasma measurements, have formed a barrier which has severely limited the comparisons that can be made between theory and experiment. Thus, it is recommended that:

- Consideration be given to conducting a series of experiments with a geometry, or set of geometries, conceived by discussions between experimentalists and theoreticians, with particular attention being given to performing accurate plasma diagnostic measurements with as many different techniques as possible. Provisions should also be made, either through the selection of geometry or through measurements, to provide a determination of the electric field distribution.
- Parallel analytical studies be undertaken so that absolute magnitude predictions can be made for the selected geometry, or set of geometries, described above.

The purpose of this chapter is to summarize the results of the present investigation, to compare these results with the observation of other investigators, and to present the conclusions in terms of their implications on ECM antenna design. Particular attention is devoted to the following factors:

- Power breakdown levels
- Input impedance
- Plasma produced pattern distortion
- Effects of non-linear and collisional attenuation

which are relevant to ECM antenna design, have been areas of interest in the present investigation, and which have received considerable attention in both the analytical and experimental literature.

#### 4.2 ANTENNA BREAKDOWN CHARACTERISTICS

A great deal of attention has been devoted to the measurement of the breakdown characteristics of slot antennas. Particular attention has been given to the determination of the relative influence of the following:

- The ambient gas density in cold air breakdown
- Ambient ionization
- Convection
- Elevated gas temperature
- Effects of chemical additives

Bisbing, McMenamin and Scherer<sup>25</sup> have recently surveyed the literature with emphasis on these effects and the reader is referred to their report for details.

##### 4.2.1 Influence of Ambient Gas Density in Cold Air Breakdown

The experimental investigations of microwave breakdown in gases has been reviewed by MacDonald in a recent book.<sup>26</sup> Although a great deal of attention has been devoted by many investigators to the measurement of the cold air breakdown characteristics of X-band slot antennas, the wide variety of geometries employed, and the failure of most authors to provide a complete description of their experimental parameters, makes systematic comparisons difficult. Nevertheless, a representative comparison will be made.

The cold gas breakdown experiments described in Section 3.4 determined the breakdown characteristics of a full-sized, teflon-filled, X-band slot located in a conical shaped ground plane. In comparing these data with the results of other investigators the following parameters are of interest:

- The influence of the slot shape
- The influence of a dielectric filling or layer at the slot exit
- The influence of the shape of the ground plane

Scharfman measured the initiate breakdown power of a slot aperture, covered with a dielectric cover, as a function of the ambient air pressure for slot heights\* of 1.016, 0.254, and 0.127 cm (see Figure 7 in Reference 20). Scharfman's results clearly show the influence of the increased electric field strength (that results from a reduced slot height) in decreasing the required breakdown power.

In Figure 3-5 the results from the present investigation are compared with Scharfman's result for a full sized waveguide. It will be noted that the data agree quite well on the low pressure side of the minima; however, they depart appreciably at the higher pressures. It should also be noted that Scharfman used a polonium source to provide a repeatable initial charge density. Such a source was not used in the Litton tests.

One would expect a teflon-filled waveguide to exhibit a slightly increased breakdown power because of a reduction in the electric field at the waveguide exit. However, comparison of data is often difficult because authors do not include a detailed description of the dielectric configuration and an indication of the nature of the impedance match at the dielectric interface. For example, Covert<sup>21</sup> has measured the breakdown power of a teflon-filled slot located on the surface of a metal cone. The height of the X-band slot was 0.254 cm. The minimum in the breakdown power curve was found to occur at a lower power level than the data of Scharfman for the same size of waveguide, but with a teflon cover rather than a teflon filling. On the other hand, the minimum in power breakdown level data obtained in the present program, with the full-sized teflon-filled slot, is greater than the value for the same sized slot as obtained by Scharfman.

One would expect the wall loss rates to be slightly reduced for the conical geometry. Therefore, there is a temptation to ascribe

---

\* The slot height is defined as the length of the slot in the direction of the electric field (assuming  $TE_{10}$  mode propagation).



some of the above discrepancies to this configuration difference. However, when the results of other investigations with planar geometries are also considered, it must be concluded that such a judgment cannot be made at this time.

The current status of the theoretical prediction of microwave breakdown has also been surveyed by MacDonald.<sup>26</sup> MacDonald directs particular attention to the problems of breakdown in uniform fields. Epstein<sup>27</sup> has recently treated CW breakdown in non-uniform fields and indicated procedures for performing engineering calculations rather rapidly and by hand. Epstein's work, which considers both non-uniform fields and non-uniform gas properties, has recently been extended to include pulsed breakdown and the effects of convection.<sup>28</sup> It is believed that Epstein's work represents the current state-of-the-art with regard to predicting cold air breakdown.

Direct comparison of the results of the current experimental program with Epstein's model is not possible because an essential parameter, namely the spatial variation of the non-uniform electric field, is not known.

#### 4.2.2 Ambient Ionization Effects

If a "large" initial electron density exists before the microwave power is applied to the slot antenna, it is well known that the initiate breakdown power level will be significantly reduced. This is due to alterations in the electron production/loss mechanisms that control breakdown. These effects have also been surveyed by Bisbing,<sup>25</sup> who suggested that ambient ionization could alter initiate breakdown power level by:

- Providing an initial plasma in which the diffusion wall loss is by ambipolar rather than free diffusion (reduces required breakdown power).
- Reducing the absolute electron density increase required to drive the ambient plasma to the critical electron density where  $\omega_p = \omega$ ; (reduces required breakdown power).

- Increasing the rate of electron attachment loss for low antenna power levels; (increases required breakdown power).

Figure 3-19 shows the effects of preionization on the initiate breakdown power level and compares the results with those obtained using cold ambient gas over the slot. It is noted that the initiate breakdown power level is reduced by 6 to 10 db depending upon the ambient gas density and the ambient electron density.

MacDonald is currently studying the effects of preionization in modifying initiate breakdown levels in an S-band cavity arrangement.<sup>29</sup> Although the results reported to date are for neon rather than air, the detailed knowledge expected from this study should be particularly useful for predicting the effects of preionization on the initiate breakdown power levels of jamming antennas.

#### 4.2.3 Convection Effects

Convection effects increase the power required for breakdown. A survey of the state-of-the-art of convective effects has recently been given by Bisbing et al.<sup>30</sup> He notes that the flow field about a slender cone re-entry body can be divided into three distinct flow regions: (1) the ambient free stream, (2) the inviscid shock layer, and (3) the boundary layer. Although the re-entry environmental effects are generally different between the three regions, convective effects are common to all. An exception occurs in the region of high electron density gradient in the boundary layer adjacent to the body. In this region, which may be important for shunt effects in VHF antennas, diffusion losses could dominate over convective effects.<sup>31</sup>

The characteristic particle residence time  $\tau$ , defined as<sup>30</sup>

$$\tau = \frac{L}{u}$$

where  $u$  is the velocity, and  $L$  is the length of the high field region, is a useful parameter for indicating the magnitude of the convection effect. If we assume that the length of the field region is about equal to the height of the slot,  $\tau \sim 2$  microseconds for a full size

X-band slot, and a re-entry velocity of 20,000 fps.

Re-entry velocities cannot be simulated steady state in the laboratory. First order effects of convection in simulating the flight performance can be included by varying the pulse width to represent varying flow times across the slot aperture. Alternatively, the slot aperture can be squeezed down to minimize  $L$ ; however, this generally results in a spatial distortion of the local fields and thereby introduces an additional change in the experimental configuration. For example, Covert<sup>21,22</sup> did not observe behavior that could be related to convection effects for free stream velocities of up to 3200 ft/sec using a teflon-filled X-band slot 0.254 cm high; i.e.,  $\tau \sim 3$  microseconds.

There seems to be general agreement on acceptable methods for including the influence of convection in analytical studies. Therefore, no attempt was made in the present investigation to reduce the slot height or pulse width in an attempt to simulate convection effects.

#### 4.2.4 Elevated Gas Temperature Effects

A survey of recent experimental work is given in References 25 and 30. The interpretation of such experiments is difficult because of effects, such as ionization or the presence of wall impurities, which may accompany the presence of a high temperature gas and exert a more pronounced influence than the gas temperature on the required breakdown power. However, although the effect of high temperature is not understood completely at the present time, there appear to be enough experimental shock tube data to establish the legitimacy of the effect.<sup>30</sup>

It is generally agreed that the high temperature effect is a consequence of the presence of excited molecular states. The most reasonable models would appear to be those which relate the electron energy distribution to the presence of vibrationally excited molecules which provide superelastic collision centers for the electrons.<sup>32</sup>

A note of caution should be made about devices such as the



plasma accelerator used in the present study. The plasma beam constitutes essentially an afterglow plasma since the ionization is produced primarily in the accelerator proper, and the beam region is characterized by recombination and diffusion losses. The process of recombination and subsequent bound-bound electron cascading is a prolific generator of excited states. Thus, in this type of plasma device the excited state population densities are far in excess of what one would expect for the actual gas temperatures ( $\sim 1000^\circ\text{K}$ ), and gas temperature effects per se cannot be identified.

#### 4.2.5 Effects of Chemical Additives

The effects of ablation products and of quenchants have been studied recently by several investigators.<sup>33-35</sup> As discussed in Section 3.5.4, such additives can be expected either to increase or decrease the breakdown power, depending on the species involved. Thompson, et al,<sup>33</sup> observed the following, when twenty percent by volume of CO (carbon ablation),  $\text{CF}_4$  (teflon ablation) and  $\text{SF}_6$  (electrophilic quenchant) were added to the plasma flow in the vicinity of an X-band antenna:

- CO  $\longrightarrow$  No effect on electron density or breakdown power.
- $\text{CF}_4$   $\longrightarrow$  Reduction in electron density by a factor of 2 or 3, with attendant increase in breakdown power by a factor of 3.
- $\text{SF}_6$   $\longrightarrow$  Reduction in electron density by more than a factor of 3. Breakdown power was increased by a factor of 2.

Similar results were obtained in the ablation tests conducted during the present investigation; i.e., teflon ablation in argon produced a bluish glow and a reduction of the electron density by a factor of about 3 (based on Figure 3-18).

A number of complex attachment, dissociation, and metastable related reactions can occur when an electronegative species is introduced into a plasma.<sup>36</sup> When ablation products are introduced into the high field region of an antenna the situation becomes even more

complex because direct ionization processes become important and the electron distribution function is non-Maxwellian. It is believed that an understanding of this situation awaits the performance of a program of carefully designed experiments - where each experiment is conceived to limit the number of chemical reactions which are occurring.

#### 4.3 INPUT IMPEDANCE CHARACTERISTICS

The calculation of the input admittance or impedance of a slot aperture covered with a plasma layer having a spatial variation in electron density has been a popular analytical problem. Galejs is currently preparing a monograph summarizing the present state-of-the-art in this area.<sup>37</sup> In addition, experimental studies are reported<sup>17,24,38-42</sup> in which the input impedance of a slot aperture covered with a plasma has been measured.

A meaningful comparison between theory and experiment requires that the electron density gradients in the plasma layer be accounted for, both in the analytical model and in the experimental measurements. In order to achieve the required spatial resolution the electron density measurements must be made with electrostatic probes. Furthermore, the desired operating conditions generally involve electron density ranges where thick sheath effects are important, and gas densities where collisionless probe theories cannot legitimately be applied. Unfortunately, such precautions are not generally taken in the reported work and it is believed that generalizations concerning agreement between theory and experiment cannot be made at the present time. Indeed, it is believed that the agreement that is often reported by invoking other factors, such as elevated ion temperatures,<sup>17</sup> is probably fortuitous and does not serve as a critical test of the adequacy of the theoretical models. Because of waveguide thermal expansion effects it was generally not possible to make meaningful impedance measurements in the present program. This is unfortunate, since sheath and collision effects were accounted for in the electrostatic probe data interpretation.



It is recommended that, for the purpose of comparison with theory, input impedance experiments be undertaken with the simplest possible geometry and with particular caution being exercised in the electrostatic probe measurements, both with respect to probe surface considerations (see Section 2.5.3), and to data analysis (see Section 2.5.2.2).

#### 4.4 ANTENNA PATTERN MEASUREMENTS

The far-field radiation pattern of an antenna is of particular interest both for ECM decoys and for lifting re-entry communications. Although a large volume of literature is available on theoretical predictions of the radiation patterns for radiators having various geometries, it appears that relatively few experimental measurements using a plasma layer have been made.<sup>24,40,42</sup> Jacavano<sup>42</sup> and Cloutier<sup>40</sup> used horn radiators and receivers, with the plasma produced in a glass container and interposed between them. Taylor<sup>24</sup> used an X-band slot, with a horn as a receiver. The plasma was produced by an RF discharge and the experiment was conducted with a glass test section.

It was noted in Section 3.5.3.3 that Taylor had observed significant attenuation and pattern distortion. Jacavano and Cloutier also observe attenuation and distortion, but to a much lesser degree. The peak electron density (determined from the stated values of  $\omega_p$ ) is quite close for some of the plasma conditions used in the two investigations (i.e. conditions such that  $\omega_p/\omega = 0.8$ ). Under these comparable operating conditions, the data from both investigations indicate the surprising result that the largest attenuation is observed with the thinnest plasma layer. Furthermore, the same behavior was noted with the pattern distortion; namely, that the greater the plasma layer thickness, the less the distortion.

It is believed that the work performed on the present program constitutes one of the few cases in which microwave slot antenna patterns have been measured under the following conditions:



- The presence over the slot of a plasma layer that was not confined by walls.
- The location of the receiving horn in the antenna far-field.
- The performance of the experiments within an anechoic chamber.

The results of these experiments permit the following conclusions to be drawn with regard to the antenna field pattern:

- No antenna pattern distortion was observed under conditions ( $\omega_p/\omega = 0.8$ ) at which considerable attenuation and pattern distortion had been observed by other investigators.
- The complexity of the geometry does not permit a detailed comparison with theoretical computations.

**BLANK PAGE**

## 5. REFERENCES

1. R. G. Fowler, "Experiments with the Electric Shock Tube", Lecture presented at the Gas Dynamics Colloquium, Northwestern University, Evanston, Illinois (November, 1962) (Not published).
2. R. C. Warder, Jr., R. M. Rosen, A. S. Penfold and G. R. Seemann, "Experimental Study of Voltage Breakdown Characteristics of Transmitting Antennas", Litton Space Sciences Laboratories Report ATD-11-67-006, Quarterly Technical Report No. 1, Contract No. F19628-68-C-0001, AFCRL-67-0687 (September, 1967).
3. R. C. Warder, Jr., R. M. Rosen, and A. S. Penfold, "Experimental Study of Voltage Breakdown Characteristics of Transmitting Antennas", Litton Space Sciences Laboratories Report ATD-11-67-043, Quarterly Technical Report No. 2, Contract No. F19628-68-C-0001, AFCRL-68-0086 (December, 1967).
4. G. R. Seemann, J. A. Thornton and A. S. Penfold, "Subsonic Plasma Tunnel for Evaluating Re-entry Flight Instrumentation", AIAA J., Vol. 6, 1592 - 1594, (August, 1968).
5. J. A. Thornton, G. R. Seemann, and A. S. Penfold, "Development of a Continuous Flow Electromagnetic Alternating Current Traveling Wave Accelerator for High-Density, Hypervelocity Wind Tunnel Applications", AFFDL-TR-67-45 (1967).
6. G. R. Seemann, J. A. Thornton, and A. S. Penfold, "Experimental Study of a Traveling Wave Accelerator", AIAA J., Vol. 4, 1870-1872 (October, 1966).
7. G. R. Seemann, J. A. Thornton, and A. S. Penfold, "Development of Electrodeless MHD Accelerator Technology", Proceedings of the Fifth Hypervelocity Techniques Symposium, Denver (March 1967).
8. J. A. Thornton, "An Approximate Theory for Interpretation of Ion Saturation Current Measurements over a Wide Range of Gas Densities", to be submitted for publication (1968).



9. D. Bohm, E. H. S. Burhop, and H. S. W. Massey, Characteristics of Electrical Discharges in Magnetic Fields, edited by Guthrie and Wakerling, McGraw Hill Book Co., New York (1949).
10. V. M. Zakharova, Yu. M. Kagan, K. S. Mustafin, and V. I. Perel, "Probe Measurements at Medium Pressures," *Soviet Physics-Tech. Phys.*, Vol. 5, pp 411-418 (1960).
11. D. Bradley and K. J. Matthews, "Double Spherical Electrostatic Probe Continuum Theory and Electron Temperature Measurements" *Phys. Fluids*, Vol. 10, #5, pp 1336-1341, (June, 1967)
12. J. R. Cozens and A. von Engel, "Theory of the Double Probe at High Gas Pressure", *Int. J. Elec.*, Vol. 19, pp 61-68 (1965)
13. G. R. Seemann, and J. A. Thornton. "Ground Testing of Flush Electrostatic Probe Package", Final Report Contract No. 192533, AF 04(694)-913, Litton Publication No. 11-68-089 (June, 1968).
14. A. H. Shapiro, The Dynamics and Thermodynamics of Compressible Fluid Flow, Vol. I., The Ronald Press Co., (New York, 1953).
15. L. Spitzer, Jr., Physics of Fully Ionized Gases, Interscience, New York, (1956).
16. I. P. Shkarofsky, M. P. Bachynski and T. W. Johnston, "Collision Frequency Associated with High Temperature Air and Scattering Cross-Sections of the Constituents," appearing in Electromagnetic Effects of Re-entry, edited by Walter Rotman and Gerald Meltz, Pergamon Press, New York (1961).
17. J. Galejs and M. H. Mentzoni, "Waveguide Admittance for Radiation into Plasma Layers - Theory and Experiment", *IEEE Trans. AP-15*, pp 456-470 (1967)
18. E. H. Ginzton, Microwave Measurements, McGraw-Hill Book Co., Inc., New York (1957).
19. C. G. Montgomery (ed.) Technique of Microwave Measurements, McGraw-Hill Book Co., Inc., New York (1947).
20. W. E. Scharfman and T. Morita, "Voltage Breakdown of Antennas at High Altitude", *Proc. IRE.*, Vol. 48 pp 1881-1887 (November, 1960).
21. E. E. Covert, and J. B. Coffin, Jr., "Wind Tunnel Studies of Antenna Breakdown, Part I, Influence of Forced Convection Only", Report No. AFCRL-64-282 (I), prepared by Aerophysics Laboratory, Massachusetts Institute of Technology (March, 1964).

22. E. E. Covert and L. R. Boedeker, "Studies on Antenna Breakdown in the Presence of a Plasma Sheath Including Effects of Forced Convection", Report No. AFCRL-67-0190, prepared under Contract No. AF 19(628)-5518, by Aerophysics Laboratory, Massachusetts Institute of Technology (February, 1967).
23. M. A. Heald and C. B. Wharton, Plasma Diagnostics with Microwaves, John Wiley, New York (1965).
24. W. C. Taylor, "Study of the Effect of a Plasma in the Near-Zone Field of an Antenna", Final Report, NASA Contract NAS 1-4973, Stanford Research Institute (May, 1966).
25. P. E. Bisbing, D. L. McMenamin, and P. Scherer, "Study to Obtain Design Data for Re-entry ECM Antenna Systems (U)", Report No. AFCRL-67-0585, Second Quarter Technical Report, prepared under Contract No. F 19628-67-C-0210, by Missile and Space Division, General Electric Co. (September, 1967).
26. A. D. MacDonald, Microwave Breakdown in Gases, John Wiley, New York (1966).
27. M. Epstein, "High-Frequency Breakdown of Nonuniform Gases in Spatially Varying Fields", Physics of Fluids, Vol. 11, No. 4, pp 896-902 (April, 1968).
28. M. Epstein, (Aerospace Corp.), Private Communication.
29. A. D. McDonald, "Antenna Breakdown Phenomena in Re-entry Plasmas", Proceedings of the Conference on the Applications of Plasma Studies to Re-entry Vehicle Communications, Vol. 1 (October 3-4, 1967).
30. P. E. Bisbing, D. L. McMenamin, and A. K. Jordan, "Study to Obtain Design Data for Re-entry ECM Antenna Systems (U)", Volume 1 of 2, Report No. AFCRL-68-0037, Third Quarter Technical Report, prepared under Contract F 19628-67-C-0210, by Missile and Space Division, General Electric Co. (December, 1967).
31. P. M. Chung, and V. D. Blankenship, "Electrostatic Probe for Electron Density Measurements on Re-entry Vehicles", Aerospace Report No. TR-669 (S6240-10)-2, Aerospace Corp., San Bernardino, Calif., (March, 1966).
32. G. C. Light and R. C. Taylor, "Antenna Breakdown in High-Temperature Air", Aerospace Report No. TR-1001 (2220-10)-3, Aerospace Corp., El Segundo, Calif. (June, 1967).

33. W. P. Thompson, M. Epstein and C. J. Lenander, "Microwave Break-down of the Re-entry Boundary Layer", TR-1001 (2240-20)-11 Aerospace Corporation, El Segundo, California (May, 1967).
34. W. P. Thompson (Aerospace Corp.), Private Communication.
35. C. W. Haldeman (MIT), Private Communication.
36. E. A. Sutton and R. F. Weiss, "A Preliminary Calculation of the Necessary Wake Quench Fluxes (U)", (Secret), Paper No. 36, Presented at 25th AMRAC Meeting, Arlington, Virginia (April, 1968).
37. J. Galejs, (Sylvania Elect. Sys.), Private Communication.
38. W. C. Taylor, "An Experimental Study of Nonlinear Plasma-Wave Interaction", Report No. AFCRL-65-654, prepared under Contract AF 19(628)-4800, by Stanford Research Institute (August, 1965).
39. W. C. Taylor, "The Effect of a Plasma in the Near-Zone Field of an Antenna-II", Final Report, NASA Contract NAS 1-7024, Stanford Research Institute (April, 1968).
40. G. G. Cloutier and M. P. Bachynski, "Antenna Characteristics in the Presence of a Plasma Sheath", in Symposium on Electromagnetic Theory and Antennas, pp 537-548, Pergamon Press, New York (1963).
41. M. H. Mentzoni and J. Donohoe, "Admittance of a Slot Antenna Following R. F. Voltage Breakdown", Electronics Letter, Vol. 2, Page 459 (December, 1966).
42. D. J. Jacavanco and G. Meltz, "An Experimental Investigation of Antenna Pattern Distortion Due to a Plasma Layer", IEEE Trans. Ant. and Prop., Vol. AP-12, pp 365-366 (May, 1964).



## DOCUMENT CONTROL DATA - R&amp;D

(Security classification of title, body of abstract and indexing annotation must be entered when the overall report is classified)

1. ORIGINATING ACTIVITY (Corporate within) Space Sciences Laboratories Litton Systems, Inc. 336 No. Foothill Rd., Beverly Hills, Cal. 90213		2a. REPORT SECURITY CLASSIFICATION UNCLASSIFIED	
		2b. GROUP	
3. REPORT TITLE EXPERIMENTAL STUDY OF VOLTAGE BREAKDOWN CHARACTERISTICS OF TRANSMITTING ANTENNAS, VOLUME 1 of 2			
4. DESCRIPTIVE NOTES (Type of report and inclusive dates) Scientific - Final - Period covered July 1967 - July 1968 Approved: 9/17/68			
5. AUTHOR(S) (Last name, first name, initial) Richard C. Warder, Jr. John A. Thornton			
6. REPORT DATE July 1968	7a. TOTAL NO. OF PAGES 125	7b. NO. OF REFS 42	
8a. CONTRACT OR GRANT NO. F19628-68-C-0001, ARPA Order No. 693		9a. ORIGINATOR'S REPORT NUMBER(S) Publication No. 11-68-110-I	
8b. PROJECT NO. 8671 DOD Element 6.25.03.01.R DOD Supplement N/C		9b. OTHER REPORT NO(S) (Any other numbers that may be assigned this report) AFCRL-68-04050	
10. AVAILABILITY / LIMITATION NOTICES This document is subject to special export controls and each transmittal to foreign government or foreign nationals may be made only with prior approval of AFCRL (CRDM/ <del>unclassified</del> ) L.G. Hanscom Field, Bedford, Mass. 01730			
11. SUPPLEMENTARY NOTES This research was sponsored by the Advance Research Projects Agency		12. SPONSORING MILITARY ACTIVITY Air Force Cambridge Research Laboratories (CRD) L.G. Hanscom Field Bedford, Massachusetts 01730	
13. ABSTRACT This document is part of the final report describing an investigation of the breakdown characteristics of selected microwave and VHF transmitting antennas under both cold air and simulated re-entry conditions. The purpose of the program was to provide experimental data which will aid in the selection of re-entry jammers. Of particular interest were the power-handling capabilities, the pattern of the radiated fields, and the input impedance, of antennas which are compatible with the geometry of a conical re-entry vehicle.  The report is divided into two volumes. This volume is unclassified and describes the investigation of a microwave slot antenna. Volume II, which is classified Secret, describes the investigation of a VHF antenna.  The microwave antenna consisted of a teflon-filled X-band slot, located on a conical surface which served as a conducting plane. The microwave experiments consisted of performing initiate and extinguish breakdown tests with both cold gas, and a plasma environment over the antenna. Transmitted and reflected power measurements were also made, together with preliminary ablation tests.  The antenna plasma tests were conducted in the large size, steady state, plasma flow environment produced by the <del>Litton</del> electrodeless MHD plasma accelerator.			

14. KEY WORDS	LINK A		LINK B		LINK C	
	ROLE	WT	ROLE	WT	ROLE	WT
Microwave Antennas Antenna Breakdown Re-Entry Plasma Simulation Traveling Wave Accelerators Plasma Diagnostics						

## INSTRUCTIONS

**1. ORIGINATING ACTIVITY:** Enter the name and address of the contractor, subcontractor, grantee, Department of Defense activity or other organization (corporate author) issuing the report.

**2a. REPORT SECURITY CLASSIFICATION:** Enter the overall security classification of the report. Indicate whether "Restricted Data" is included. Marking is to be in accordance with appropriate security regulations.

**2b. GROUP:** Automatic downgrading is specified in DoD Directive 5200.10 and Armed Forces Industrial Manual. Enter the group number. Also, when applicable, show that optional markings have been used for Group 3 and Group 4 as authorized.

**3. REPORT TITLE:** Enter the complete report title in all capital letters. Titles in all cases should be unclassified. If a meaningful title cannot be selected without classification, show title classification in all capitals in parentheses immediately following the title.

**4. DESCRIPTIVE NOTES:** If appropriate, enter the type of report, e.g., interim, progress, summary, annual, or final. Give the inclusive dates when a specific reporting period is covered.

**5. AUTHOR(S):** Enter the name(s) of author(s) as shown on or in the report. Enter last name, first name, middle initial. If military, show rank and branch of service. The name of the principal author is an absolute minimum requirement.

**6. REPORT DATE:** Enter the date of the report as day, month, year, or month, year. If more than one date appears on the report, use date of publication.

**7a. TOTAL NUMBER OF PAGES:** The total page count should follow normal pagination procedures, i.e., enter the number of pages containing information.

**7b. NUMBER OF REFERENCES:** Enter the total number of references cited in the report.

**8a. CONTRACT OR GRANT NUMBER:** If appropriate, enter the applicable number of the contract or grant under which the report was written.

**8b, 8c, & 8d. PROJECT NUMBER:** Enter the appropriate military department identification, such as project number, subproject number, system numbers, task number, etc.

**9a. ORIGINATOR'S REPORT NUMBER(S):** Enter the official report number by which the document will be identified and controlled by the originating activity. This number must be unique to this report.

**9b. OTHER REPORT NUMBER(S):** If the report has been assigned any other report numbers (either by the originator or by the sponsor), also enter this number(s).

**10. AVAILABILITY/LIMITATION NOTICES:** Enter any limitations on further dissemination of the report, other than those

imposed by security classification, using standard statements such as:

- (1) "Qualified requesters may obtain copies of this report from DDC."
- (2) "Foreign announcement and dissemination of this report by DDC is not authorized."
- (3) "U. S. Government agencies may obtain copies of this report directly from DDC. Other qualified DDC users shall request through \_\_\_\_\_."
- (4) "U. S. military agencies may obtain copies of this report directly from DDC. Other qualified users shall request through \_\_\_\_\_."
- (5) "All distribution of this report is controlled. Qualified DDC users shall request through \_\_\_\_\_."

If the report has been furnished to the Office of Technical Services, Department of Commerce, for sale to the public, indicate this fact and enter the price, if known.

**11. SUPPLEMENTARY NOTES:** Use for additional explanatory notes.

**12. SPONSORING MILITARY ACTIVITY:** Enter the name of the departmental project, office or laboratory sponsoring (paying for) the research and development. Include address.

**13. ABSTRACT:** Enter an abstract giving a brief and factual summary of the document indicative of the report, even though it may also appear elsewhere in the body of the technical report. If additional space is required, a continuation sheet shall be attached.

It is highly desirable that the abstract of classified reports be unclassified. Each paragraph of the abstract shall end with an indication of the military security classification of the information in the paragraph, represented as (TS), (S), (C), or (U).

There is no limitation on the length of the abstract. However, the suggested length is from 150 to 225 words.

**14. KEY WORDS:** Key words are technically meaningful terms or short phrases that characterize a report and may be used as index entries for cataloging the report. Key words must be selected so that no security classification is required. Identifiers, such as equipment model designation, trade name, military project code name, geographic location, may be used as key words but will be followed by an indication of technical context. The assignment of links, rules, and weights is optional.